An Investigation into Flow Properties of Self-Healing Agents in Damaged Zones of Cementitious Materials

A thesis submitted for the Degree of Master of Philosophy

by

Andrea Hoffman B.Eng. (Hons)

School of Engineering

May 2012

Acknowledgements

The support that has been given to me from my family throughout the whole of this MPhil has been incredible, so therefore I would like to dedicate this thesis to them.

Dr. Diane Gardner, my supervisor for this research project has assisted me through learning and she has taught me a lot and not just in the studies looked at in this thesis. I feel that I have made such a large progression in my education and skills from this MPhil and would like to thank her for this as she has encouraged and guide me every step of the way. Thank you.

I would also like to thank my personal tutor, lecturer and other supervisor, Dr. A. D. Jefferson. Throughout my time at university he has provided me with the best guidance any supervisor or tutor ever could and without his help and support, this would not have been possible. Thank you.

The technician staff; Carl, Iain, Harry, Des, Brian and Len have been amazing and I have enjoyed every minute down in the laboratory with them. They have been so amazing and helpful and I cannot thank them enough. I had the best time down in the labs with Carl and Iain and they have made this an unforgettable experience. I would also like to thank Len, for putting up with me when I used the scales from his lab without asking and not returning them and also Harry for all of his hard work and expertise down in the lab helping me with experimental difficulties.

Lastly, I would like to thank everyone in office W1.32, Iulia, Ben, Simon D, Simon C, Adrianna and Rob; you guys have been amazing and are friends I will never forget.

Summary

This thesis is concerned with the experimental and numerical study of capillarity in cementitious materials. Capillarity is a phenomenon that has been researched by many; however, literature shows few studies completed on capillarity in cementitious materials, in particular discrete cracks. This thesis presents experimental and numerical data to further those areas in research that rely on capillary flow mechanisms, such as the deterioration process in concrete and the flow of healing agents in self-healing cementitious materials.

Experimental simulations of capillary flow through five different crack configurations in cementitious materials have been studied. Alongside the experimental work capillary flow theory has been used to validate the experimental results with the use of numerical formulae. This thesis presents details of the Lucas-Washburn equation traditionally used in capillarity and glue flow theory in chapter 5 and the experimental results alongside the theory are used to assess the performance of the numerical models.

Some of the conclusions that have been made are listed below however, a more in depth view is shown in chapter 4:

- results looking at the effect of crack configuration show that the crack path does not have a large effect on capillarity;
- specimen age of mortar was another area that was looked at and results and readings do show that the rate of rise is affected by age;
- the difference between the healing agents used in experiments does show that viscosity does play a large part in rate of capillarity and
- specimen saturation, one of the parameters also touched on in this thesis does show that the more saturated the specimen, the higher the flow of the healing agent.

Conclusions are made and are presented in chapter 6 based on the analysis of the experimental results and the validation of the numerical solution. Comparisons between the experimental work and numerical solution show that the numerical solution for various crack configurations is reliable to determine the glue flow theory for healing agents.

Contents

Chapter 4 Page no.

Chapter 5

Chapter 6

List of tables

List of figures

Chapter 4

Main notation

Parameter	Symbol/formula	Units
Viscous flow	$v(x)$	m/s^2
Viscosity	μ	Ns/m^2
Pressure	p	N/m^2
Gravity	g	m/s^2
Inclination angle of capillary/crack	ϕ	$^\circ$
Distance of fluid front from the reservoir	z	m
Capillary potential pressure	P_c	N
Angle meniscus forms with crack/solid face	θ	$^\circ$
Surface tension (liquid-air)	γ	N/m
Cross sectional area of capillary	$A(x)$	m^2
Cross sectional area of meniscus interface	$A(z)$	m^2
Crack aperture	b	m
Density	ρ	kg/m^3

Chapter 1

Introduction

1.1 Introduction

The last twenty years have seen significant growth in sustainable construction materials being developed in response to global demand. This is being done primarily to reduce the carbon dioxide emissions associated with the construction industry as concrete structures are the prime contributors to costs spent within the construction industry (Corporatewatch, 2009). This particular source states that 45% of these costs are spent on structural repair and maintenance and a significant proportion of this is directly related to the nations ageing concrete civil infrastructure. The development of sustainable construction materials consider the use of not only low carbon materials but also aim to enhance the longevity of the structure via improvement of long term material properties such as durability. The presence of pores and cracks in a cementitious matrix, the latter caused as a result of plastic shrinkage, structural loading and thermal effects amongst other actions, allows the movement of water and gases throughout the microstructure. This may lead to the promotion of deterioration processes such as freeze-thaw action, chloride ingress or carbonation and the independent or sometimes concurrent actions of these processes have reduced the service life of structures and have forced extensive repairs. (Gardner et al. 2011) This is of significant importance when considering the design and performance of critical civil infrastructure such as water reservoirs, radioactive waste disposal facilities and confining enclosures of nuclear power plants.

Capillary absorption is a force driven primarily by surface tension and has been frequently noted throughout literature as one of the primary transport mechanisms by

which aggressive agents from the environment ingress concrete. Conversely, capillary absorption is also the mechanism by which concrete is able to self-heal and novel work in the area of self-healing cementitious materials has proved promising in enhancing the longevity of structures. Such healing processes involve either the internal release of healing agents as a result of damage to the host material (autonomic healing) or the movement of moisture through the host material to promote natural healing (autogenic healing). The ability to measure and predict the movement of healing agents and moisture through cracks in the cementitious material will therefore allow the effectiveness of such healing systems to be evaluated. When considering autonomic self healing in cementitious materials a number of adhesives have been used as the healing agent (Joseph et al. 2010). The ability of the healing agent to flow into a discrete fracture is dependent on capillary action and in autonomic healing studies the healing agents have been explicitly chosen such that the viscosity of the fluid and its curing/setting time does not delay the flow of the healing agent.

Numerous experimental studies have been performed on capillarity in porous media, including brick, stone and concrete, with the majority of researchers using sorptivity, the absorption of water via capillary action through a network of capillaries, as a measure of capillarity. It is evident that few researchers have considered capillary flow in a single capillary (i.e. a discrete crack) and the studies which are available offer limited data due to the low number of crack apertures and configurations employed. Numerical simulations and predictions of capillary absorption in cementitious materials have been presented by a number of researchers, although again a far greater body of work has been published on capillary rise in porous media in general, rather than in concrete in particular (Gardner et al 2011).

1.2 Aims of work

The overall aim of this work was to identify and measure capillary flow of water and glue in discrete cracks in mortar. This included exploring some of the factors that influence the rate and level of capillary rise height in mortar specimens. The lack of detailed experimental data in the literature to enable accurate modelling of the movement of water in discrete cracks was the primary driving force behind the design of this research programme. One of the main areas of investigation focuses on the effect of crack aperture on the rate of capillary rise in concrete. This in the past has proved difficult to measure due to size constraints of the measuring apparatus and the inability to simulate a variety of crack configurations and apertures.

The objectives in achieving the main aim of this thesis were:

• to undertake a series of experimental studies to determine how the crack aperture affects the rate and level of capillary rise height with the use of mortar specimens and a range of fluids;

• to determine how the rate and level of capillary rise height in a naturally formed cracks differs to that of a planar crack at equal crack aperture and

• to identify the capillary flow parameters for varying flow agents in cementitious materials through the examination of fluid flow in discrete cracks.

1.3 Layout of the Thesis

This thesis has 6 chapters including this introduction. Chapter 2 presents literature concerning capillarity and deterioration processes in concrete, along with previous studies that have observed capillary flow in porous media and developments in autonomic and autogenic self healing.

The experimental procedure to obtain data of capillary uptake of water and a potential healing agent (flow agent) in simulated discrete cracks in mortar, obtained via high speed video measurement is reported in Chapter 3. Such a technique allows capillary rise measurements over very short time intervals to be captured, along with measurement of several of the parameters governing capillary flow in cementitious materials.

Chapter 4 reports and discusses the experimental results with respect to crack configuration, specimen age, flow agent and specimen saturation.

In Chapter 5 the theory of capillary flow in discrete cracks is presented and a numerical model which simulates capillary flow in cementitious materials is developed. A comparison of the measured and simulated capillary rise response in the discrete crack is used to validate the model.

The final section of this thesis, Chapter 6 draws conclusions from the experimental and numerical studies undertaken and provides suggestions for further investigation and development of the model to consider the curing effect of healing agents.

Chapter 2

State of the art review

2.1 Introduction to State of the Art Review

The literature review presented here introduces and discusses the issues related to capillary flow in porous media. It has been noted that there are gaps in the knowledge associated to capillary flow in porous media and this review identifies the shortcomings of existing research and suggests possible areas of investigation.

The first area discussed in the literature is why and how durability relates to the key topic in this thesis, capillarity. Cracks in cementitious materials provide flow paths directly into the structure and as certain agents such as chloride ions pass through these cracks they cause deterioration of these structures. Therefore it is necessary to have an understanding of how fluids flow through cracks in cementitious materials. Researchers who have investigated the strength and durability of cementitious materials, including the new research area of self-healing materials, acknowledge that moisture flow contributes to the deterioration of structures. It is therefore important to have an understanding of the transportation of liquids in porous media.

Twenty-five years ago the concrete industry noted the importance of the durability of concrete and the need for it to be developed into a working material that could withstand certain conditions that had previously not been taken into consideration. It was considered to be far from maintenance free as many structures that were considered ‘young’ with respect to their designed service life had to be demolished. (Neville 1981).

Historically, durability problems associated with concrete can be attributed to the lack of compliance by designers to the requirements that relate to durability. The requirements of structures were that they needed to be durable and safe and there are a number of British Standards that have addressed these requirements.

At the same time it was noticed that concrete structures needed protection, so that they could remain aesthetically pleasing, safe and most importantly they needed to be protected against damage. Durability of concrete thirty years ago was considered to be a rather narrow definition as those who knew about concrete would have seen it as a structural material that was designed to obtain its required strength. Although an overview of durability was published in the early 1980s, the ability of engineers to analyse properties of structures as was in its infancy and in recent years great advances have been made in understanding and modelling the behaviour of concrete in relation to its durability.

2.2 Causes of concrete decay 30 years ago

In 1969 Halstead discussed the causes of deterioration of durability and also how durability of existing structures could be maintained. Halstead noted that if concrete is exposed in a normal atmospheric environment to clean air at a temperature in the region of 15 – 20˚C and having a standard relative humidity of 65% it can somewhat be considered to be infinitely durable. At this time, information was being published regarding the topic of the aggressiveness of the environment and the effect that it has on concrete. Nowadays this topic is still being examined in greater depth and as stated previously, is still an area of concern to researchers.

Halstead (1969) noted that water containing crystals in porous voids in concrete can alter the strength of concrete. This can happen by severe temperature changes within voids containing water crystals. The changes in temperature are caused by freeze-thaw cycles and as this happens, strength is lost through the concrete bonds. This therefore relates to capillarity, not directly, but the freeze-thaw cycles produce inherent cracks in a cement matrix, providing direct voids and pathways towards the steel

reinforcement. Halstead (1969) did not further his studies; he only looked directly at what happens to a cement matrix through freeze-thaw cycles. Therefore, an opening for future work was created by where the effect of ion flow through cementitious materials subsequent to freeze-thaw cycles could be studied, and this has been looked at in detail in the last 40 years.

2.3 Carbonation of concrete

Although concrete specimens may be cured properly, if exposed to the atmosphere many changes in the matrix can happen which can severely affect their structural integrity.

Erlin and Hine (2004) provides a well rounded theory of carbonation. When concrete surfaces are in contact with air, solid compounds react together and carbonic acid is produced from the reaction of carbon dioxide dissolving in water. This acid must be prevented from being produced as when the calcium compounds contained in cementitious materials react with carbonic acid, the by product is silica and alumina gels. Carbonation produces chemical reactions between carbon dioxide from the air and products from cement hydration cause reduction in alkalinity of the concrete and as this happens, levels of steel protection are reduced.

Although concrete actually increases in strength, the passive protection to steel is lost as alkalinity drops.

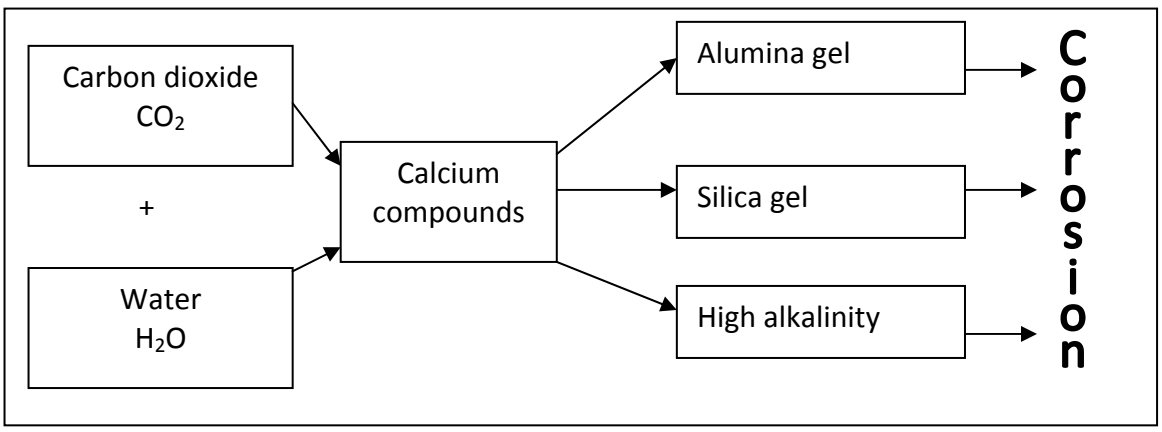

Figure 1: Process of carbonation through cementitious materials – based on literature from Erlin and Hine (2004).

Steffens (2002) created a numerical model to assess carbonation to predict corrosion risk of steel in concrete structures. At this period in time researchers felt that information on how carbonation affects structural integrity was lacking. They note that concrete itself is a porous compound material consisting of mineral aggregates and the cement matrix that form a durable structure. They studied the porosity of the concrete and also noted that it provides further possible movement and retention of water and other substances.

Their model uses finite element analysis alongside their experimental findings to assess how temperature, moisture and carbon dioxide move through cementitious materials and initiate the process of carbonation. Using the laws of diffusion a new mathematical model was created and successfully represents how moisture is stored in voids in cementitious materials.

Most parameters and variables were covered experimentally to provide an overall model including the change in atmosphere looking at the change in temperature and humidity and how it affects structures. Their work does not directly focus on capillarity or movement of fluid through a network of voids, it only focuses on the deterioration properties of concrete due to moisture movement through cementitious materials. Their work could potentially be developed further if they had a better idea of different types of capillaries or voids in cementitious materials.

Song et al. (2006) performed experiments to try and examine how carbonation of concrete structures can be prevented, as this is the main accelerator for steel corrosion and deterioration of concrete structures. The review of Song et al.'s work (2006) states that it is necessary to control the cracking of structures to try and determine an evaluation of crack resistance for structures in early ages. This is something which is hard to do as even when concrete cures and hydrates, cracks are produced and these cracks provide a direct path for carbon dioxide to enter and therefore the process of carbonation is accelerated.

The study completed by Song et al. (2006) looks at experimental and analytical techniques to predict carbonation in early aged cracked concrete as they identified that this is the main reason for depletion of concrete structures. Areas where there are high industrial fumes being produced, induce environmental pollution containing high amounts of carbon dioxide and therefore additional care must be taken in designing concrete for such applications and situations. This is significant as it demonstrates the necessity to have an understanding of the role of capillary flow in cementitious materials.

Carbon dioxide diffusion of pore water in sound concrete and cracked concrete was analysed by Song et al. Using equations of diffusion and with the use of finite element analysis characteristics of diffusivity on the carbonation of early age cracked concrete was used to predict the carbonation depth in pre-cracked concrete.

Song et al. (2006) were successful in their findings especially when specimens were tested at a premature age, this was due to their ability to use finite element analysis models along with multi component hydration models to handle the diffusion of carbon dioxide in concrete. An extra addition to their model was that the model was able to handle extra features of 'real-life' situations such as degree of saturation and temperature effects. Modelling saturation directly relates to the phenomenon of capillarity and there is the potential to further develop their model by seeing how the finite element model can relate capillarity as it does to saturation.

2.4 Permeability of concrete

Song et al. (2007) took a step forward into looking at the capillary pore structure of carbonated concrete specimens. Unlike previously, their findings create a more in-depth analysis of what happens to a cement matrix when it comes into contact with the atmosphere.

It is stated that the rate of carbonation depends entirely on the void ratio of a structure and the moisture content of a structure, especially in foundation structures

such as piles where the base of the structure could be exposed to wet soil or underground water. This is a limitation in their work as in practice the aggregates will contribute to permeability.

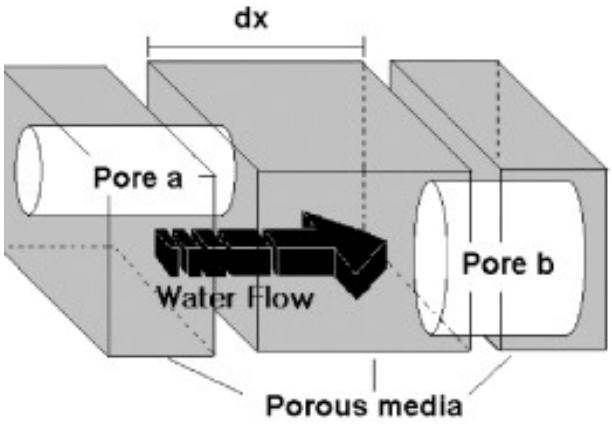

Figure 2: Flow of water through porous media Song et al. (2007)

Song et al. (2007) completed a model to determine permeability to assess the capillary pore structure in carbonated cement mortar. Assumptions taken into their model are that the aggregates do not affect carbonation processes in early aged concrete.

Figure 2 shows the model that they used to determine water flow in pores in mortar specimens. It is a clear concise way to show the flow through the specimens. Permeability was measured from models undertaken looking scales of a small magnitude (micrometres) and was verified with results from an accelerated carbonation test and a water penetration test in cement mortar. This particular property of cementitious materials potentially defines the resistance to carbonation of structures. With a less permeable matrix, ions such as carbon dioxide passing through the concrete matrix will be less successful in simulation of moisture transfer.

With work based in the lab and in field studies assessing carbonation a model was produced which can not only assess structures in the atmosphere but also those underground. Although, it is evident that even though they have looked into permeability via models using carbonation, they have not considered a range of fluids that could flow through a cement matrix and hence this is a research area that could be developed.

Stated above in the work of Song et al. (2007) it is important to have an idea of permeability through concrete. Gardner et al. (2008) completed experimental and numerical work of gas flow characteristics through concrete.

Tests were performed with the use of a pressure cell apparatus, to monitor nitrogen gas flow through concrete. Most experimental work previously has been assessing water flow through cementitious materials; as such tests provide accurate measures of permeability as they investigate the time to reach steady state flow and also the long term response of the experimental system. However, they can be timely to prepare and run. The permeability calculated from experimental work using gas permeability measurements has both values and variations consistent with those from other investigations.

All of the work undertaken in this study was executed to look at cementitious materials long-term performance and durability. Many day to day processes when in contact with cement based structures, such as landfill sites with the use of concrete barrier structures, accurate modelling of fluid flow through cementitious materials is essential.

Gardner et al. (2008) discovered that permeability increases rapidly with a reduction in moisture content. Data found in the literature was obtained for concrete in which moisture had been removed by heating. A large range of parameters were investigated including measurement of the connectivity of a range of pore sizes but not individual pores and capillaries. However, permeability measurements of saturated specimens, as well as specimens less than 28 days old are still lacking in the literature. These are areas which if discovered would provide another step towards a full understanding of fluid flow through cementitious materials.

2.5 Corrosion of concrete

Corrosion of steel reinforcement is known as a major cause of degradation of reinforced concrete structures. Therefore looking at properties of flow through concrete can directly relate to flow of harmful ions through concrete which affect the serviceability and life of concrete structures.

Work by Vidal et al. (2007) assesses the predicted time taken for different fluids or ions to reach a specific location in discrete cracks in a beam of 17 years old. 36 reinforced concrete beams (300×28×15cm), were cast and then stored in a chloride environment under service load to take into account the influence of the flexural cracks.

Results and readings of chloride flow through the induced cracks of less than 4mm showed that they do not influence significantly the corrosion process of tension reinforcing bars and then the service life of the structure. However, the bleeding of chloride ions through the smaller cracks in concrete was a cause of interface de-bonding which could lead to early corrosion in the reinforcement.

Vidal et al. (2007) could have studied a larger range of crack apertures through their specimens. It has been stated that fluid flow through the cement matrix is a larger cause of corrosion than direct flow through the induced cracks. Studies through smaller cracks could have benefited their work to see if smaller cracks affect corrosion.

Cabrera (1996) has used numerical models to assess losses in serviceability of reinforced concrete specimens. Data recorded in the laboratory was collected to look at the rate of corrosion and was used in the numerical models and against the numerical model looking at issues of serviceability of cementitious materials, such as the strength of concrete after corrosion.

His models were developed further to not only look at loss of serviceability through corrosion but also look at the rate of corrosion from the width and intensity of cracking and the bond stress through corrosion rate. Models to determine the rate of cracking

due to loss of bond strength were completed. However, no work was done to look at the flow rates of ions through the cracks generated. Yet again this suggests that ion flow through cracks in cementitious materials is an area which could be investigated further.

Granju and Balouch (2005) focus on corrosion attack of steel fibre reinforced concrete (SFRC.) The effect that the steel fibres have on the cement matrix is looked at in large detail. It was a concern that the steel fibres could be weakened by corrosion, or the opposite, they could burst the cement matrix by swelling and cracking the matrix.

Their specimens were cut exposing fibres to higher levels of corrosion than from an induced crack. They induced cracks of known apertures of 0.5 and 0.8mm and the range in between. Only crack widths in this range were looked at as shown in figure 3. Their work was somewhat limited in this respect and the effect of flow through a larger range of crack apertures would yield a greater quantity of data that would support their numerical work.

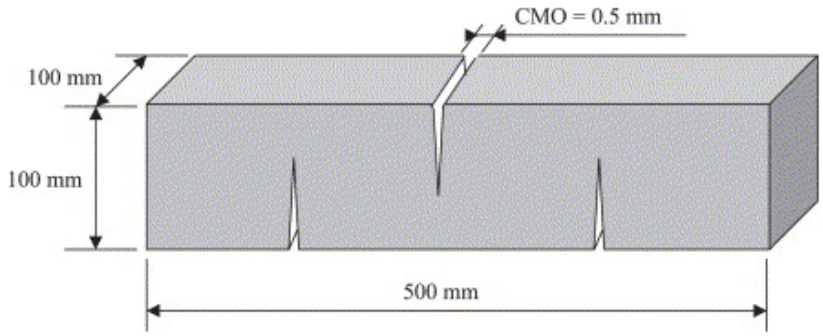

Figure 3: Crack positions generated for experimental work Granju and Balouch (2005)

Again Granju and Ballouch (2005) look at their studies with not only experimental work but also numerical work. They show that it is important to model experimental processes from theory and then match the experimental results to the theoretical results.

Corrosion over a long period of time was investigated by Vidal et al. (2007). This was achieved through experiments of a reinforced concrete beam being exposed to a

chloride environment. Their experiments show that the bleeding of chloride ions through concrete is an important cause of deterioration and that corrosion occurs earlier in the compressive section of the beam. Capillarity was not mentioned directly although their conclusions stated that the crack widths less than 0.4mm do not influence corrosion process directly.

2.6 Chloride attack

As previously discussed in section 2.1 chloride ion attack is one of the main causes of concrete deterioration and steel reinforcement corrosion. The literature discussed in this section look at chloride ion ingress into many different types of specimens whilst looking at the key method of transportation of ions through cement matrices due to capillarity.

Azari et al. (1993) used microsilica concrete to determine chloride ingress and water absorption into the cement matrix. Looking at flow of ions through microsilica concrete is an aspect that demonstrates flow properties and interaction between healing agents and ions that severely affect concrete serviceability. Determining the absorption and flow rate of water ions into concrete specimens relates to capillarity such that certain flow properties can be deduced.

Results from experimental studies showed that a mathematical relationship is apparent between the chloride concentration and the changes in microsilica content. Flow of chloride ions through microsilica concrete are reactive at low quantities of microsilica in the specimens. Water absorption is another area that was investigated as flow of water was modelled through microsilica concrete. They looked at the effect of high water contents and lower water contents of microsilica concrete. Results showed that water absorption in low quantities of microsilica in concrete was more prominent in comparison with high quantities of microsilica in concrete. Although the results and readings reflected the water absorption in microsilica concrete, no work was done looking at the effects of water absorption in concrete without microsilica. Therefore a

comparison was not made between the two different composites, and a complete analysis on flow through different types of cementitious materials was not presented.

Studies completed by Gowripalan et al. (2000) focus on the flow of ions in pre-cracked beams. Gowripalan et al. used reinforced concrete beams that were cracked in known places with known crack widths. Using a 3 point bending tests the beams were loaded until the desired crack width was achieved. They were then submerged in a chloride ion solution and chloride ion profiling was used to determine the rates at which the ions reached the steel reinforcement.

Flow of ions through cracked specimens was considered through setting exact locations where two sample holes were dry drilled and powdered samples from taken from these locations and the chloride content was determined. Their studies were successful in that they discovered how to model and determine the flow of chloride ions through cracked specimens however; they did not determine the rate of flow of other fluids through pre-cracked specimens. Yet again, this illustrates an area of research for future investigation.

Corrosion of steel reinforcement in concrete due to transportation of chloride ions in concrete structures in a marine environment has received increasing attention in recent years due to the high cost of repair. Song et al. (2008) examined concrete specimens subjected to marine environments. They look and review previous work on chloride transportation by means of diffusion of concrete structures exposed to these environments. Their findings show that exposure to sea water does not have a relationship with the chloride content contained in the surface of the structure and higher chloride content was found places where the cement had not been cured.

However, they do not take into consideration the flow of ions through voids and capillaries formed in concrete specimens. Their work solely looks at the effect of how the ions have penetrated the cracks in the specimens used.

2.7 Capillarity

2.7.1 Introduction to capillary action

Capillary action can be summarised by the tendency of a liquid to be drawn into a pore or a small opening. Many studies have looked at the theory of capillary flow. These studies have shown how capillary flow can be applied to many different processes that occur in the world today. For instance flow through soils and flow through other porous media.

Capillary action in this study is considered in the context of self-healing concrete, whereby its role in the transport of moisture of healing agents to sites of damage within a cementitious material is crucial for healing to occur.

For many years capillary action has been considered to be a fundamental process in a number of applications, as noted previously. However, capillary action in concrete has received little research attention since the 1970s. (Halstead, 1971). Recent research in concrete structures has shown that flow properties such as permeability, sorption, absorption and adsorption of concrete play a significant role in the deterioration of structures and the need to ensure the longevity of structures is one of the primary aims in the development of self healing concretes.

2.7.2 Surface tension, cohesion and adhesion

Cohesion is the attractive force that acts between liquid molecules and is responsible for the formation of drops of water. Adhesion is the force of dissimilar particles and surfaces to attract to one another (cohesion refers to the tendency of similar or identical particles/surfaces to cling to one another).

Surface tension γ, is a property of the surface of a liquid that allows it to resist an external force. Objects that are dense allow other liquids to be supported on the fluid surface. This is a key point when identifying certain flow properties (Martys and Ferraris 1997).

Fluid flow through any medium can also be altered by another force, adhesion. Adhesion is the force that causes a fluid to adhere to the surface to which it is in contact. When the cohesive force of the fluid is lower than the adhesion, the fluid will curve upward on the edge of the boundary as shown in figure 4 (a). This curvature is more commonly known as the meniscus. Alternatively, when the cohesive forces are greater than the adhesive, the fluid will curve down at the boundary, shown in figure 4 (b).

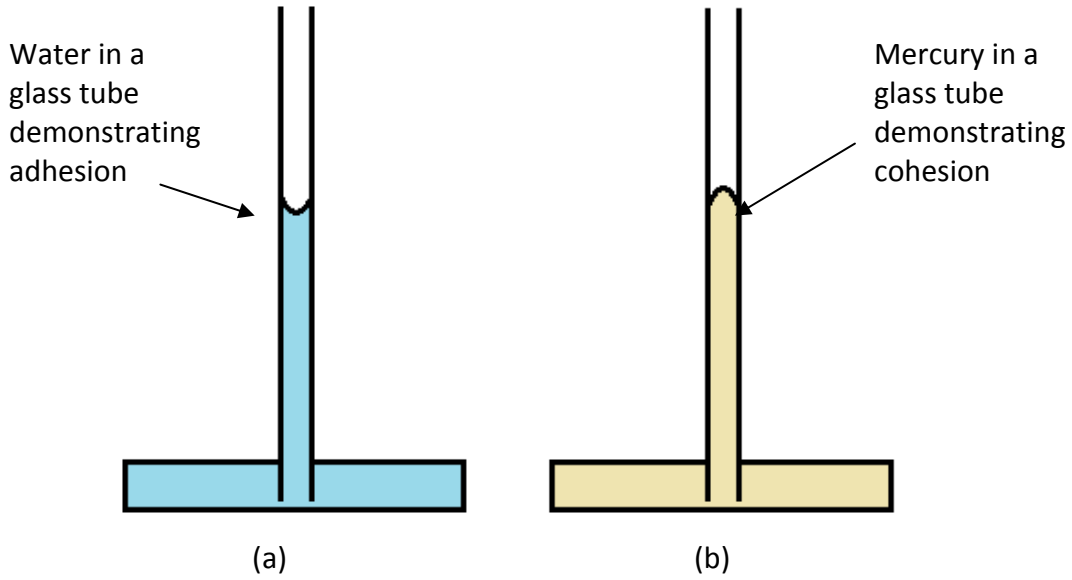

Figure 4: a) Cohesion forces are less than adhesion & b) Adhesion forces are greater than cohesion

A combination of cohesion and adhesion causes the phenomenon known as capillary flow or capillarity. Without these two forces, the phenomenon of capillarity would not occur. A change in pressure results from changes in forces in a void or a tube caused by adhesion and this causes the fluid to rise upward in the void/tube. (Martys and Ferraris 1997).

2.7.3 Sorptivity

Previous reviews on literature stated above have stated that cementitious materials are porous. (Gowripalan et al 2000) These pores and void spaces within a cement

matrix either contain liquid or gas. Porosity is recorded as a ratio of the volume of voids to the total volume of material and is normally represented as a percentage.

Concrete and cementitious materials form pore and void matrices and networks which connect together in random ways. This has been demonstrated previously by Song et al. (2007) shown in figure 2. Pores can be completely isolated, such as small single nodes or a linked network that leads nowhere. A pore structure in a cementitious material cannot be modelled as they never form in the same way and therefore only random generations of microstructure can be obtained.

However, permeability of cementitious materials is the flow of fluids under pressure and is a function of the flow paths that create a route from face to face or surface to surface of the material. These can be direct paths through linked pores and capillaries, direct routes through macro-fractures or slow and tortuous routes through one or combinations of many means of transport. (Marshall 1990)

Sorption acts as part of the diffusion process where fluids and solutes distribute within a material but no fluid flow through the media is incurred by it.

To get accurate estimations and predictions on transport through the permeable matrix of cementitious materials it is necessary to understand the internal structure.

Whilst porosity is the measure of void space by volume and permeability the measure of fluid flow through or into the material, sorption is the uptake of water into a permeable porous structure through capillary action. Sorption acts without a pressure head but through the capillary process described by Marshall (1990) and acts only in a dry or partially dry pore network.

The water uptake in a material is dependent upon its coefficient of sorptivity, *S*, in grams per millimetre^2 (of the wetted area) per root time (g/mm^2·min$^{0.5}$). Equation 2.1 shows the relationship between sorptivity, absorption and time (Martys and Ferraris 1997):

$$i=S\sqrt{t} \quad (2.1)$$

where:

i = the water absorption in g/mm^2 representing the mass increase of the sample per unit area of the wetted perimeter

t = the time elapsed in minutes representing how long the sample has been in contact with the water.

Neville gives typical values for the coefficient of sorptivity for concretes with water/cement ratios of 0.4 and 0.6 as 0.09 g/mm^2/min$^{0.5}$ and 0.17 g/mm^2/min$^{0.5}$ respectively. (Neville 1999)

Roels et al. (2003) found apertures in cementitious materials and their surrounding matrices, this was completed by a series of experiments. Larger models showed the difference between the matrix porosity and the fracture porosity. This was found to be that they both contain hydraulic properties although connect to one another through pressure and mass.

Roels et al. (2003) has provided research with a larger understanding of fluid flow with experiments which identify that a fractured medium is “characterised as a network of flow channels in which saturated flow is described using the Poiseuille equation.” Later experiments relating to this equation for laminar, continuous fluid flow through a uniform straight pipe, the flow rate (volume per unit time) is given by Poiseuille's Equation.

X-Ray diffraction was used by Roels et al. (2003). Roels et al. used 1D numerical simulations looking at fluid flow. These simulations were used to assist further studies of liquid flow through cracks in cementitious materials. Roels et al. noticed that the waterfront in the fracture quickly reaches the opposite side of the specimen as absorption occurs through the surrounding matrix with the use of crack apertures in the region of 0.1mm.

2.7.4 Equation of capillarity

The Lucas-Washburn equation was developed in 1921. Washburn undertook a theoretical investigation in which he considered the effects of the capillary force and viscous drag on circular capillaries and porous bodies. Lucas-Washburn's equation was fundamental to developing understanding of capillary flow.

The Lucas-Washburn equation is considered in more detail in Chapter 5 by where a numerical simulation of flow equation is analysed for capillaries.

Analytical modelling of liquid rise in a capillary tube has been investigated thoroughly by Liou et al. (2009) with various fluid models. They start from the original Navier-Stokes equations which represent incompressible fluid flow in capillaries which is written as;

$$\frac{\partial u}{\partial t} + u. \cdot \nabla u = -\frac{\nabla P}{\rho} + \nu \nabla^2 u \qquad (2.2)$$

Where: ν - is the kinematic viscosity, Ns/m^2

u - is the velocity of the fluid parcel, m/s^2

P - is the fluid-pressure, N/m

ρ- is the fluid density. kg/m^2

From this equation Liou et al. (2009) derive a model for time dependant interface capillary rise.

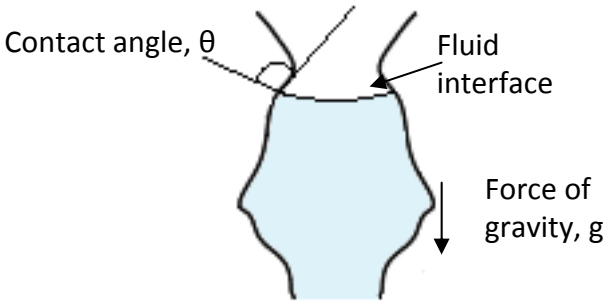

Figure 5: Capillary flow adapted from Liou et al. (2009)

With the use of the Navier-Stokes equations Liou et al. proceeded to derive the Lucas-Washburn equation. The contact angle is measured between the meniscus of the fluid against the solid surface with which it comes into contact.

The Navier-Stokes equations describe the motion of fluid substances and dictate the position of the fluid rather than the velocity of the fluid; the Lucas-Washburn equation predicts flow with respect to time. With the use of Navier-Stokes' and Washburn's work, Liou et al. (2009) derived equations to model different types of capillaries; a circular cylindrical capillary, a uniform rectangular cylindrical capillary, a circular convergent- divergent and a divergent-convergent capillaries, a parabolic non-uniform capillary, a sinusoidal non-uniform capillary and divergent-sinusoidal non-uniform capillary.

The seven models produced by Liou et al. (2009) have proved to be very successful with the use of MatLab coding. Their results show that for capillaries that have large variations in cross-section there are significant effects on flow for non-uniform geometry. The flow varies with respect to the capillary geometry. Results and conclusions showed that the model was successfully validated by comparing the solutions for a circular cylindrical tube, rectangular cylindrical micro-channels, and convergent-divergent and divergent-convergent capillaries with existing numerical models which do not allow for non-uniformity in the capillary geometry. The validated model has been applied to capillaries with parabolic varying wall, sinusoidal wall, and divergent sinusoidal wall. The inertial and viscous effects on the dynamic capillary rise and the equilibrium height were investigated.

Stevens et al. (2009) take the work of Bahramian and Danesh (2004) to measure contact angles from capillary pressure measurements from packed beds of particles which are partially saturated with liquids.

Zhmud et al. (2000) examined the analysis of the original theory of capillarity. Experimental work and numerical work was performed by the researchers to try to capture the phenomenon of capillary rise. Capillary rise was measured with the use of borosilicate glass capillaries with radii of 0.1, 0.15, 0.25 and 0.5mm and the liquids used in experimentation were surfactant solutions, such as ethoxylated trisiloxiane, liquids with a low surface tension. These solutions were used to ensure that there was no interference between the fluid and the capillaries. The dynamics of capillary rise was captured as soon as the liquid was put in contact with the capillary. The capillary rise was recorded with the use of high speed camera software. One-thousand frames a second were recorded to assess the phenomenon of capillary flow. However, a limited number of glass capillaries over a relatively small size range were used. The range of fluids was also limited as only two surfactants were used and other fluids with high surface tension were not used.

Funada and Joseph (2002) created a numerical tool to model the instability of capillary flow in a viscous tube. The phenomenon of their model is shown below in figure 6.

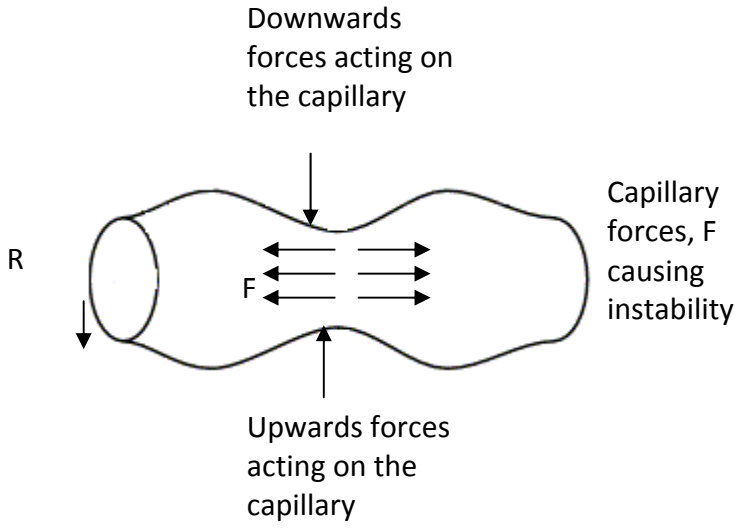

Figure 6: Adapted from Funada and Joseph (2002), instability of viscous flow in a capillary

The model completed by Funada and Joseph (2002) model has been compared against the original Navier-Stokes Equations. More updated studies by Funada and Joseph in 2002 show that in a numerical form capillary instability (where the forces of a fluid in a capillary are not equal) of a liquid cylinder of mean radius R leads towards capillary collapse. This phenomenon of an instable capillary is described by Funada et al. as a 'neck down' due to surface tension γ, in which fluid is injected from the throat of the neck, leading to a smaller neck and greater neck down capillary force, F as seen in figure 6.

Theory of instability along a long capillary cylinder was initially studied by Rayleigh in 1897 and his findings are now considered to be somewhat inaccurate as they neglect the outer fluid. This outer fluid that is in contact with the outer surface provides a force known as viscosity. Rayleigh then developed his methods to account for this viscous force, although his findings were found as incomplete. In later years Fundada and Joseph (2002) looked at viscous potential flow analysis and now the issue of capillary instability can be assessed with the use of new model by Funada and Joseph (2002) in the fully viscous and potential flow cases so no forces are neglected. They show that capillary instability is prominent in places where there are pressure changes.

It is necessary to have an understanding of the different types of forces apparent in a capillary. Funada and Joseph successfully show through their numerical work flow of fluids through a capillary and how different capillaries can affect the flow rates.

Viscosity is one of the key properties of a fluid and the Reynolds number represents a fluids viscosity. A fluid's viscosity is an important parameter as it represents the property of a fluid which resists the force making the fluid flow. For instance, when two fluids are next to one another they do not necessarily mix. Transportation within the surface molecules and the fluid molecules are then transported through diffusion. Funada and Joseph (2002) state that is important to have an understanding about how a fluid's viscosity related to diffusion as they can affect the phenomenon of capillarity.

2.7.5 Capillary flow and contact angles

Young (2004) forms a model of the interface progression in a non-uniform capillary based on analysis of the Lucas–Washburn equation.

Young (2004) demonstrates the effect that capillary geometry has on the progress of the interface. A solution of the time required for interface advancement without gravity in a non-uniform capillary was developed using theory based on the Lucas-Washburn equation. It was discovered that for capillary advancement along horizontal pipes without gravity, the wetting time was found to depend on some parameter of the capillary geometry. This model developed by Young (2004) is used in chapter five as the theory is used to model the experiments presented in chapter 3.

Bahramian and Danesh. (2004) explore how to predict the solid-vapour and solid-liquid interfacial tension with the use of a numerical model. The necessary parameters for this to be possible are the liquid critical temperature and volume, the solid melting temperature and the volume of liquid and solid compounds. The results were produced each evaluating the solid-fluid interfacial tension values to predict the contact angle of the liquid drop on the solid surface. This was done with the use of Young's equations (2004). Bahramian and Danesh (2004) were successful in the prediction of the contact angles along side their experimental data proving that their models are accurate and reliable. The contact angles were measured by a microscope image of a droplet on a plate and the angle subsequently recorded. This is a good method and is later shown to be developed in chapter 5 where a discussion on contact angles is presented.

The theory behind their work shows that the difference in solid–liquid and solid–vapour tension has a close relationship with the liquid's surface tensions, viscosity and the contact angle between the liquid drop and the surface, shown in figure 7.

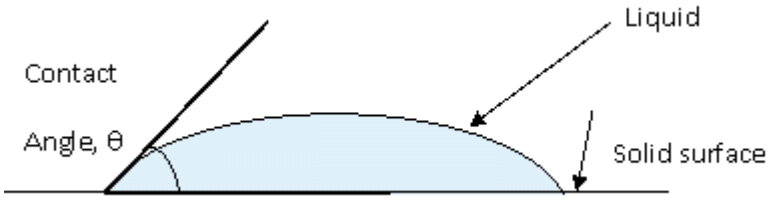

Figure 7: Fluid on solid planar surface

As all of these parameters are either known, or measureable so therefore with different fluids and the contact angles measured, these values can be used in the model to determine the solid-fluid and solid-vapour interfacial tension.

Bahramian and Danesh (2004) successfully predicted, via experimental work and numerical models, the contact angles to predict the interfacial tension. Although their work was successful, it does not verify interfacial tension. Therefore highlights an area of research that could involving different fluids to predict contact angles for certain fluids to be furthered.

Behaviour of fluids at an infinitely small scale has been an interest throughout history of science and microfluidics is an area where this concept is investigated. Behaviour of fluids at a large (marco) scale is different to the behaviour of a fluid at a smaller scale as surface tension, energy dissipation and fluidic resistance start to dominate the system. The studies that have been completed on microfluidics look at how behaviours change at this small scale and how they can addressed, or eliminated for new uses. (Roels et al. 2003)

The work completed by Roels et al. therefore relates to capillarity as it is important to have an understanding of how fluids behave at certain scales. The capillaries used in this thesis range from 0.094 to 1.170mm so parameters like surface tension do need to be taken into consideration.

Stevens et al. (2009) have completed a model where a uniform capillary acts as a porous medium. Their model is shown in figure 8 by where it is evident that a framework has been completed to determine the contact angles. A bed of packed particles has been submerged in a specific fluid and a corresponding model for a capillary has been established alongside the contact angle, θ. This has been measured using an accurate scale.

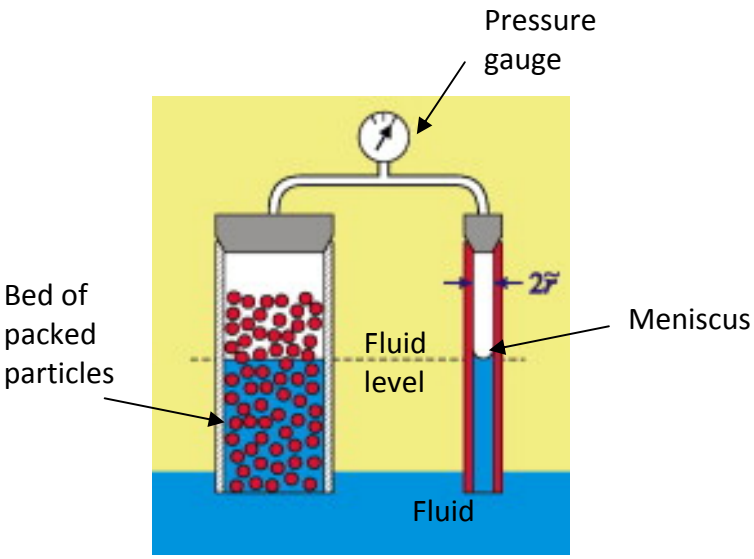

Figure 8: Image of experimental set up to determine contact angle of liquid-solid interface

The value of the contact angle, cosθ is determined by the intermolecular interactions of the interfacial tensions. In the capillary the liquid interface is considered to be approximately spherical and the capillary pressure can be calculated with the formula in equation 2.3.

$$\Delta P = \frac{2\gamma}{R} = \frac{2\gamma}{r}\cos\theta \qquad (2.3)$$

Where R is the radius of interfacial curvature and r is the radius of the capillary. The contact angles were measured for various fluids and this was done with capillary pressure measurements. Stevens et al. (2009) conclude that the particle shape has a large influence on the contact angles measured.

Hanzic et al. (2010) state that it is hard to determine the difference of the contact angle between the fluid and the concrete wall. It is also shown that at a nano-scale the contact angle changes so much more when it is in contact with the capillary wall. This is due to the roughness of the wall.

2.7.6 Capillarity and cementitious materials

Gospodinov (2005) looks at the phenomenon of diffusion and in this case diffusion of sulphate ions into cementitious materials. The other areas also looked at in detail are microcapillary filling and the following liquid push out of capillaries. He created a numerical model and looked at an in-depth view of ion diffusion through cementitious materials. He then compared the results with experimental observations of corrosion processes in concrete. Experimental work and numerical studies explored by Gospodinov (2005) include the diffusion of ions in saturated and nonsaturated concrete systems. Studies were also completed on the effects of environments that are particularly aggressive and contain large quantities of ions that degrade cementitious materials. The conclusions drawn through the experimental work conclude that the movement of the ions throughout the concrete matrix can only flow in the liquid phase. Therefore the movement of ions through a concrete matrix move due to diffusion. Tests that identify migration and diffusion of ions through concrete were also conducted; these were used to provide an estimation of the diffusion coefficients of the cementitious materials used. From the results and simulations discussed in Gospodinov's work, real transfer conditions of ions through a cement matrix could be simulated. The numerical algorithm looked at solutions to differential equations to simulate liquid push out by where ions are removed from one pore to another in situations in structures.

Lepech and Li (2009) researched the water permeability of high performance fibre-reinforced cementitious composites of HPFRCC. Again, experimental work was undertaken and compared with a numerical model. As the specimens of HPFRCC undergo tensile deformation cracks are formed. Microcracking was the key area of observation as the authors did not want the micro cracks to develop into larger cracks.

The micro-cracks formed were in the region of approximately 60 μm in width. The cracks were then saturated in a chloride ion solution and using micromechanics the theoretical basis for tailoring materials for tight crack width and correspondingly low permeability was established. Tests were then used after to determine if the new materials HPFRCC could maintain tight crack widths under tensile strain. Lepech and Li (2009) were successful in that they established models and results for flow in micro-cracks of HPFRCC concrete, however they only examined one crack aperture and their work may have been improved by looking at a larger range of crack apertures.

A study by Hoffman (2009) focussed on capillary flow and looked directly at experimental and numerical studies of capillary flow simulated through a number of experimental methods that analysed different capillary rise heights with respect to different crack apertures. The general trend in the readings showed that as crack aperture increased over a time period of three minutes the final rise height decreased. The theory behind this phenomenon is due to the surface tension and viscosity parameters relating to the equation governing capillary action which is explained in depth in chapter 5 of this thesis.

A limitation of this work is that the author only looked at fluid flow in cracks at a period of time greater than 10 seconds. This thesis takes a step forward and looks at the crack aperture with respect to rise height within 6 seconds and flow is captured using high-speed cameras.

2.7.7 Kinetics of capillary absorption

Fluid flow through a cement matrix occurs in voids. This happens as diffusion, suction and capillary absorption force the fluid through the matrix. Diffusion and suction happens while there is a change in the pressure gradient of gas and fluids. Capillary flow and absorption is different as it is altered by surface tension and surface tension changes depending on the fluid used or the surface with which it is in contact.

Hanzic et al. (2010) explore the kinetics of capillary absorption; this is done by creating experiments to find a capillary coefficient for a concrete matrix. Transport of liquids in porous media such as concrete takes place in open pores mainly due to diffusion, suction and capillary absorption.

With the use of calculated capillary coefficients through experimental work; the flow and kinetics of fluids through cement matrices was studied in depth. Studies completed by Hanzic et al. (2010) used ethylene glycol to look in depth at concrete matrix porosity and liquid viscosity. Ethylene-glycol is the fluid chosen to complete the experimental work as it is a fluid which does not react with cement gel. Hence, the flow of fluid can be modelled using Neutron radiography, and their results demonstrated capillary flow through cementitious materials. For the determination of capillarity with the use of neutron radiography the height of the liquid front was measured in three vertical profiles either by measuring the distance directly on the digital neutronograph.

The experiments were completed to study reasoning for capillary flow of water through concrete with use of the Lucas- Washburn equation. Hanzic et al. (2010) show that the Lucas-Washburn equation is only valid for up to 25 hours. This implicates that swelling and rehydration within the cement-matrix is not a valid reason for deviation of the capillary coefficient in the concrete-water experimental work. Therefore this experiment is not suitable for long term applications, greater than 25 hours.
Through experimental work Hanzic et al. (2010) concluded many reasons behind capillary flow:

- Diffusion through the cement matrix is very low and is found to be a rare phenomenon in this case. This was found from their work on neutron radiography and it is shown by movement of the molecules.
- Suction shows that liquid is represented by its viscosity, it occurs in larger pores.

Capillary absorption occurs in small pores as well as larger pores, however the experimental studies focused on those in the range from 10 nm–10 µm. In this range of size, the forces arising from surface tension are in the same range as gravity forces present in the liquid and therefore the phenomenon of capillarity is not as prominent.

2.8 Self healing cementitious materials

Self healing is of particular interest in this study as flow properties and capillarity play a large part in the area of the ability of concrete to self-repair. There are two main categories of self healing, autogenic healing and autonomic healing. These are discussed in more depth below.

2.8.1 Definitions

Below the different types of self healing materials are discussed and how they play a part in cementitious materials.

2.8.1.1 What are smart self healing materials?

"Smart structures are engineered composites of conventional materials, which exhibit sending and actuation properties, due to the properties of the individual components." (Joseph et al. 2010)

2.8.1.2 Autogenous self healing

Autogeneous healing is the natural ability of concrete to self repair. There are three primary mechanisms of autogenic healing. These are as the following.

- When a specimen is rehydrated, the water can react with unhydrated cement in the concrete matrix and repair any cracking.
- Movement of fragments in water
- Precipitation of calcium carbonates

2.8.1.3. Autonomic self healing

Autonomic healing is where the cementitious material, whether it is either a beam, slab or any other concrete composite, has been manufactured to have the ability to self heal.

The most common healing agents that are used for autonomic healing are epoxy resins, cyanoacrylates and alkali-silica solutions.

2.8.2 Autogenic healing studies

Recently, concrete has been discussed in further detail in many articles of progression of the phenomenon of self-healing concrete. McAlpine (2010) debates the differences between the phenomenon of self-healing concrete and the production of calcite with the use of bacteria. Previously stated, concrete is susceptible to deterioration and Jonkers (2010) of Delft University of Technology in Delft, the Netherlands, summarizes the key problematic area "Water is the culprit for concrete because it enters the cracks and it brings aggressive chemicals with it.” A key issue is that it seeps through the cement matrix and corrodes the steel.

A conclusion between the scientists was that they should be able to locate, and to some form ‘seal’ the crack. Jonkers (2010), believes that healing concrete should and potentially can be done by using water flow as the start and by packing the concrete with bacteria that use water and calcium lactate "food" to make calcite, natural cement.

However, concrete has a very alkaline pH of around 10 and might be higher. Calcite producing organisms cannot survive in this alkalinity. Jonkers and colleagues discovered natural bacteria known by Bacillus present in soda lakes in Russia and Egypt. Another interesting fact is that these bacteria, Bacillus, can survive without any

food and spore for long periods of time, up to 50 years long. The significance of these bacteria is that if its by-products can spore for long periods of time and are used in healing mechanisms these will last for long periods of time.

Their experimental work consisted of producing ceramic pellets ranging from 2 to 4 millimetres in diameter, and adding them to the concrete mix. Preventing the bacteria from activating in the mixture was seen to be challenging. This was because they wanted for the spores to only produce calcite when opened by microcracking in the concrete.

When cracking occurs in the concrete, the pellets open and water seeps inside the cracks. As this occurs, the bacteria feed off of the water and the embedded nutrients and produce calcite and carbon dioxide. Calcite is pure limestone so essentially this by product heals the cracks.

In 1983 Hannant and Keer (1983) discovered the ability of autogenous healing of thin cement based sheets. Natural weathering was examined on pre-cracked fibre reinforced mortar. Weathering on specimens was examined for a period of up to two years. Results showed that cracks will heal sufficiently under natural weathering but the healed cracks are unable to carry high tensile stresses.

Hannant and Keer (1983) did not look into autogenous healing of large crack widths, therefore there is a lack in their data which should be addressed in the future.

Van Tittelboom et al. (2010) come up with a more environmentally friendly method to help towards self healing cementitious materials. They use a biological repair technique; Ureolytic bacteria such as Bacillus sphaericus can precipitate $CaCO_3$ in their micro environment by conversion of urea into ammonium and carbonate. The precipitated crystals produced by the bacteria can fill the cracks produced in a concrete matrix.

Through experimental work the analysis showed that this type of bacteria was able to precipitate $CaCO_3$ crystals in the matrix to fill up and voids or created capillaries. However, although Van Tittelboom et al. (2010) reported some success in their findings the results did not reflect any work on durability or serviceability of structures with the bacteria in concrete.

Jefferson et al. (2010) research into the smart self healing field by looking at the potential for a crack closure system with the use of shrinkable polymer tendons. Their experimental work includes unbonded pre-oriented polymer tendons in cementitious beams. The tendons are activated through an increase in temperature after the cement based material has undergone initial curing.

The system is demonstrated with the use of a series of small scale experiments of pre-cracked mortar specimens. Results show that upon thermal activation of the tendons, the tendon completely closes the macro-cracks. Therefore this system is successful in its ability to enhance autogenous healing and improve structural durability.

Qian et al. (2009) look at the self healing behaviour of cementitious materials using blast furnace slag and limestone powder to determine what effect they have on the recovery of a specimen's deflection capacity. Four point bending tests were used to crack the beam at 28 days. Results showed that beams submerged to water healing recovered strength in the region of 65-105% which is much higher than those healed in air.

The work completed by Qian et al. (2009) has furthered research in that their work can potentially reduce or even eliminate the maintenance of civil infrastructure.

2.8.3 Autonomic healing studies

Li et al. (1998) initiated the feasibility of smart healing in cementitious materials. The smart materials in their work include the sensors and actuators in the form of controlled micro cracks and hollow glass fibres carrying air-curing chemicals.

One self-healing concept is to release chemicals which seal the tensile cracks, followed by air curing of the released chemicals in the cracks, leading to regaining the mechanical properties of the uncracked composite. The experiments conducted in the studies look at controlled micro-cracking. Afterward, the effectiveness of the self healing is confirmed by the elastic modulus of the composite after it undergoes self-healing with the use of air curing chemicals. Li et al. (1998) produced encouraging results as they showed that after the first loading cycle the composites regain their strength and return to their original elastic modulus. Studies looked at by Li et al. include those that look at sealing/healing chemicals contained in hollow brittle glass fibers and this work was furthered by Joseph et al. (2010)

Joseph et al. (2010) state that there are definite properties that a self-healing flow agent must possess. One of these is that it is necessary to have a low viscosity to ensure a wider repair area and a sufficiently strong bond between crack surfaces and that there should be adequate capillary forces to draw the agent into the crack. Later work by Joseph et al. (2010) examined in more detail studies on self healing of mortar beams.

Figure 9 shows the concept that has been addressed through the work of Joseph et al. (2010) and the process of capillary action that occurs through cracks induced in cementitious materials via 3 point bend tests.

Cyanoacrylates that come into contact with moisture react and cure very rapidly forming a bond often stronger than the material it is bonding, i.e. concrete. Figure 9 again shows the developed system by Joseph who shows that if a system is damaged and healed and then damaged again, a new crack will form around the healed crack.

Their work directly relates to the studies undertaken in this thesis. This is a successful model for autonomic healing, and depending on the different types of crack propagations and fluids, models and experiments have been completed to relate to determine the length of time it takes for the fluid to fill up the crack or capillary.

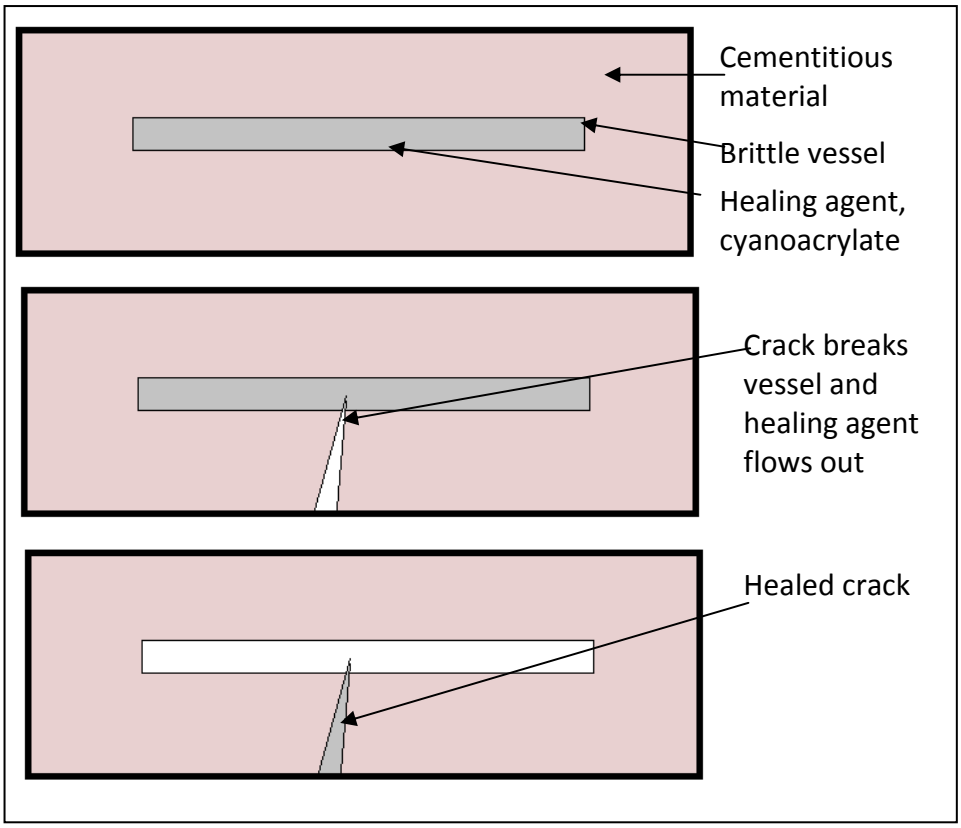

Figure 9: Autonomic healing concept for cyanoacrylate adapted from Joseph et al. (2010)

2.9 Final literature summary

It has been identified through the literature that there are numerous studies on flow of moisture and water through diffuse (networks) of cracks in concrete. Whilst these contribute to the deterioration processes in concrete and will determine the flow of healing agents away from damage locations it is the capillary flow in a discrete crack that is of most importance in self healing materials and this has received significantly less attention in the literature.

Therefore, having gained an understanding of literature presented on capillarity in other research areas, it will be possible to apply this to the novel research area of self-healing cementitious materials in order to understand the process of capillary flow and how effective these new materials may be in healing cracks which if left unattended may compromise structural integrity. This is a novel and exciting element to this field of research that has not been previously explored.

Chapter 3

Experimental Procedure

3.1 Introduction

Self-healing and capillary flow through cementitious materials are two key areas that can be combined together to provide an in-depth investigation of the potential for self-healing in concrete. The investigations conducted in this thesis assess how fluid flow through capillaries, in the form of discrete cracks, can influence the rate at which self-healing may occur in cementitious materials. Glass capillaries have been previously used in research to determine properties of capillary flow (Zhmud et al. 2000) and are used in this experiment to compare capillary flow in glass to capillary flow in manufactured mortar capillaries. Many variables including, but not limited to, the characteristics of the capillary surface and the nature of the fluid need to be considered such that a rigorous experimental procedure can be completed.

The experimental work undertaken in this thesis uses mortar specimens and fluids with varying viscosities in order to examine the effect of different crack/capillaries on the rate and level of capillary rise height. Coarse aggregates were not used in these experiments as it was necessary to omit the effect of the absorption of fluids by the coarse aggregate during capillary rise. Moreover, it is assumed that cracks originate at the aggregate-mortar interface and propagate through the mortar matrix and therefore it is the flow properties of the mortar phase alone that are of most interest.

3.2 Materials

The cement used in this study was CEMII/B-V32,5R supplied by Lafarge and manufactured to conform to BS EN 197-1:2000. The fine aggregate component of the mix consisted of sea-dredged sand from the Bristol Channel, conforming to BS EN 12620:2002. The fine aggregate was air-dried for 24 hours before use. Particle size distribution tests according to BS EN 933-1:1997 were performed to establish the gradation of the sand. The sand was placed in an oven at 110°C ± 1°C for two hours prior to sieving. The sample size selected was 600g on the basis of the maximum particle size of the aggregate being 4mm (BS EN 12620:2002). The results from the test can be seen in Table 1.

The results shown in table 1 demonstrate the size of the particles being used in the mortar specimens. This is necessary to know as later when experimental results are being discussed in chapter 4, the particle size could affect overall capillary flow and could potentially interfere with the surfaces of the capillaries used.

Table 1: Calculation of sand grading for dry sieving

Sieve aperture size (mm)	**Mass of material retained (g)**	**Percentage of material retained (%)**	**Cumulative percentage passing (%)**	**Cumulative percentage retained (%)**
8	0	0	100.00	0.00
4	48.50	8.08	91.92	8.08
2	57.00	9.50	82.42	17.58
1	63.50	10.58	71.84	28.18
0.250	422.50	70.42	1.42	98.58
0.063	8.50	1.42	0.00	100.00
TOTAL	**600.00**	**100.00**	**-**	**-**

The mix proportions were selected on the basis of a standard mortar mix used in previous laboratory work. The composition of the mix was 540kg/m^3: 1618kg/m^3: 242kg/m^3 (cement:sand:water). The resulting mortar had an average compressive strength of 36.7 N/mm^2 and was used in each experiment.

3.3 Specimen manufacture

3.3.1 Specimen numbers and form

Twelve prisms of dimensions 255mm x 75mm x 75mm were cast for each crack configuration experiment. It was decided that this number of specimens would allow 11 different crack apertures to be explored and enable sufficient specimens to be cut from each prism to allow repeat tests to be conducted. Seven to eight pairs of specimens (a pair comprised Specimen 1 and Specimen 2 as shown in table 2) for the tests were taken from each prism cast. The specimen designation was selected depending on the age (old or young), crack configuration (planar, tapered, tortuous and natural), flow agent (water or cyanoacrylate) and wire thickness in the range shown in table 2 for each of the experiments.

Table 2: Specimen referencing and form

Experiment	Specimen 1	Specimen 2	Range of crack apertures (mm)
Old, planar, water & cyanoacrylate	1a-36a	1b-36b	0.094-1.170
Old, tapered, water & cyanoacrylate	2a-22a	2b-22b	0.094-1.170
Old, tortuous, water & cyanoacrylate	t1a-t28a	t1b-t28b	0.094-0.714
Old, natural, water, with reinforcement	t1-t14	N/A	0.094-1.170
Old, natural, water, without reinforcement	t1a-t14a	t1b-t14b	0.094-1.170

The video files, providing the full fluid flow history through the various crack configurations have been named in a similar manner and are provided on the CD-ROM accompanying this thesis. Typically 3 tests were performed for each crack width for all crack configurations, specimen ages and degrees of saturation. An exact breakdown of the number of specimens tested is provided in Appendix A.

3.4 Casting

3.4.1 Mix procedure

As previously mentioned the mix proportions were kept consistent throughout all of experiments to ensure that the specimens all had a similar composition. The constituent materials were weighed, in buckets to an accuracy of 0.05kg. The dry materials were mixed together for approximately five minutes in a Cumflow horizontal pan mixer with a capacity of approximately 250kg. The water was then added to the pan in three stages using a visual inspection of the mix to achieve a suitable workability. Once fully mixed the mixture was then placed into the moulds.

The moulds were filled in thirds. After each third was added the moulds were vibrated for 30 seconds. This process was repeated for the remaining two thirds of the moulds. Once all of the mortar was placed in the moulds, the tops were leveled using a pallet knife.

3.4.2 Specimen curing

Two curing procedures were used to obtain old and young specimens and these are described in more detail in the following sections.

3.4.2.1 Curing procedure for old specimens

After casting the specimens were left for 24 hours before being demoulded. They were then wrapped in damp hessian for 14 days and covered in plastic so the moisture content was kept constant. Every two days the hessian was re-soaked to prevent the

specimens from drying out. After the specimens had been cured under hessian for 14 days they were then left to cure in air in general lab conditions at a temperature of 21˚C for a further 14 days. After this time the specimens were wet cut using a circular concrete cutting saw. Each prism of dimension 255mm x 75mm x 75mm yielded 8 pairs of specimens, each specimen of dimensions 30mm x 30 mm x 75mm. During this time the specimens were likely to have absorbed water from the cutting process, which may have had an impact on the measured capillary rises and therefore the specimens were left uncovered for a week at 21˚C in general lab conditions such that they could return to their pre-cut condition. The actual age of the specimens at the time of testing was therefore 35 days. The surface finish of the sawn face of the specimens was particularly rough and therefore to ensure the two specimens met uniformly the sawn surfaces were lightly filed.

3.4.2.2 Curing procedure for young specimens

After casting the specimens were left for 24 hours before being demoulded. However, upon demoulding the specimens were still 'soft' and were unable to be cut. After an additional 24 hours they were sufficiently hard to enable them to be wet cut using a circular concrete cutting saw. Similarly to the old specimens each prism of dimension 255mm x 75mm x 75mm yielded 8 pairs of specimens. The sawn faces of the specimens were again lightly filed prior to experimentation to remove the rough surfaces. These specimens were then left to cure in air at 21˚C in general lab conditions until the time of experimentation (maximum 5 days of air curing). The resulting ages of the young specimens at the time of experimentation ranged between 4-7 days old.

3.4.2.3 Saturation of specimens

Specimens designated old were soaked in water for a week prior to testing (between the ages of 28 and 35 days). This gave the specimens sufficient time to become fully saturated.

3.5 Crack configurations and apertures

Four crack configurations have been used in this study and their form and method of manufacture is discussed in more detail below. In summary the four crack configurations include planar, tapered, tortuous and natural cracks. A range of crack apertures were achieved with short lengths of steel, nickel or tin wires with diameters varying from 0.094 – 1.214 mm. The diameters of the wires were measured using a vernier caliper over various positions along a piece of the wire. The apertures created were then measured with a portable crack width microscope and the actual crack aperture recorded.

3.5.1. Planar and tapered cracks

The planar and tapered experiments use both old and young specimens. For the planar tests wires of a constant diameter were placed between the two specimens at the bottom, middle and top of the specimens, as indicated in figure 10a. For the tapered experiments wires were placed at the bottom and the top of the specimens only, with the wire at the top of the specimen having a smaller diameter than the wire at the base of the specimen, as shown in figure 10b. The ensemble was then clamped together to keep the wires in place.

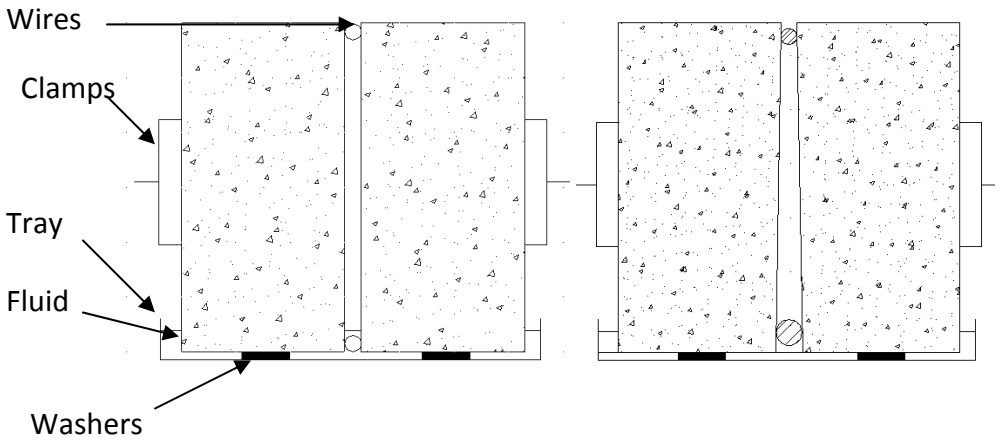

Figure 10: A Schematic representation of a) planar and b) tapered crack configuration

3.5.2 Tortuous crack investigation

Tortuous cracks were created with the use of 2mm folded steel plates. These plates were manufactured so that angle of the flow path deviated from the vertical by ± 5° Tortuous cracks with 2 flow path angles (3 nodes) and 4 flow path angles (5 nodes) were created, as shown in figure 11 a and b respectively. Prior to casting, the plates were covered in demoulding oil to ensure that they would not bond to the mortar. They were then manually held in place during casting. The same mixing and casting procedure was used as described in section 3.4.1.

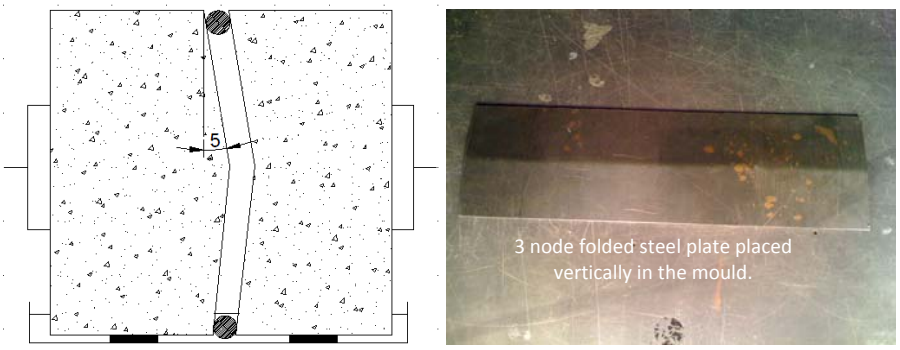

(a)

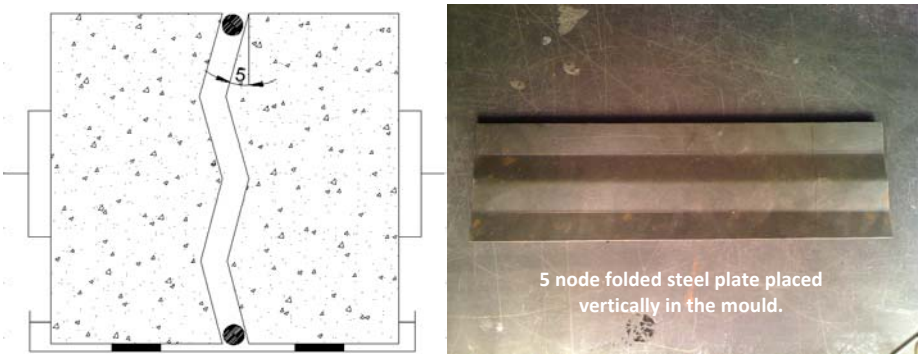

(b)

Figure 11: Tapered crack of a) 3 nodes and b) 5 nodes achieved using folded steel plates

Upon demoulding and removal of the steel plates, the surfaces in contact with the mould oil were wiped thoroughly with acetone to ensure that no oil was left on the surface to influence capillary flow measurements. Wires of constant diameter, over a

range of wire diameters, were then used to obtain tortuous cracks of uniform aperture.

3.5.3 Natural crack configuration

Specimens with naturally formed crack surfaces were manufactured from prisms loaded in three-point bending as shown in figure 12a. In order to control the rate of crack opening 14 prisms were cast with a 3mm diameter reinforcing bar. The prisms were notched with a 5mm notch prior to testing such that cracking was initiated in the centre of the specimen and to encourage a near vertical crack path. This was important to achieve as this would allow capillary flow through planar specimens with naturally cracked surfaces to be compared to planar specimens with smooth surfaces with similar crack orientations. Once the prisms were fully cracked a pair of specimens was then cut from the central portion of each prism as indicated in figure 12 b.

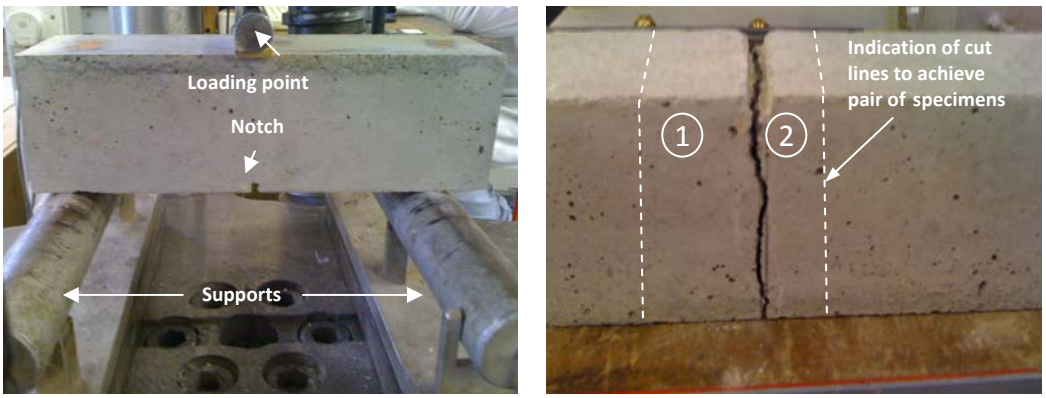

Figure 12: Manufacture of naturally cracked specimens a) Three point bend test arrangement b) Extraction of specimens from cracked zone of prism

A variety of crack apertures were achieved following the procedure outlined for planar specimens.

3.6 Flow agents

3.6.1 Water and Cyanoacrylate

Two types of fluid were used as flow agents in the experiments, the physical parameters of which are given in table 3. The first fluid was tap water at room temperature (21°C). The second fluid was a low viscosity, single agent, cyanoacrylate adhesive (PC20 supplied by Cyanotech Ltd.) The data sheet for the cyanoacrylate is supplied in Appendix B. The capillary flow of cyanoacrylate is particularly relevant as it has been successfully used by Joseph et al. (2010) in a number of self healing studies performed in the same laboratory.

Glass capillary tubes of known diameter were used to calculate the viscosity of the cyanoacrylate in the experiments. Images of the contact angle between the meniscus and the wall of the capillary tube were captured using a portable crack width microscope and digital camera and together with the level of capillary rise height observed and the density of the cyanoacrylate, the viscosity could be calculated. However, the viscosity of cyanoacrylate changes over time when in normal atmospheric conditions. Therefore, measurements of the change in viscosity have been recorded.

Table 3: Physical properties of flow agents used in the experimental work

Fluid	**Viscosity (Ns/m^2)**	**Surface Tension (N/m)**	**Density (kg/m^3)**
Water	0.892	0.0728	1000
Cyanoacrylate	Varies see calculation Chapter 5	0.0334	1060

Silica fume/water slurry in a 50:50 mix by mass was considered as a flow agent, but was dismissed during the early stages of the experimental programme due to difficulties in achieving capillary flow with the silica fume in small capillaries.

3.6.2 Xanthan gum

In order to investigate the capillary flow time of a fluid with a viscosity equal to that of cyanoacrylate without the 'curing effect', xanthan gum was used. Xanthan gum is a biological additive that can be added to fluids to increase their viscosity. Xanthan gum is a unique substance commonly found in food, cosmetic and industrial additives. It is a polysaccharide, a carbohydrate and is usually produced by fermentation process. During fermentation, a strain of bacteria (Xanthomonas campestris) is added to glucose or sucrose (i.e. corn sugar) which turns them into a gum. Different concentrations of xanthan gum in water were used to obtain a fluid of equivalent viscosity (i.e. with the same rise height) as that of cyanoacrylate. The amount of Xanthan gum used in the experiments was calculated as 0.016g per 100ml of water.

It must be noted that rise height depends on equation 5.1 in Chapter 5. Therefore adding the equivalent xanthan gum means that there is the same combined surface tension and contact angle term but not necessarily the same viscosity.

3.7 Experimental details

3.7.1 Data capturing technique

High-speed video cameras have been an excellent tool for capturing a moving process at an accelerated rate. High speed cameras are used to look at capturing process control, process engineering and other small areas of research. Motioneer high-speed video cameras that have been selected for these particular experiments and can record up to 32,000 frames a second. This method allowed the rise height of the fluid through the crack to be recorded and then replayed at a slower rate for data processing purposes.

In order to capture the full rise height of the fluid the experiments were recorded at 250 frames per second. This was chosen after preliminary testing using the cameras to determine an appropriate frame rate for this particular experimental arrangement. The previous work performed by the author presented in the literature review informs the reader that a shortcoming in the experimentation was that capillary flow had only been recorded at one final height at a time at three minutes. The use of the high-speed video cameras enabled the full flow history of the fluid in the capillary to be recorded accurate rise height with time measurements to be obtained.

A scaled piece of laminated graph paper was used as the measurement tool for looking at the overall capillary rise height within the specimen. This method allows rise height to an accuracy of 0.5mm to be measured. The rise height with respect to the rise time was then obtained. Capillary flow was measured over a total time of 16 seconds which includes the addition of the flow agent to the container where the specimens are placed.

3.7.2 Lighting

Lighting was required in order to gain clear visibility through the simulated cracks. Two spot lights were used to illuminate the front of the specimens so that the laminated scale could be seen on the camera, and two halogen lights, with adjustable intensity were placed directly behind the specimens to illuminate the crack. The larger the crack size, the less light was needed, therefore the lights behind the crack were adjusted in response to this. Lighting in the experimental work looking at natural cracks was a particular challenge due to the tortuosity of the crack in two dimensions and therefore there was difficulty in shining the light provided by the halogen lamp through the entire crack plane. The solution employed was to add fluorescein to the water and conduct the experiment in a darkened cabinet under an Ultra-Violet (UV) light. The UV light also provided sufficient light to illuminate the laminated scale. This set up can be seen in figure 13.

Figure 13: Image of natural crack experimental arrangement under UV lighting

3.7.3 Experimental arrangement

The experimental arrangement is shown in figure 14. Initially, each specimen was weighed and its weight recorded. The wires were then placed onto the specimens and then they were clamped together (as discussed previously). The clamped specimens were then placed into a tray of dimensions 12 x 125 x 125 mm on top of two washers. Washers were used to raise the specimens 1.38 mm above the base of the tray to ensure the fluid would be able to flow underneath the specimen and have access to the base of the capillary.

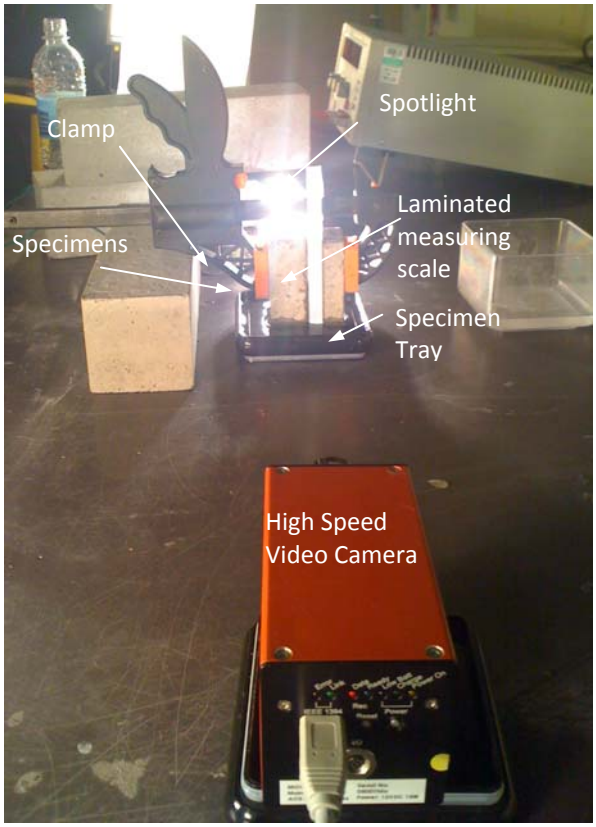

Figure 14: Experimental arrangement

The horizontal distance between the specimen and the camera was approximately 300-400 mm. This distance varied as a result of the focal range of the lens. Accurate measurements of rise height depended on the legibility of the scale and clarity of the meniscus position in the crack. For measurement of capillary flow on naturally cracked specimens the camera was placed inside the darkened cabinet with the specimens, maintaining the same horizontal spacing as stated above.

Once the experiment was set up the camera recording sequence was then triggered and a predetermined volume of fluid, as detailed in Table 4 was poured immediately into the tray. The volumes for the cyanoacrylate tests varied as it was a known fact that once cyanoacrylate is in contact with air, it starts to cure therefore it was difficult to establish exact cyanoacrylate quantities in the experiment. However, each volume of flow agent used was sufficient to allow for capillary flow.

Table 4: Quantities of fluid used in each experiment

Fluid	**Volume of fluid used (ml)**
Water	50
Cyanoacrylate	30-50
Xanthan gum	50

Once capillary rise had occurred recording was stopped and the specimens were immediately taken from the tray and each one weighed. This was to examine the quantity of fluid adsorbed into the mortar matrix during the experiment to determine whether this had an effect on the rate and level of capillary rise observed. By weighing them immediately, absorption of the fluid over the same timescale for all specimens was achieved.

3.7.4 Data processing

As there were a total of 16800 frames for each video clip, only the frames showing the movement of the fluid in the crack were retained. The end of capillary flow was taken as the point where no further rise height occurred with time. The reason for this is that it is the initial stages of capillary flow that are of importance, particularly in autonomic healing when there is a high potential for rapid hardening of the healing agents and therefore, even though there will be further capillary rise over time, it is the first few seconds that are of interest.

Chapter 4

Experimental Results and Discussions

This chapter considers the results from the experimental work undertaken in the laboratory. The experimental results can be considered in five distinct sections. These are the effect of crack aperture; effect of crack configuration; effect of flow agent; effect of specimen age and effect of specimen saturation on the capillary rise response of liquid flow in discrete cracks in cementitious materials. The results presented in each section are generally grouped and discussed in terms of crack configuration before further comparisons are made.

The majority of the experiments were performed in triplicate and therefore, due to the substantial quantity of data available, only the average result from the experiments has generally been selected and presented in this chapter. However, all results are given in Appendix C.

Due to the positioning of the spacers, the field of view of the camera and the tray covering 12mm of the base of the scale, the rise heights are only available from 12mm upwards and the time at which 12mm was observed was taken as zero. Therefore the time and rise heights indicated in the figures do not represent the full history of fluid flow. Therefore, when comparing results and looking at the rate of capillary rise it is important to recognise the adjustment that has been made. All data has been extracted from the experimental videos that can be found in Appendix D.

4.1 Effect of crack aperture

The effect of the crack aperture on the capillary rise response of water is presented in this section and is discussed for a planar crack configuration only. The capillary rise

response for flow in a planar crack aperture between 0.094mm up to 1.170 mm wide is given in figure 15.

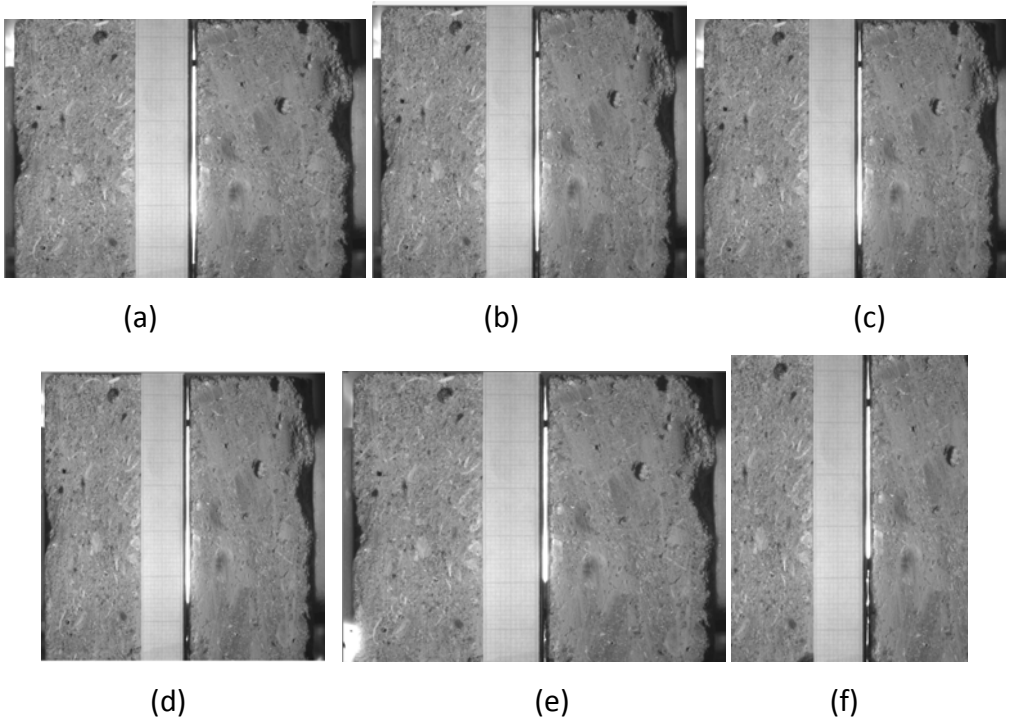

Figure 15: Capillary rise front for old planar water with a crack aperture of 0.502 mm a) 16mm at 0s b) 19mm at 0.036s c) 21mm at 0.072s d) 24mm at 0.160s e) 30mm at 0.716s f) 33.8mm at 5.600s

Figure 16 shows the rates of rise for an old planar water experiment for all crack apertures.

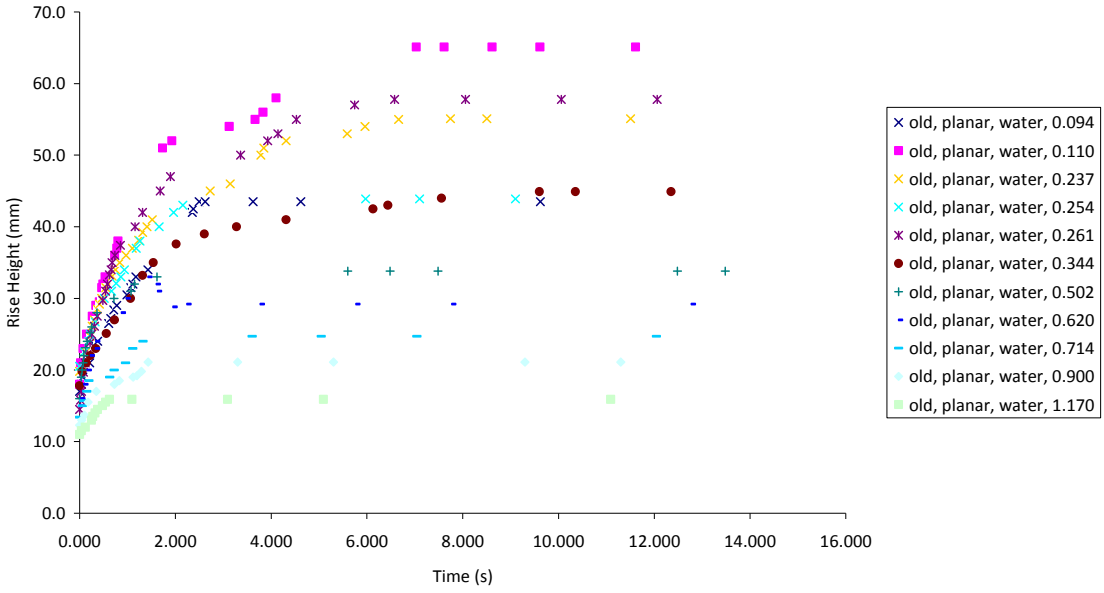

Figure 16: 35 day planar water experimental results

Although the equation of capillary flow potential is introduced in chapter 5, it is introduced here in order to support the experimental observations made.

$$h = \frac{2\gamma \cos\theta}{\rho g r} \tag{5.1}$$

Equation 5.1 is the equation of capillary flow potential where γ is the liquid-air surface tension in N/m, θ is the angle that the meniscus forms with crack/solid face in degrees, ρ is the density of liquid in kg/m^3, g is the force due to gravity acting on the fluid in the capillary in m/s^2, and r is radius of the capillary in mm.

The specimens under examination were in the laboratory dry state. It is apparent that for planar crack apertures greater than 0.237 mm the equilibrium capillary rise height is equal to that predicted from capillary flow theory (equation (5.1)) assuming an equilibrium contact angle of zero and surface tension of water of 0.0728 N/m.

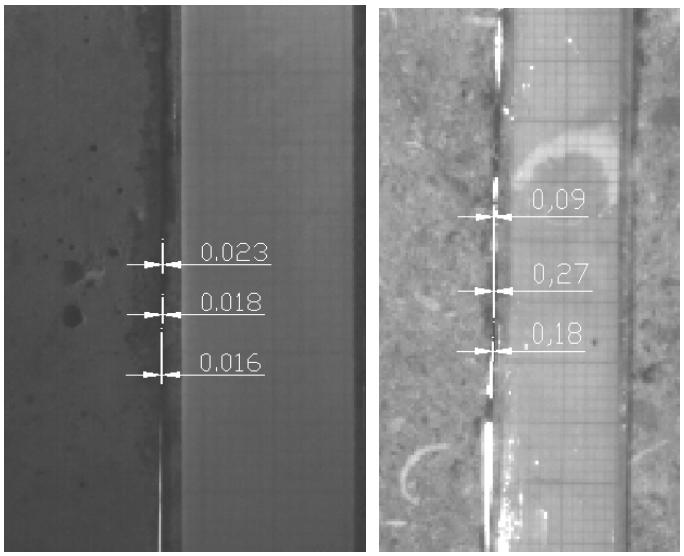

a) 0.094 mm b) 0.110mm

Figure 17: Measured Crack apertures for a crack aperture of a) 0.094mm and b) 0.110mm

For crack apertures smaller than 0.237mm the theoretical equilibrium capillary rise height was not reached in any of the experiments performed. One of the reasons for this may be attributed to the actual crack width being larger than that suggested by the thickness of the wire used. Figure 17 shows the actual crack apertures of the

experiment determined from a video image. It is shown in figure 17 that for an assumed crack aperture of 0.094 measurements of actual crack apertures range from 0.016mm to 0.023mm. This is due to variations of the mortar faces caused through the manufacture of the specimens and achieving a uniform clamping force over the height of the specimen. Although, this effect will be apparent in the majority of the tests it has a greater effect on the capillary rise heights in the narrower capillaries. This is why the final rise height is a lot lower than the expected rise height. Using the average value of rise height from the experiment and the equation of flow 5.1 the comparisons of rise height versus crack aperture can be made. These are presented towards the end of this section.

Another reason for the changes in final rise height differences could be attributed to the changes of the specimen weight due to absorption of fluid during the experiment. These values are given in Table 5. The table also gives an indication of the magnitude of variation observed in the experimental results.

Table 5: Changes in weight of 35 day planar water experiments

Crack aperture (mm)	**Weight increase of specimens (g)**			**Equilibrium rise heights (mm)**		
	Test #1	**Test #2**	**Test #3**	**Test #1**	**Test #2**	**Test #3**
0.094	2.0	1.5	2.5	35.0	43.5	40.5
0.237	2.5	3.0	3.5	30.0	55.1	65.0
0.261	2.0	2.5	2.5	16.0	57.8	57.8
0.620	1.5	1.5	2.0	24.0	29.2	30.5
1.170	1.0	1.0	2.0	20.9	15.9	14.5

As seen in the table above, the experiments with a lower equilibrium rise height have greater increases in weight indicating greater absorption of water into the matrix of the mortar specimen. As absorption occurs through the open pores in the cement matrix, fluid stays in the voids therefore increasing the overall weight of the specimen. It can be concluded that flow away from the main capillary channel into the cement

matrix retards flow in the main capillary. This is explained further in figure 18. The fluid flow through the specimens was observed over a few seconds where by the initial capillary rise height happened in a matter of seconds. The longer the time of recording of capillarity the more fluid absorption can be seen in to the cement matrix.

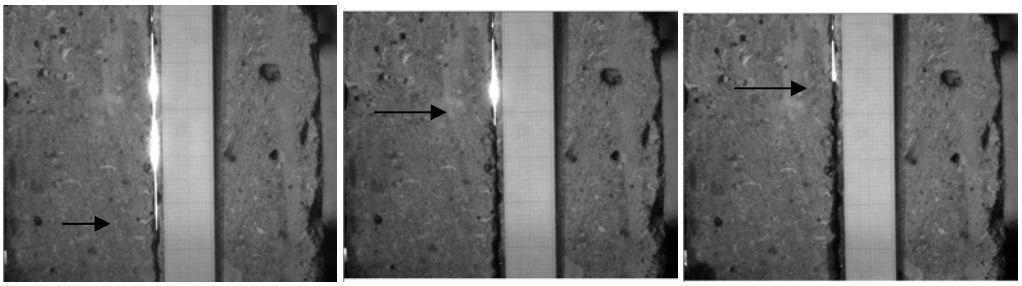

(a) (b) (c)

Figure 18: Difference in maximum rise heights and changes in weight of old planar water 0.261mm aperture over a period of 3 seconds showing fluid absorption into cement matrix

The arrows in figure 18 indicate the change in the fluid surface and therefore indicate fluid absorption. Although it is shown that over a period of time that the absorption into the cement matrix does increase it is also shown that the moisture content into the matrix retards behind the capillary fluid front throughout flow.

It is thought that the larger the change in weight of the specimen, (c) above in figure 18 means that there is a lower overall rise height. The capillary flow for (a) and (b) in figure 18 is over the same time scale. This happens as there are more voids in the concrete matrix available for the fluid to flow through, effectively giving an apparently wider aperture. With a higher amount of void space available, due to the capillary pore pressure the fluid flows into the voids, henceforth increasing the weight of the specimen and lowering the capillary rise heights.

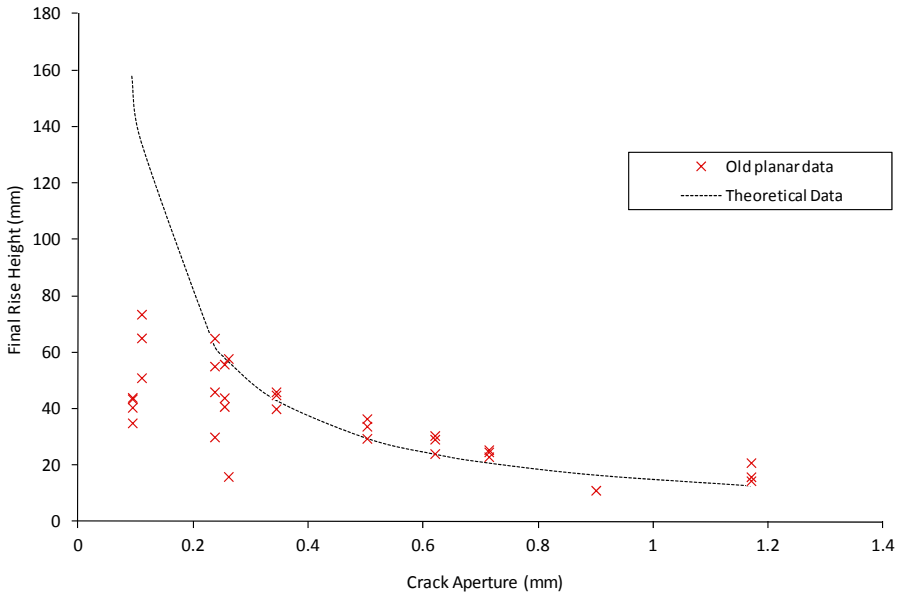

Figure 19: Comparison of planar crack aperture with final rise heights for 35 day old specimens

Previously, average results for each specimen have been presented to demonstrate the effect of crack width on the capillary rise response and the final rise height. In order to examine the variation between the tests performed at each crack aperture, the final rise height has been extracted for each experiment and is shown in figure 19 for each crack aperture.

At crack apertures greater than 0.344mm the variation in results for each crack aperture are reasonably consistent and show a lower overall spread than for crack apertures less than 0.344mm. This observation helps support the previous selection and discussion of the capillary rise response and final rise heights using only the average data points

The results presented in figure 19 confirm previous observations that the final rise height associated with the two smallest apertures are significantly lower than the theoretical final rise heights, calculated using equation 5.1. It is believed that this can be attributed to (i) the limiting effect of the specimen height (75mm); (ii) the difficulty in achieving small (less than 0.110mm) crack apertures with the methods used and (iii)

the protrusion of particles on the surface causing blockages of the flow path. At crack apertures greater than 0.261mm there is good agreement between the theoretical final rise heights and the experimental data. This gives confidence in not only the experimental procedures used but also in the surface tension, contact angle and density values assumed in the theoretical solution.

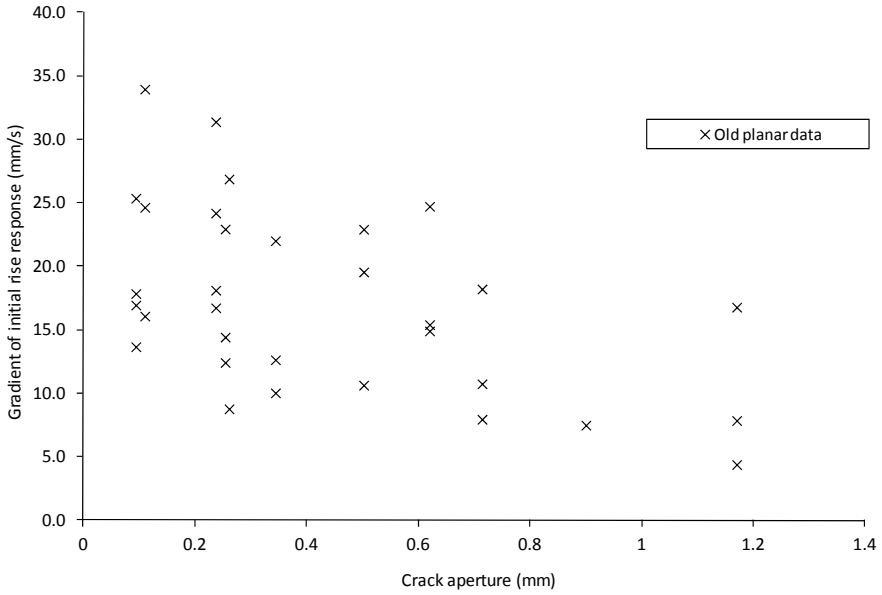

Figure 20: Gradient of the initial rise height over a period of 1 second for 35 day old planar specimens.

Figure 20 shows a large variation in the rates of initial rise. Whilst there is a general trend in the relationship between the velocity of the meniscus (gradient of the initial rise response) and the crack aperture it is contrary to what would be expected from theory, in that the larger apertures would have much higher meniscus velocities, reaching their final rise heights in much shorter times than the smaller apertures. This difference may have resulted from the difficulty in capturing the first 12 mm of capillary rise and therefore what is reported does not truly represent the initial stages of capillary rise. Additionally it has already been noted that there was some variation in the actual crack apertures used in the experiments which would also influence the magnitude of the variation in the results observed in figure 20. Finally, absorption of the fluid into the the matrix either side of the capillary will affect the rate of rise in the

main capillary channel, although without further measurement and interrogation of the video data this is difficult to quantify.

4.2 Effect of crack configuration

Five different crack configurations were examined as part of the experimental work in this thesis, these were planar; tapered; two types of tortuous cracks and natural cracks. This section looks at how a change in crack configuration affects capillary flow through cementitious materials.

The planar results have already been considered and analysed. Therefore, the next areas of investigation are tapered, tortuous 3 and 5 nodes and natural crack configurations.

Capillary flow has been examined for 35 day old tapered crack configurations. This type of crack configuration has been looked at experimentally and the observations have been recorded and discussed in detail below.

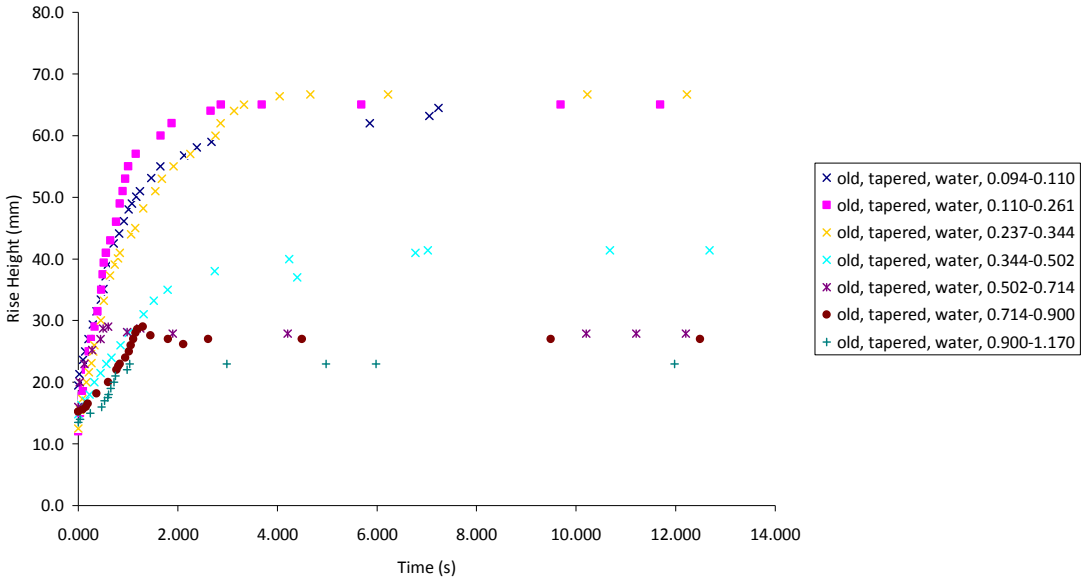

Figure 21: 35 day tapered water experimental graphs and results

Figure 21 shows that a steep gradient is shown for small crack widths of 0.094mm-0.110mm where as for 0.900mm-1.170mm a shallower gradient occurs. This goes against what is generally assumed, that the wider the crack aperture, the faster the initial rise height.

Table 6 shows using the rise heights from the experimental work and the planar crack aperture that would give the same equilibrium rise height.

Table 6: Calculation of crack apertures used in experimental work

Rise height in experimental work (mm)	**Crack aperture used in experimental work (mm)**	**Actual crack aperture using equation (5.1) (mm)**
41.4	0.344	0.301
27.9	0.502	0.523
27.0	0.714	0.541

Table 6 indicates that using equation 5.1 the actual crack aperture in experiments can be calculated. It is evident that it does vary from what the actual wire thickness was that was used in the experiments. Therefore, when analysing the data it is important to understand what the actual crack aperture to determine capillary flow was.

Experimental results and recordings have been discussed in this section on the effect of capillary flow in manufactured tortuous cracks. These were performed to simulate what would happen in a natural crack.

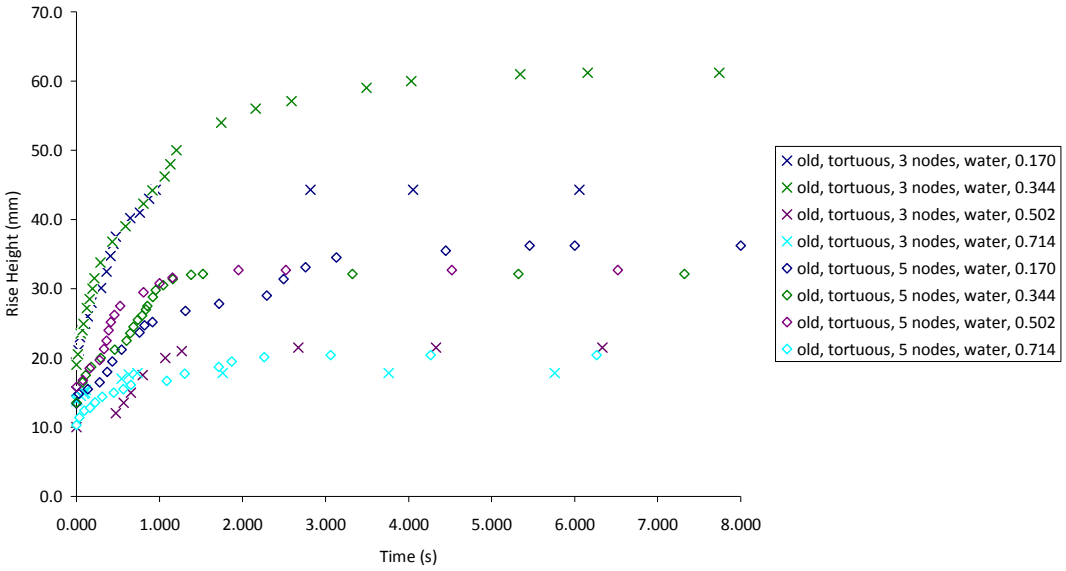

Figure 22: Effect of crack configuration, 35 day tortuous 3 nodes water and 35 day tortuous 5 nodes water

Figure 22 compares 3 & 5 nodes, old tortuous water experiments with different crack apertures. Looking at 3 & 5 nodes with a crack aperture of 0.170 mm, there is a slight difference in overall rise height. The overall rise height is affected due to the change in the nodal number, it can be seen that there is a lower rise height for a larger number of nodes. However, for the larger crack apertures the fluid does not get past the first nodal point. Therefore, for further experimentation spoken about in chapter six and an idea would be to increase the number of nodes to see what the effect of the change in angle would have on fluid flow. Also, it is clearly shown in the graph, that the higher the tortuosity of the specimens, the longer time it takes to reach maximum rise height. The fluid has further to travel to get to an absolute rise height in a tortuous crack. Change in inclination of the crack reduces the overall time for the fluid to reach equilibrium rise height. This is shown in the theory chapter 5.

Natural cracked specimens have been used to determine the rate of flow of fluids through cementitious materials representative of those found in current structures. The experimental results have been recorded below and discussed.

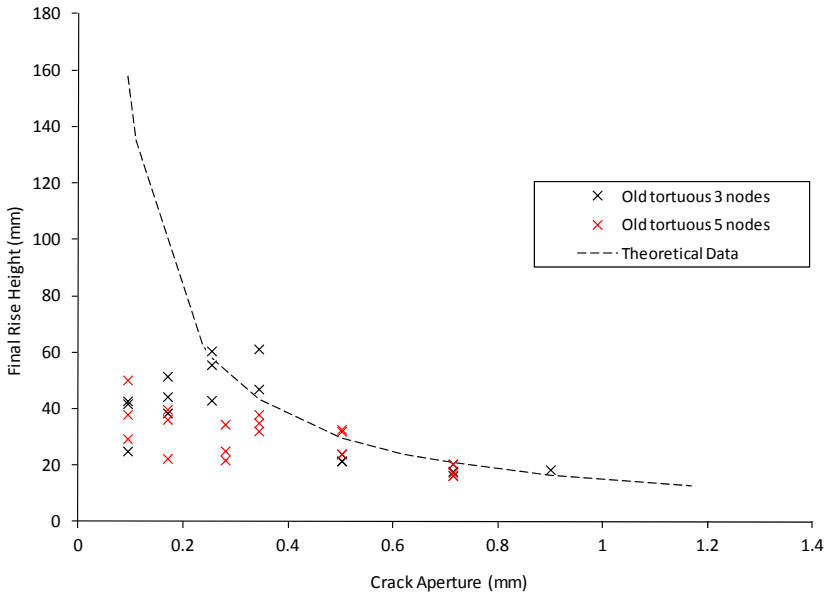

Figure 23: Comparison of tortuous crack aperture with final rise heights for 35 day old specimens

Similar to the planar crack aperture data shown previously in figure 19 at tortuous crack apertures greater than 0.344mm the final rise height results for each crack aperture are reasonably consistent with those calculated from theory, with the variation in the results decreasing with increasing crack aperture.

The results presented in figure 23 confirm previous observations that the final rise height associated with the two smallest apertures are significantly lower than the theoretical final rise heights, again confirming the difficulty in achieving small (less than 0.110mm) crack apertures with the methods used. Moreover, figure 23 shows that there is little difference in the results between the 3 and the 5 node specimens, confirming the theory that regardless of crack inclination the fluid will always reach the same absolute rise height for the same crack aperture.

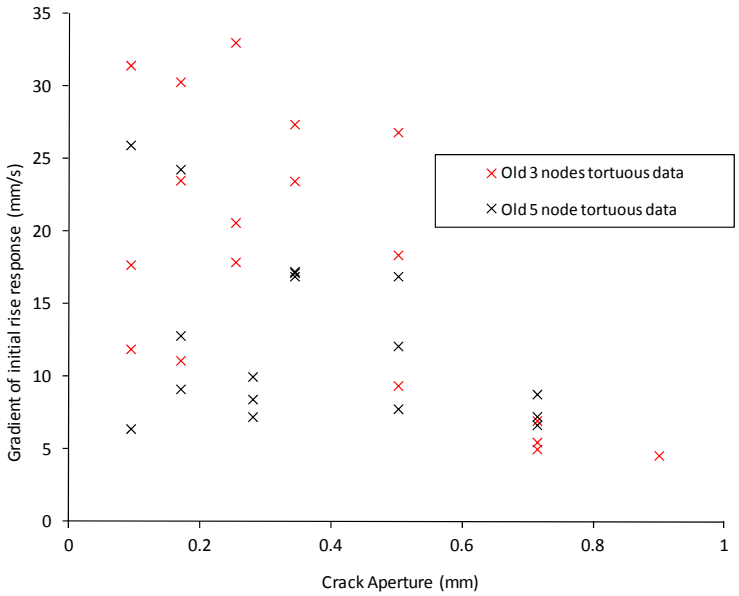

Figure 24: Gradient of the initial rise response over a period of 1 second for 35 day old tortuous 3 and 5 node specimens with water.

Figure 24 shows a large variation in the rates of the initial capillary rise response. The 5 node tortuous specimens generally have lower velocities, signifying that the meniscus takes longer to reach the same absolute rise height as the 3 node specimens, as a result of the longer flow path. As observed previously, the relationship between the velocity of the meniscus (gradient of the initial rise response) and the crack aperture is contrary to what would be expected from theory and may be attributed to the absence of capillary rise data for rise heights of less than 12mm.

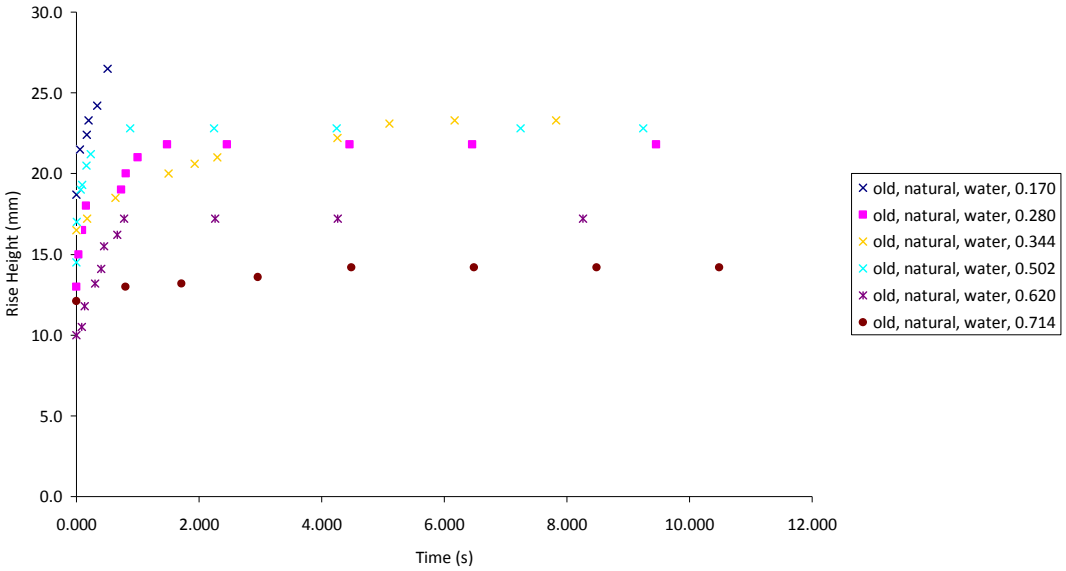

Figure 25: 35 day natural water experimental graph and results

The natural water experiments, shown in figure 25, show consistency with the theory of the capillary flow potential equation 5.1 that the greater the crack width of the capillary the lower the overall rise height. Table 7 indicates for specific crack apertures what the corresponding rise height should be and what the experimental rise heights were found to be.

The contact angles were measured using images from the capillary rise height videos for specific crack apertures. The angles were only measured for planar crack experiments not for tapered, tortuous or natural cracked specimens.

The contact was measured using images of where the light shines through the specimen.

Table 7: Comparing crack apertures for mature natural crack aperture experiments

Crack aperture (mm)	Average experimental rise height (mm)	Contact angle, θ (˚)	Theoretical equilibrium rise height (mm)
0.170	26.8	23	80.4
0.280	21.8	42	39.4
0.344	23.3	42	31.7
0.502	22.8	46	20.5
0.620	17.2	33	20.1
0.714	14.2	34	17.23

It is clear that table 7 shows some uncertainties in the experimental final rise height when compared to the calculated final rise height for capillary flow through mature, natural cracks with water as the flow agent. For crack apertures, 0.170, 0.280 and 0.344mm the experimental rise heights appear to be much lower than the rise heights calculated using equation (5.1.) However, in this instance, using formula 5.1, it is only an estimate. This is because many parameters have not been taken into consideration such as the angle of crack inclination and the absorption of flow agent into the cement matrix.

Unlike the planar or tapered experiments in which there is a crack aperture less than 0.344mm, it takes longer for fluid flow to reach the maximum rise height; the natural experiments do not display this and there are significant differences in the time taken to achieve maximum rise heights. For example the initial gradients displayed on the graph in figure 25 for crack aperture 0.620mm show a rapid increase to reach maximum rise height whereas for a crack aperture of 0.714, it is a very slow and gradual increase. Figure 25 shows that for a crack width of 0.170mm, it takes 0.5 seconds to achieve maximum rise height and with 0.280mm crack width it takes 2 seconds longer to achieve maximum rise height. However, as previously stated, the initial rise response was not recorded until a rise height of 12mm was observed due to

the experimental set up and the results shown are those from a time from 2-10 seconds into flow. Capturing the data over a short period of time enables us to look at the immediate capillary rise response of the system giving an indication of the ability and velocity of a flow agent to move through a discrete crack. The longer term response of the system will give an indication of the extent of healing that can be achieved, along with any limitations that may be faced as a result of the selection of the healing agent (i.e. hardening or curing of the healing agent within the capillary flow time).

The angle of inclination of the crack undoubtedly affects the rate of capillary flow; this is discussed further in chapter 5. The lower the angle of inclination from the vertical, the greater the overall final rise height, this is not reflected in the experimental results and readings shown on the graph as the specimens used are different crack inclinations, those with reinforcement have a straight natural crack, and those without reinforcement have a diagonal crack at an angle. The angle of inclination varies with respect to the type of crack. From the videos it has been calculated that the angle is approximately 5˚ from the vertical. Images are shown below in figure 26 where the variable brightness of the lamp behind the specimens is responsible for the impression of a wider aperture than that reported.

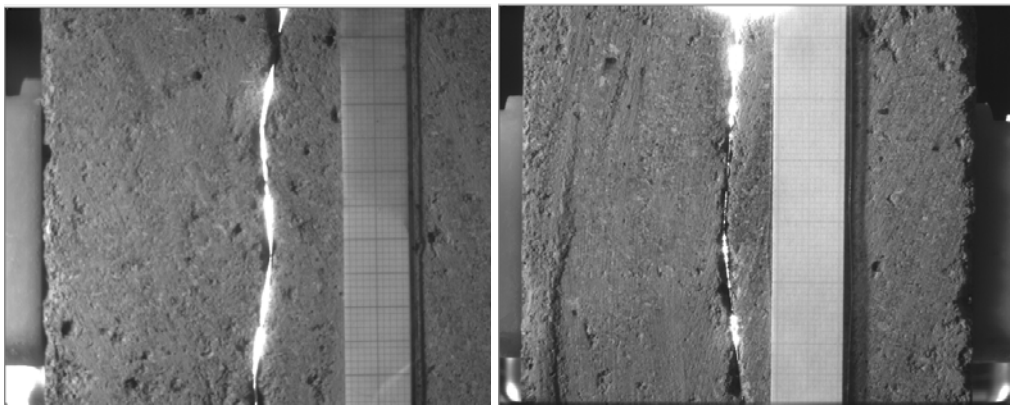

(a) (b)

Figure 26: Crack apertures of (a) 0.170mm and (b) 0.261mm for tortuous experiments of 2 and 5 nodes

It should also be noted that for natural cracks in particular that the crack is changing in three dimensions and is not necessarily planar. The standard equation does not take this into account therefore while general trends can be observed from the results they will not follow capillary theory.

All crack configurations are graphically compared here to try and determine relationships between the different types of crack configurations and what can be deduced from the overall rise heights and times.

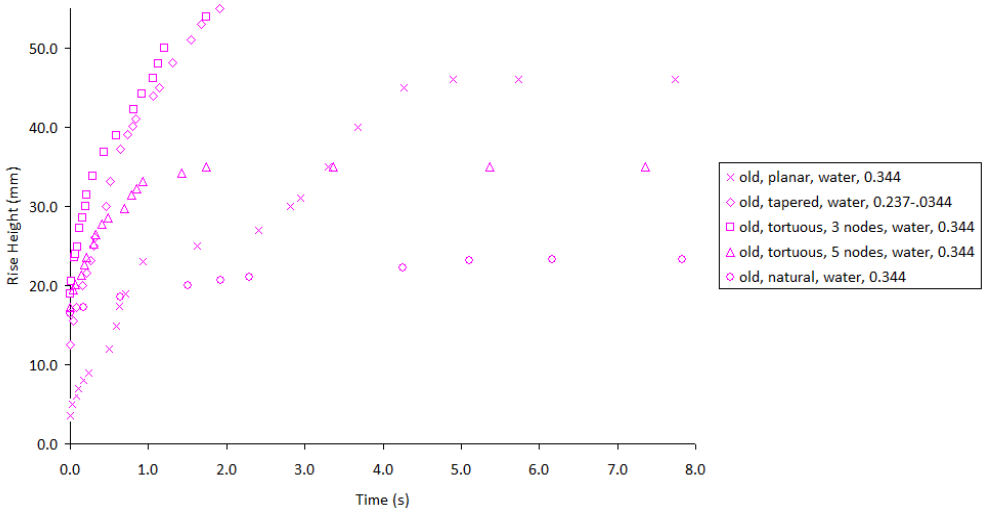

Figure 27: Old planar water, old tapered water, old tortuous water and old natural water experimental results from 0-8 seconds for a crack aperture of 0.344mm

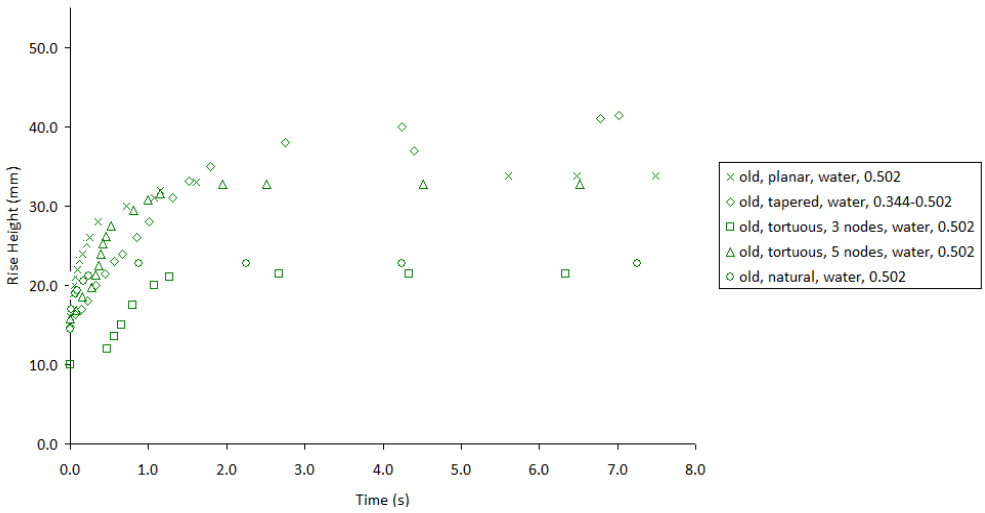

Figure 28: Old planar water, old tapered water, old tortuous water and old natural water experimental results from 0-8 seconds for a crack aperture of 0.502mm

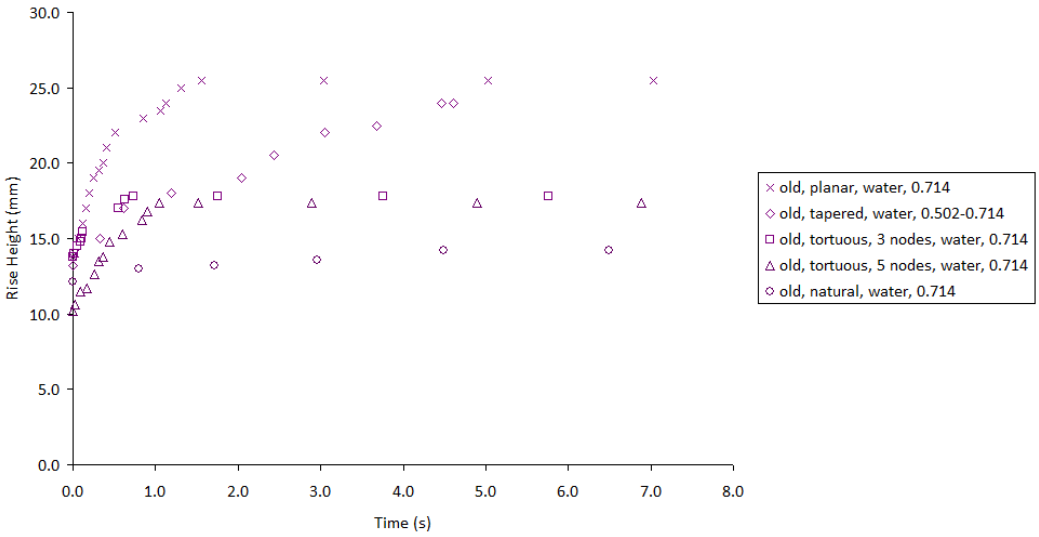

Figure 29: Old planar water, old tapered water, old tortuous water and old natural water experimental results from 0-8 seconds for a crack aperture of 0.714mm

Looking at figures 27 - 29 shows that at a crack width of 0.344mm, the experiments display a similar maximum overall rise height for all crack configurations**.** The overall rise heights for a crack width of 0.714 are in the similar region and only have an overall maximum difference in rise height of 10mm. Therefore, it is width rather than crack configuration that has importance for achieving maximum rise height. The smallest overall rise height obtained was taken from the natural crack experiments.

4.3 Effect of flow agent

This section of the results chapter looks at the difference in overall rise heights, crack apertures and flow rates between water, cyanoacrylate and xanthan gum.

This results section is introduced to look at the changes between the flow agents used in the experiments. This is because each flow agent has a different viscosity and surface tension and therefore capillary rise heights are expected to be different. Furthermore, the effect of setting times can be investigated.

The first comparison is made between 35 day old planar water and cyanoacrylate experiments at equal planar crack apertures.

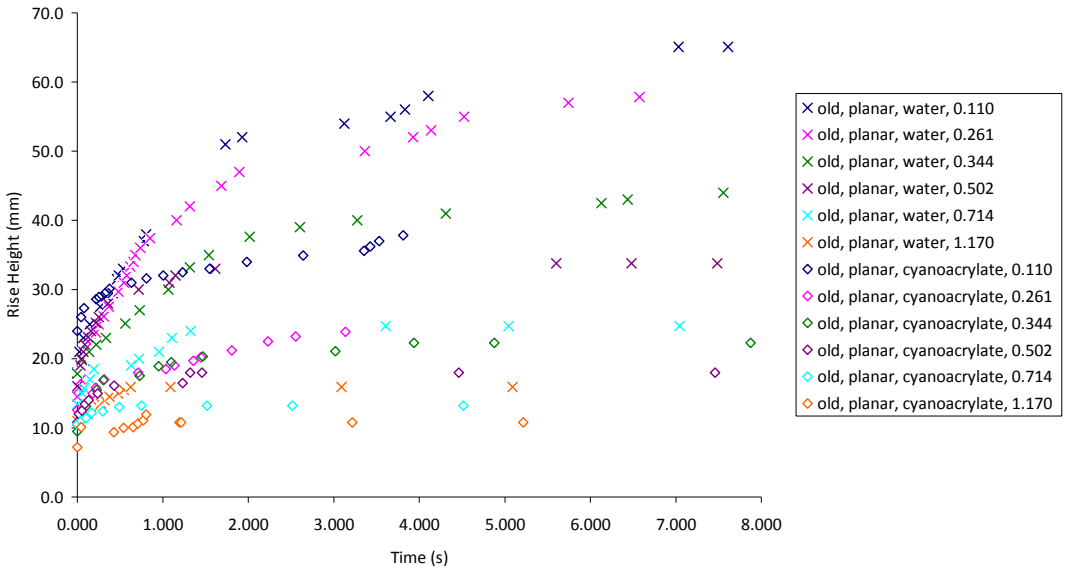

Figure 30: 35 day mature planar water and old planar cyanoacrylate experimental results

The curves displayed for each of the crack apertures in the graph in figure 30 show the effect of crack width on capillary rise height, for two different flow agents. It is known from the data sheet provided in Appendix B that cyanoacrylate has a higher viscosity than water. Moreover, an additional property of cyanoacrylate is that the viscosity changes with time as a result of the curing process that the glue undergoes when in contact with an alkaline environment in the presence of moisture. In light of this knowledge it is therefore appropriate to assume that equilibrium rise heights for all cyanoacrylate specimens may be lower than their water counterparts. It is difficult to determine at this stage whether there is any effect of cyanoacrylate curing on the equilibrium rise height and xanthan gum will be used to examine this effect towards the end of this section.

The smaller the wire thickness the larger the difference in the equilibrium-rise height between water and cyanoacrylate. For instance for 35 day mature concrete, planar water 0.110, between water and cyanoacrylate, there is a difference between overall maximum rise heights of 20mm whereas for 1.170mm crack width the difference in

overall rise height is less than 10mm. This happens due to the difference between the surface tension and contact angle of cyanoacrylate compared to water. Looking at the theory stated in chapter 5, with a higher viscosity (cyanoacrylate) the capillary rise response is going to be slower than the capillary rise response of a liquid with a lower viscosity (water).

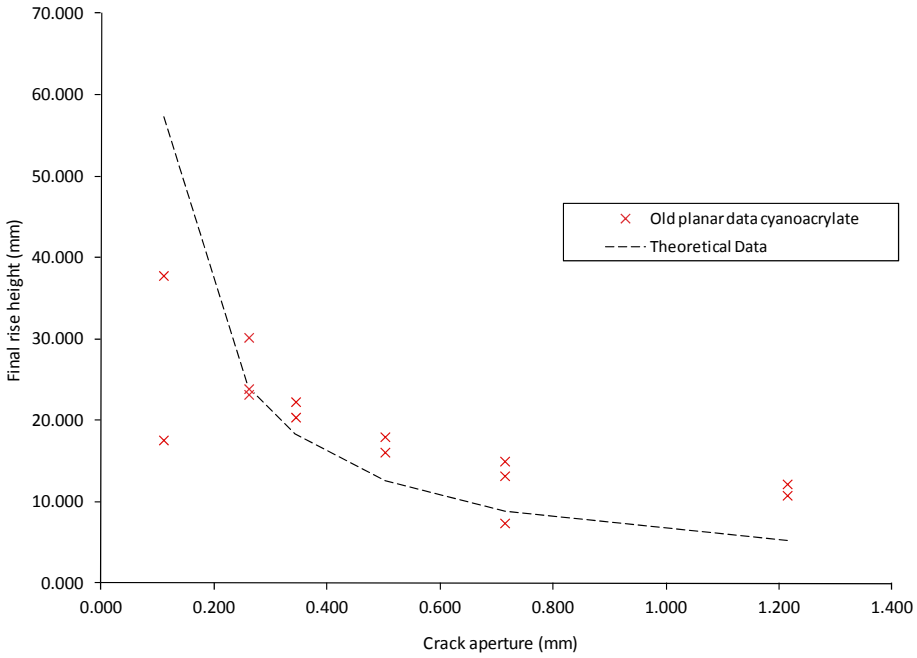

Figure 31: Comparison of 35 day cyanoacrylate planar experimental final rise height data over a range of crack apertures with theoretical data

Figure 31 presents the variation in results of final rise height with varying crack aperture for planar 35 day old specimens with cyanoacrylate as the flow agent. The theoretical values have been calculated assuming a contact angle of 10˚, surface tension of 0.033 N/m and a density of 1060 kg/m^3 as suggested in the technical data sheet found in Appendix B and used by Joseph (2010).

The variation in the results is similar to that reported for flow of water in planar cracks and demonstrates the repeatability of the experiments.

When considering the agreement between the theoretical and the experimental data it is apparent that a reasonably good agreement is achieved at crack apertures

0.237mm and greater. Better agreement may be achieved with refinement of the values assumed for surface tension and contact angle of cyanoacrylate when in contact with cementitious materials however, this would require further investigation.

The final rise heights associated with the crack aperture of 0.110mm are significantly below those predicted by theory and may be attributed to the hardening of the glue within the crack. Crack apertures of this magnitude and smaller are often quoted in product technical specifications as being close to those where bonding of the faces by cyanoacrylates occurs.

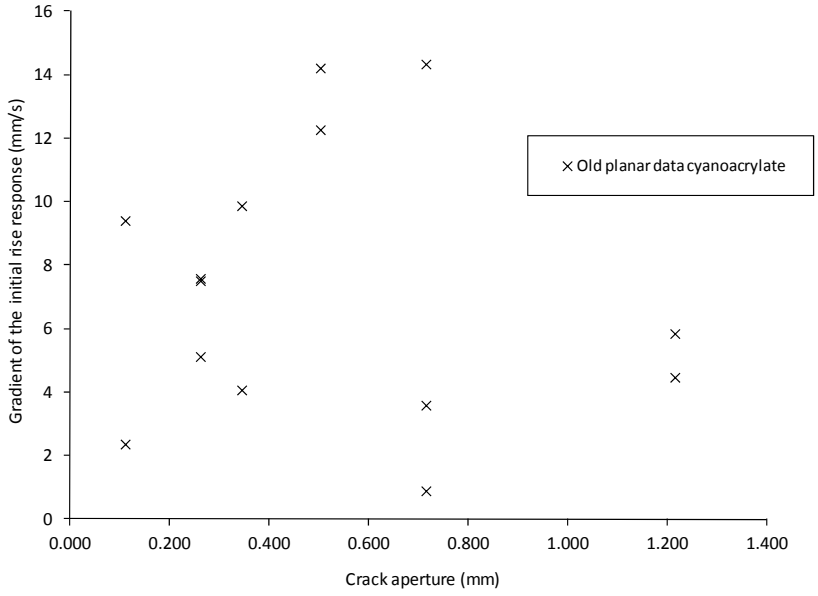

Figure 32: Gradient of the initial rise response over a period of 1 second for 35 day old planar specimens using cyanoacrylate.

Figure 32 shows a large variation in the rates of the initial capillary rise response with no discernible relationship between the crack aperture and the gradient of the initial capillary rise response in planar specimens (i.e. the velocity of the meniscus). In the experiments using cyanoacrylate the velocity of the meniscus will not just be affected by the crack aperture but there will also be additional interactions between the cyanoacrylate and the capillary walls. The latter may result in hardening of the cyanoacrylate in the capillary, resulting in retardation of the velocity of the meniscus.

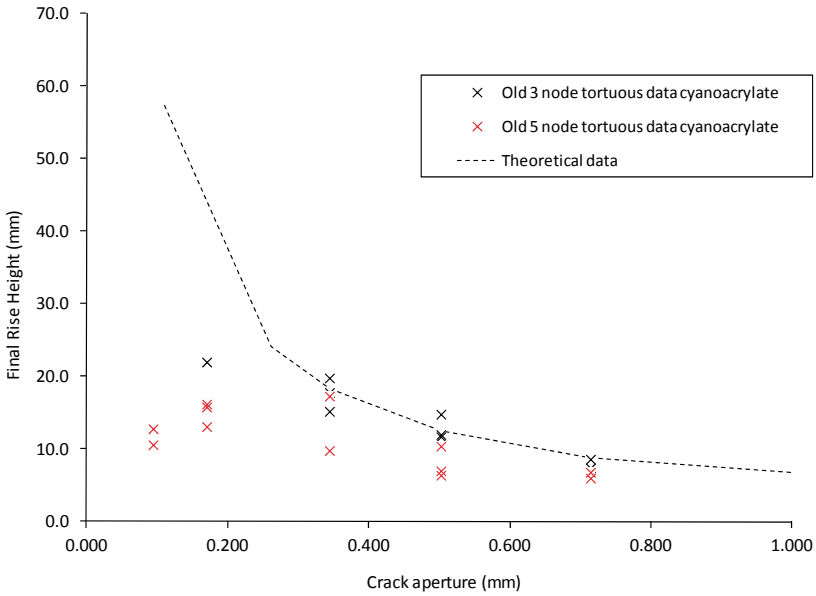

Figure 33: Comparison of 35 day cyanoacrylate tortuous experimental final rise height data over a range of crack apertures with theoretical data

As can be seen in figure 33 the cyanoacrylate experimental data for the 3 and 5 node tortuous specimens agrees reasonably well with the theory. Unlike the data presented in figure 31 the majority of the tortuous data falls slightly below the theoretical values. As has been repeatedly noted throughout Section 4 this may be due to variations in the actual crack apertures used in the experiments. Furthermore, there may be evidence of cyanoacrylate healing in the two smallest crack apertures, in which the theoretical rise heights were not achieved. This is further supported by the difficulty in physically pulling these specimens apart immediately after the capillary rise response had been captured.

For all crack apertures the rise heights associated with the 5 node tortuous specimens are generally lower than their 3 node counterparts. This may reflect the longer flow path of the cyanoacrylate in the 5 node tortuous specimens resulting in additional curing and hardening occurring, prohibiting the full rise height from being achieved.

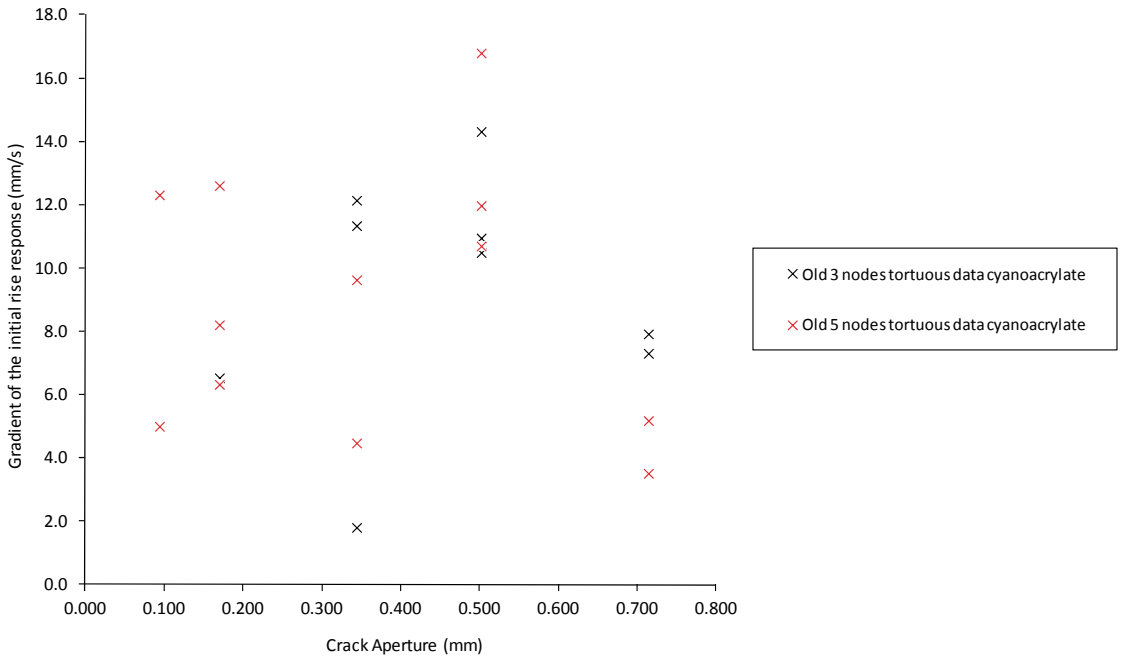

Figure 34: Gradient of the initial rise response over a period of 1 second for 35 day old tortuous specimens using cyanoacrylate.

As observed with the planar data in figure 32, the tortuous data in figure 34 shows no obvious correlation between the crack aperture and the velocity of the meniscus. The results presented in figure 34 fall within the range observed in figure 32, signifying that the capillary flow of cyanoacrylate in cementitious materials is somewhat consistent, albeit not as anticipated from theory. Unlike the difference observed in the velocities of the water meniscus between the 3 and 5 node crack configuration there is no clear difference between the velocities of the cyanoacrylate in the two crack configurations. This may be due to the varying interaction of the cyanoacrylate with the specimens during capillary flow.

The results from tapered experiments using water and cyanoacrylate are graphically presented below in figure 35.

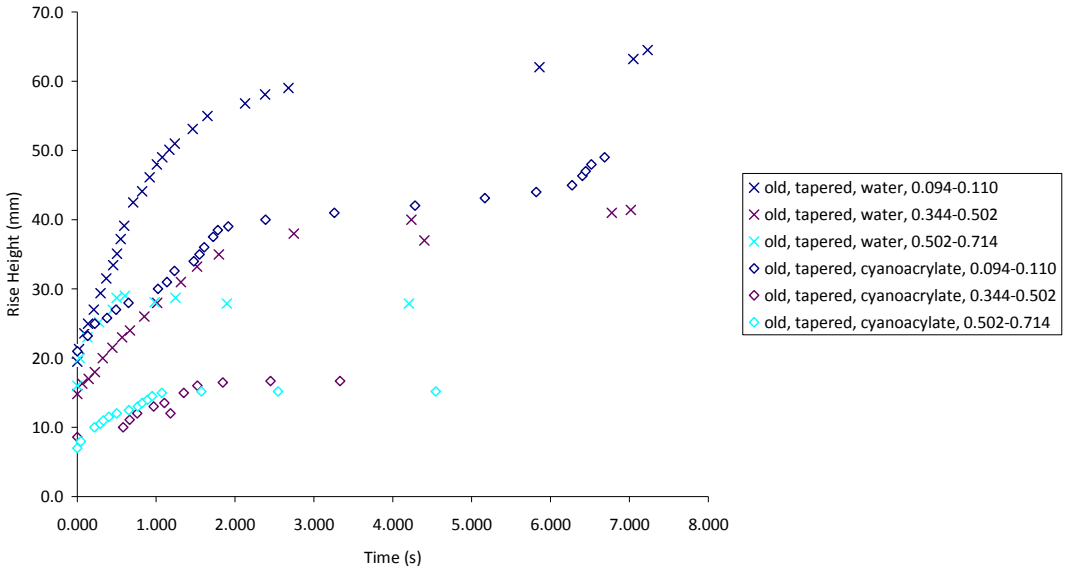

Figure 35: 35 day mature specimens tapered water and 35 day mature specimens tapered cyanoacrylate experimental results

All 35 day mature tapered water and cyanoacrylate data again follow theory, that is, the smaller the crack aperture the larger the overall rise height.

It can be seen looking at the gradients of both the water and the cyanoacrylate experiments that the water experiments initial gradients are steeper. However, previously stated, what is shown is not the initial rise height, only the response past 12mm rise height. Looking at equation 5.1 and theory in chapter 5 these observations do again follow theory as cyanoacrylate has a lower viscosity than water, however it is not certain that it can be assumed that this prevents it reaching its maximum rise height in a fast amount of time. This may also occur due to the cyanoacrylate setting.

Table 8: Comparison of cyanoacrylate theoretical rise height with experimental rise height

Crack aperture (mm)	Theoretical rise height (mm)	Experimental average rise height (mm)
0.261	24.3	23.1
0.344	18.4	22.3
0.502	12.6	18.0

Table 8 shows that the theoretical rise height of cyanoacrylate in a specific crack aperture appears to be similar to the average experimental rise height recorded. However, from the experimental tests it can be seen that the values for the experimental average rise height is higher as the crack apertures could be smaller. This is due to the wires losing shape in the process of being clamped.

When considering the effect that a change in inclination of cracks has on the rates of fluid flow through capillaries, as performed in the tortuous experiments it can be seen that for 35 day mature specimens tortuous 3 nodes water the crack aperture of 0.170mm has an unexpected capillary rise response. Between 1 and 2 seconds the overall rate of flow slows down in comparison to the rest of the experiment. The areas where there is a gentle gradient, is where there is absorption of the fluid into the cement matrix, and areas where there is a steep gradient is where the fluid rises rapidly due to the capillary pore pressure. This statement is confirmed by the videos found in the attached data to this thesis but it is also shown in figure 36.

The retardation of the fluid shown below in the graph (figure 36) for old, tortuous, 3 nodes, water, 0.170mm, is as a result of the wire restricting the flow of the fluid in the channel. The wire in this instance acted as a blockage in the flow path. In further experiments the spacer wires were placed outside of the anticipated flow areas to reduce the occurrence of this.

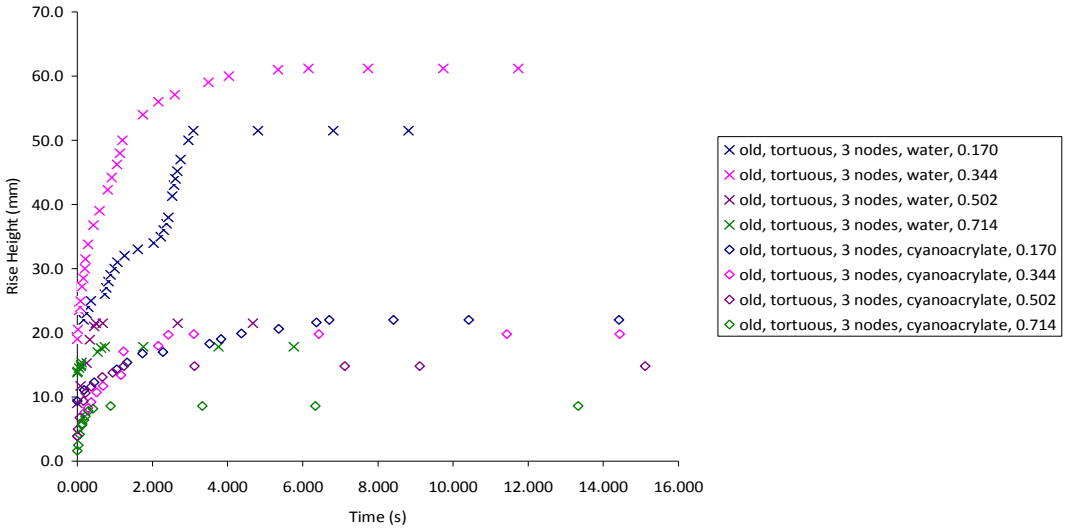

Figure 36: Effect of flow agent: 35 day mature tortuous 3 nodes water and 35 day mature tortuous 3 nodes cyanoacrylate

Figure 37 shows absorption into crack apertures of 0.254mm and 0.344mm. It is shown that through the flow 0.344mm crack aperture has a large amount of absorption through the crack aperture and also through the base of the specimen, whereas 0.254mm crack aperture does not.

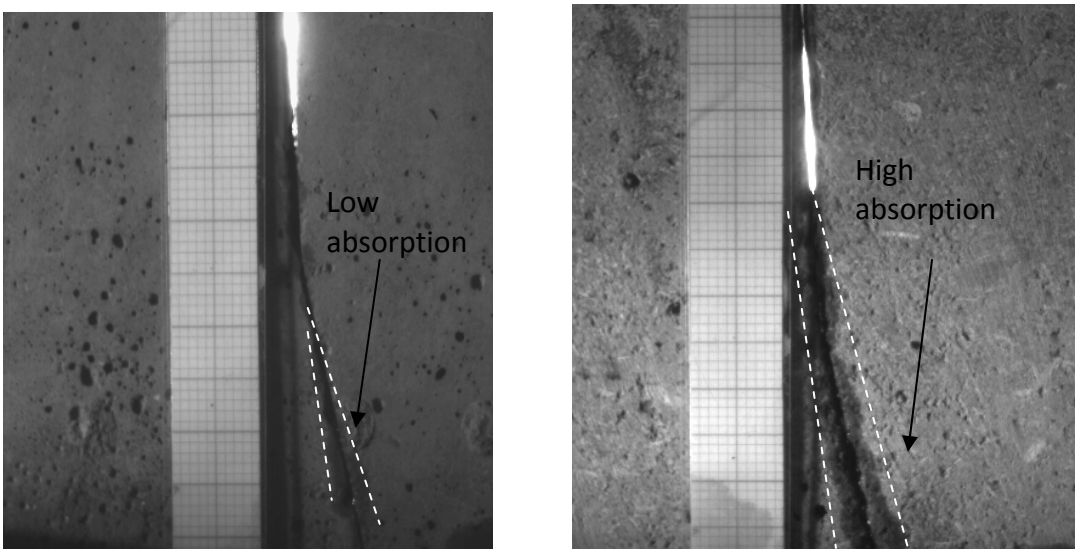

A: 0.254mm water B: 0.344mm water

Figure 37: Absorption into specimens in experiments

All of the 3 nodes water experiments achieve an overall higher rise height in comparison to the 3 nodes cyanoacrylate experiments. For the same aperture the water specimens continue to exhibit higher equilibrium capillary rises than their cyanoacrylate counterparts.

The surface of the specimens are alkaline and do not have an effect on the flow of water. When there is a small crack aperture the cyanoacrylate may cure quickly and the bonding width according to the data sheet in appendix A is 0.05mm. Conversely, at a crack aperture of 0.714 mm there is a lot more liquid in the crack to cure therefore the effect is not as noticeable.

This section, examines the effect of flow agent on capillarity through a crack configuration with a larger number of nodes.

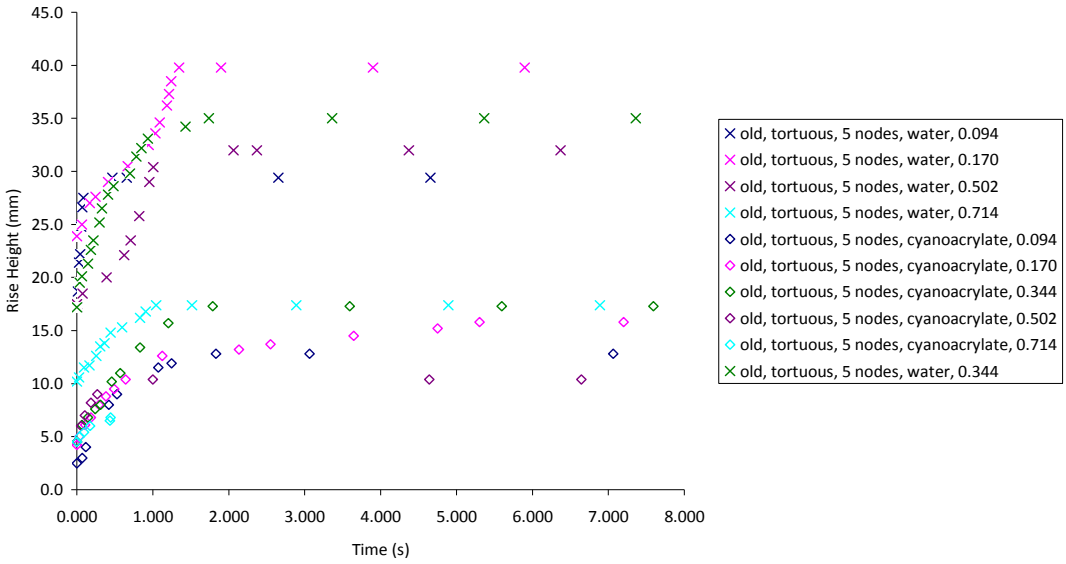

Figure 38: Effect of flow agent: old tortuous 5 nodes water and old tortuous 5 nodes cyanoacrylate experimental graphical results

Overall, the gradients for the old tortuous 5 nodes water have a faster flow rate initially compared to the 5 nodes cyanoacrylate experiments. This could depend on the viscosity of the cyanoacrylate. The results and readings are further discussed and compared against the theoretical results in chapter 5.

Xanthan gum experimental work was undertaken to compare and assess the curing/hardening effect of cyanoacrylate during capillary flow experiments. Hence the change in viscosity is looked at in detail by looking at the fluids used in the experimental work and seeing how capillary flow is affected.

Xanthan gum was measured according to the same capillary rise height for cyanoacrylate, it has the same density and surface tension and contact angle but not necessarily the same viscosity.

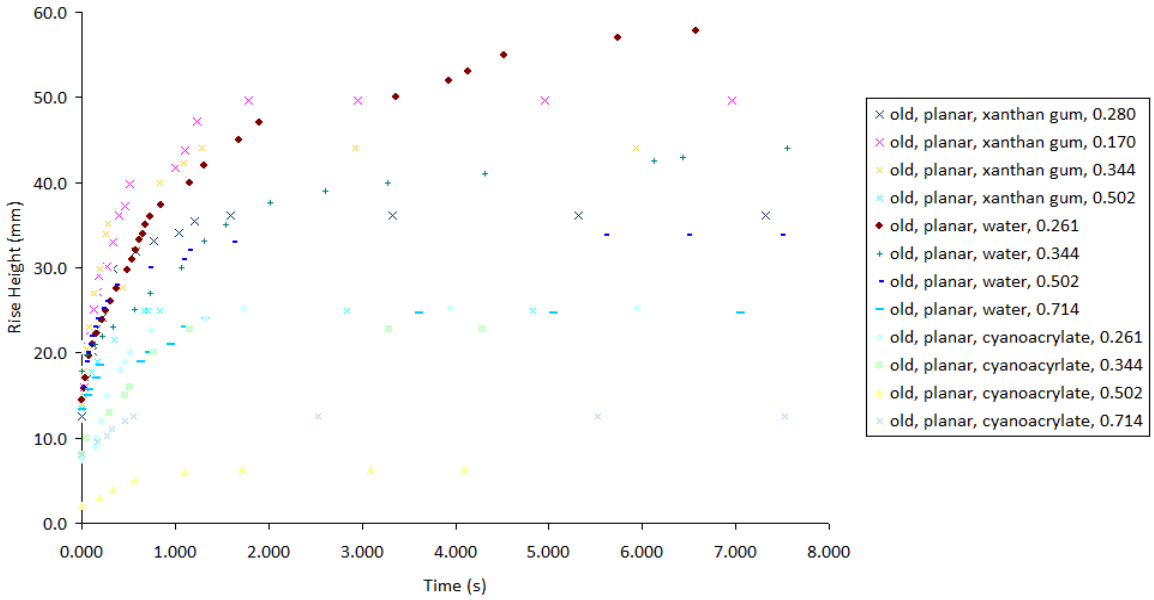

Figure 39: Effect of flow agent: Old planar xanthan gum, old planar water and old planar cyanoacrylate

Xanthan gum as stated in chapter 3 is a biological additive that has no setting characteristics whereas cyanoacrylate does cure with respect to time. Therefore xanthan gum was used to determine the difference between the capillary rise response without the curing effect. The xanthan gum additive is used to give equivalent rise heights and therefore γ, $\cos\theta$ and ρ same as cyanoacrylate but not necessarily viscosity. As cyanoacrylate sets, the viscosity increases and the final rise height is lower and comparing the final rise heights to the xanthan gum experiments the effect of cyanoacrylate curing is apparent through the lower rise heights.

The results displayed on the graph compare the rate of capillary rise height between cyanoacrylate and xanthan gum in order to establish the effect of cyanoacrylate curing in capillary rise. It can be seen that although cyanoacrylate and the xanthan gum used in these experiments have been designed to have the same capillary rise height, the cyanoacrylate tests overall have a lower equilibrium rise height compared to the xanthan gum experiments. These results and readings show that the setting time of the cyanoacrylate has a large effect on the overall rise height.

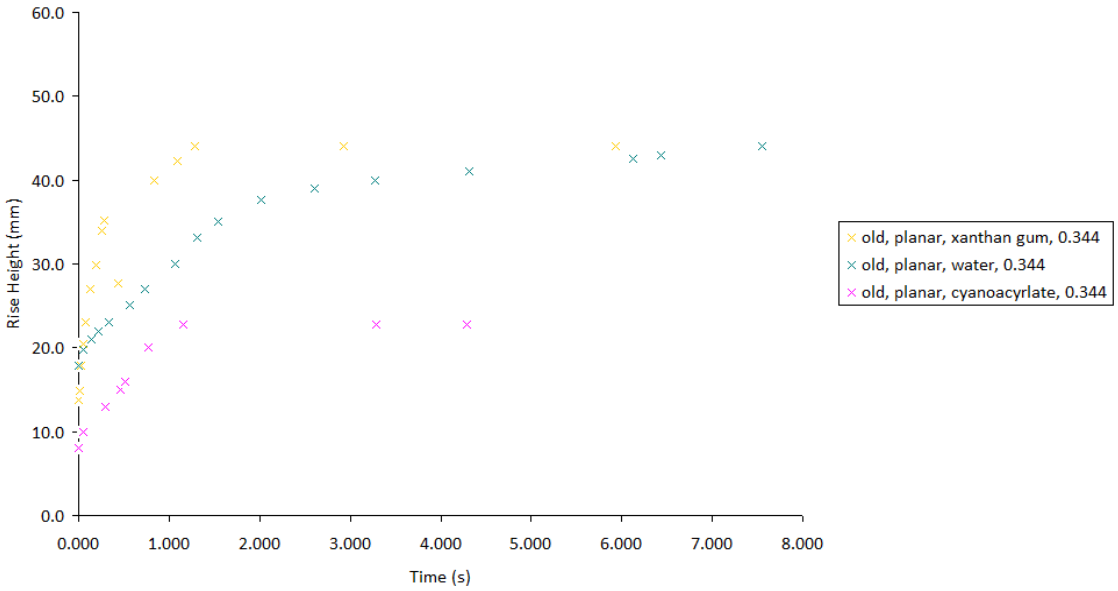

Figure 40: Graph of capillary rise rates for xanthan gum, water and cyanoacrylate

Looking at the videos and the graph gradients in figure 40 it is shown that the rate of rise is faster with the xanthan gum compared to cyanoacrylate. It can be seen that the water and the xanthan gum reach the same final rise height but not cyanoacrylate.

The surface tension of the xanthan gum was calculated on the overall rise height in a glass tube compared to the rise height in the same diameter tube with cyanoacrylate. As discussed previously it is known that the viscosity of a fluid does affect the overall rate of rise or rate of flow. Viscosity does not affect the level of rise height and in this instance the surface tensions could be different as those were not calculated. Differences such as the friction on the inside of the glass tubes could differ affecting

the overall rise height. Therefore, this method could be argued as not being the most accurate.

4.4 Effect of specimen age

An investigation into the effect of specimen age on capillary flow in discrete cracks in cementitious materials has been examined in this section. Looking at this specific parameter can give an idea of the ability of the healing agent to flow in both young and mature cementitious matrices, hence indicating the potential for healing to occur in cracks formed at early age, due to shrinkage and early thermal effects and those formed at later stages as a result of load application or deterioration processes.

The effect of age here has been examined via the comparison of old 35 day mature planar water experiments and young 7 day planar water experiments.

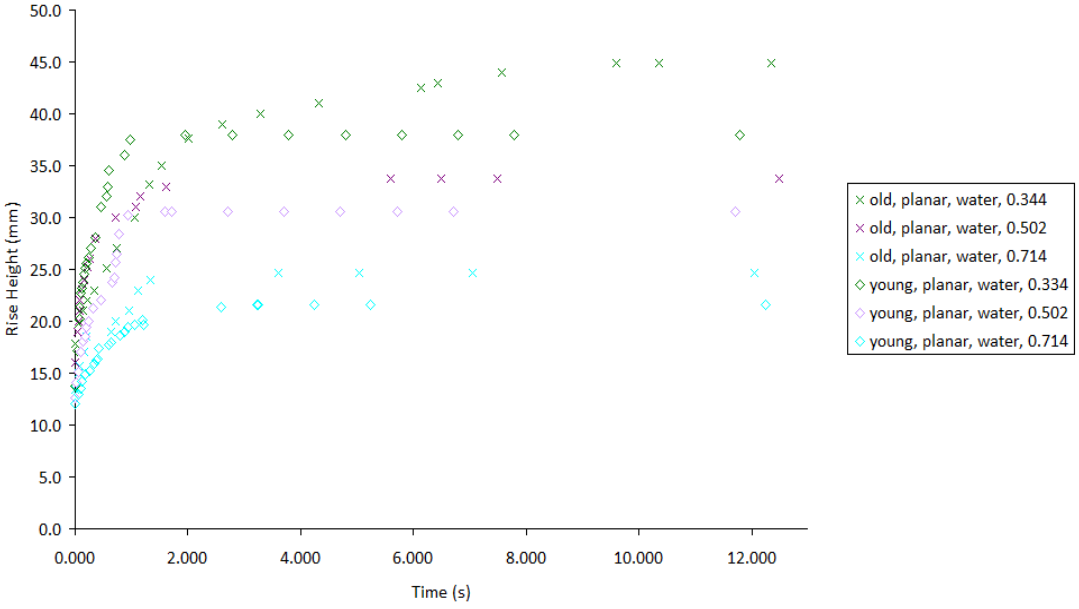

Figure 41: Effect of age, old planar water and young planar water graphical results

Old, planar, water and young, planar, water with the same crack aperture of 0.094 has a lower rise height than 0.110. This is due to the same reasons as described in section 4.2.1 where the actual crack aperture is evaluated. Therefore these results are not considered in the following discussions.

It can be seen that in general the rate of capillary rise is faster for the young specimens than for the old specimens even though the final rise heights are of similar magnitude.

The change in weight found for the young experiments can be found in appendix A and they show to have a change in weight of 0.5g and the change in weight for the old specimens is found to be 1.5g. This shows that the higher the initial rate of capillary rise the less fluid is absorbed.

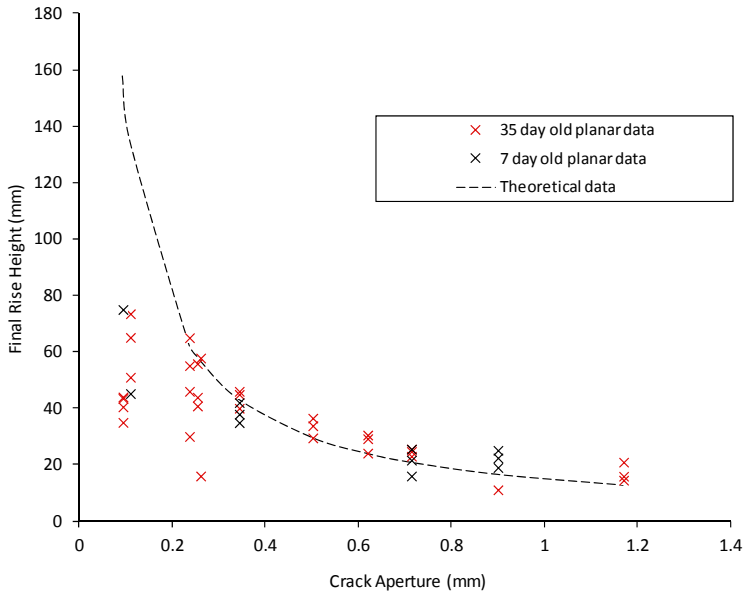

Figure 42: Comparison of planar crack aperture with final rise heights for 7 and 35 day old specimens using water

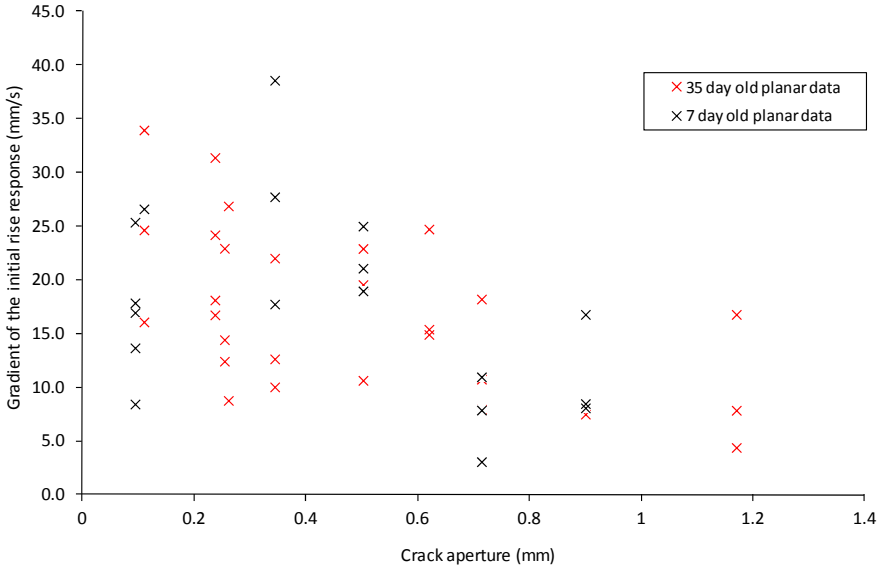

Figure 43: Gradient of the initial rise response over a period of 1 second for 7 and 35 day old planar specimens using water.

The data shown in figure 42 confirms that for the smallest crack aperture of 0.094mm that regardless of the age of the specimen the final rise height, as predicted by theory is not reached. The reasons given previously for this are also applicable here. For the remainder of the crack apertures there is no significant difference between the rise heights at either age and the rise heights predicted by theory. Similarly in figure 43 the 7 day old specimens show marginally higher meniscus velocities than their 35 day old counterparts, supporting the observations made previously. This may also be attributed to the effect of the time dependent development of the mortar microstructure on the dynamic resistive forces acting during capillary flow.

This section looks at the tapered crack configuration experiments but comparing the age of the specimens and seeing what effect the age of the mortar has on the specimen.

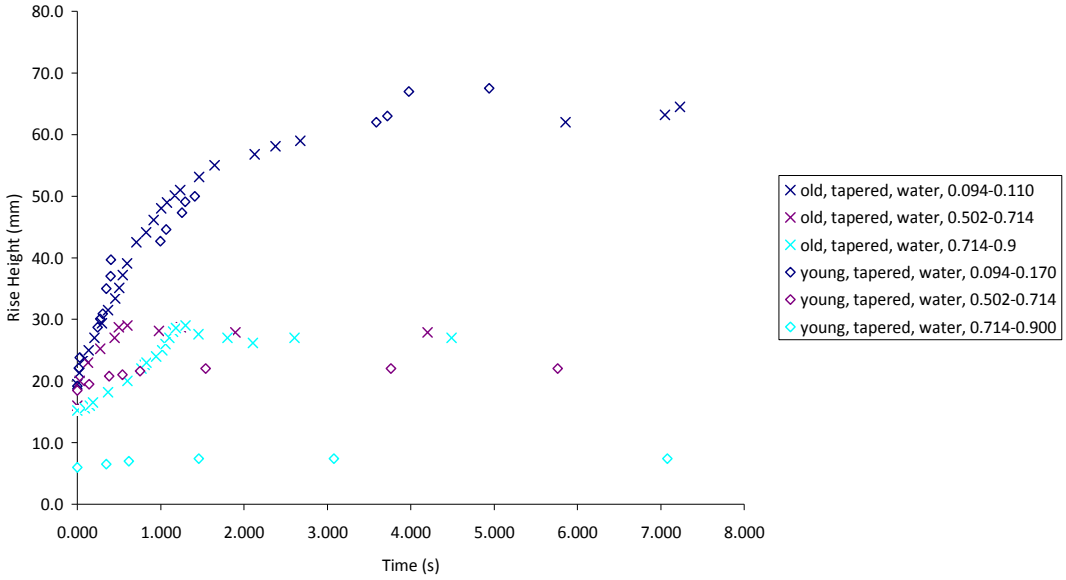

Figure 44: Effect of age: old tapered water and young tapered water

Comparing the tapered experiments with the planar experiments, as in figure 44, the young specimens have a lower overall rise height than the old specimens. The larger apertures show very low rise heights, as previously discussed this is due to the methods undertaken in experiments, where the first 12mm or so cannot be seen so therefore the overall rise height is not as accurate as it could be.

Young tapered water 0.094-0.170 experiment has an interesting flow pattern. A rise height of 30mm is achieved within a second but then its maximum rise height takes another 3.5 seconds to reach maximum rise height. The video shows that there is absorption through the cement matrix therefore decreasing the overall final rise height. With the presence of a wire at this location there is a delay in the rise height which is due to absorption taking place and then a subsequent increase in rise height.

The effect of age using cyanoacrylate is looked at here to try and determine how the healing rates of cyanoacrylate are affected by age of cementitious materials.

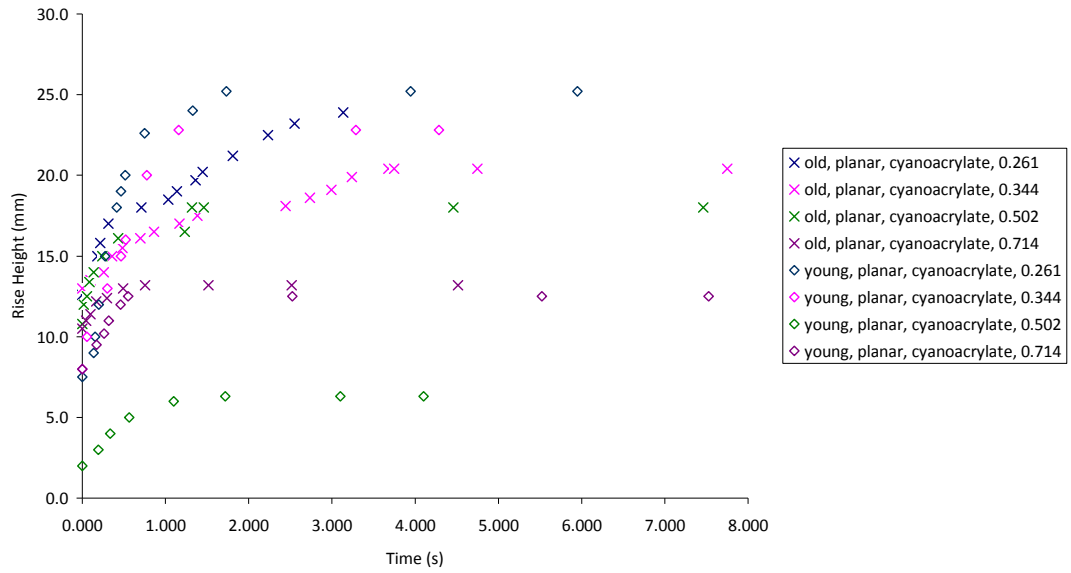

Figure 45: Effect of age: Old planar cyanoacrylate and young planar cyanoacrylate

From figure 45, for old planar cyanoacrylate crack apertures of 0.261mm and 0.344mm the overall rise height is higher than in the same crack apertures for the young experiments. Looking at theory it would suggest that they should be at the same final height but having looked at the effect of age in the water experiments the young specimens absorb less therefore the cyanoacrylate would travel further up the capillary.

Old planar cyanoacrylate and young planar cyanoacrylate specimens have similar overall rise heights at the majority of crack apertures considered, as confirmed in figure 46. However, from figure 45 it can be also seen that they take a similar time to reach the maximum rise height. From the experiments conducted the specimen age appears to have an effect on the rise response; with older specimens retarding the capillary rise response. This is somewhat confirmed by the initial rate of capillary rise data presented in figure 47. However, it is the longer timescale response of the system (1 to 8 seconds), as given in figure 45 that is a better reflection of this behaviour. This difference between the rise response of young and old specimens may be attributed to a change in the surface tension as a result of the age of specimen.

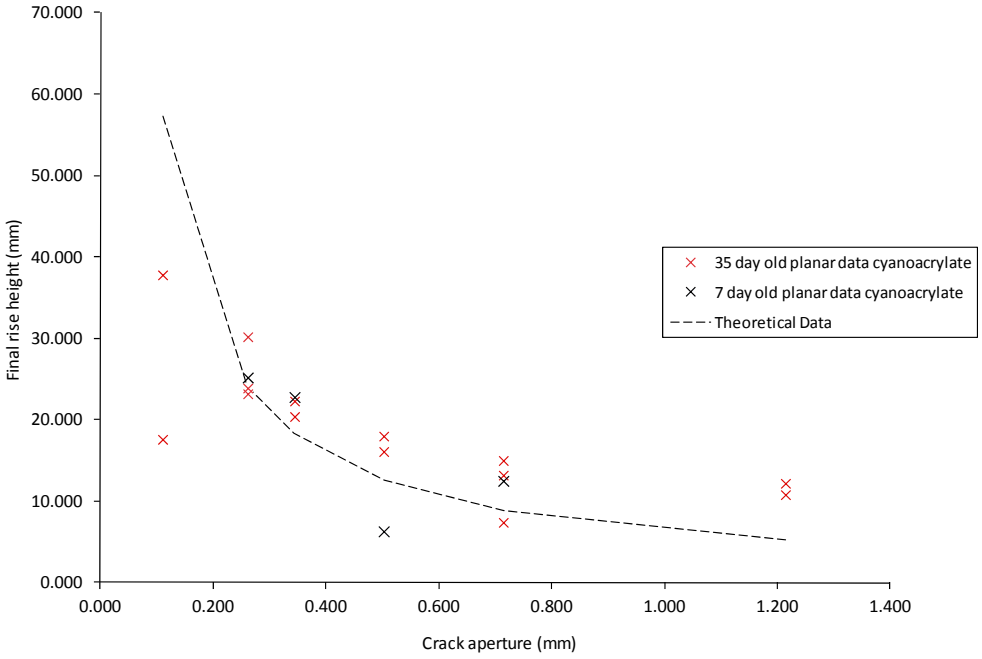

Figure 46: Comparison of planar crack aperture with final rise heights for 7 and 35 day old specimens using cyanoacrylate

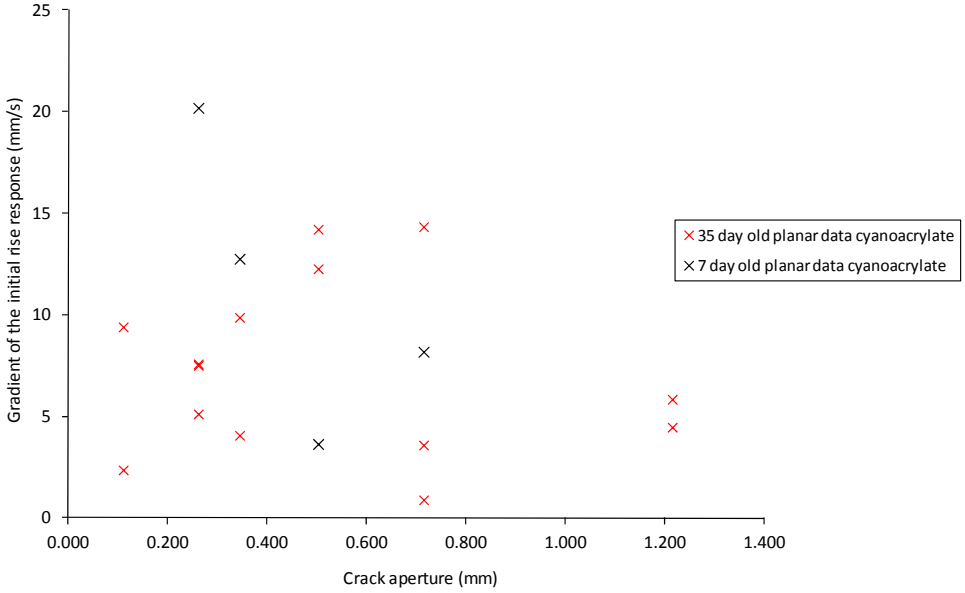

Figure 47: Gradient of the initial rise response over a period of 1 second for 7 and 35 day old planar specimens using cyanoacrylate.

One conclusion is that regardless of the age of the specimen the cyanoacrylate reaches its equilibrium rise height in under 8 seconds which indicates that it should be able to flow into the crack plane before it completely hardens. Secondly, the graphs show that

even though curing occurs the fluid still continues to flow afterward, not reaching the maximum rise height but flowing further.

The influence of specimen age on the capillary rise response of cyanoacrylate in tapered crack configurations are evaluated here, and the results presented in figure 48.

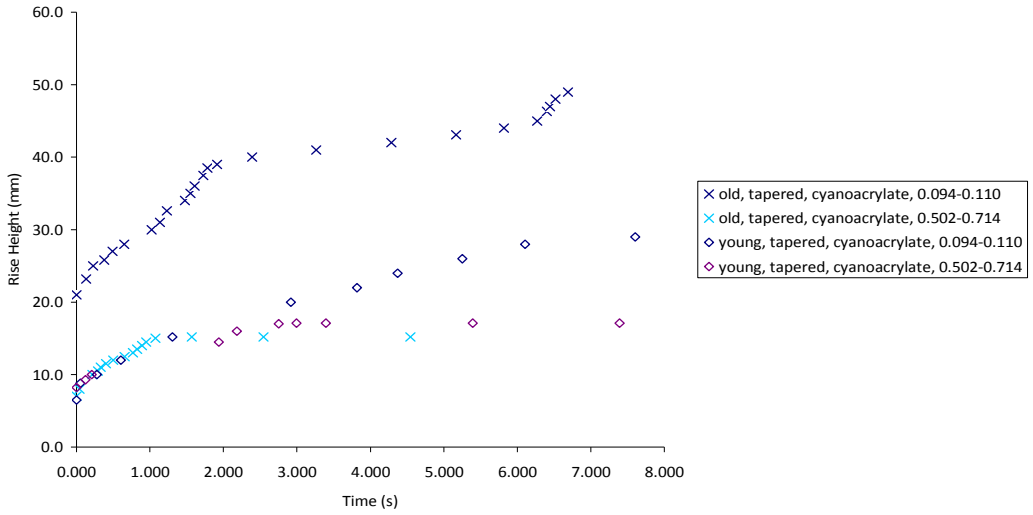

Figure 48: Effect of Age: Old tapered cyanoacrylate and young tapered cyanoacrylate

It takes a significant amount of time for the old tapered experiments with a crack aperture of 0.094 – 0.110 as it is still rising at the end, as demonstrated in figure 48. As there are significant differences in the gradients throughout the rise height the experiments do not show that it is possible for the cyanoacrylate to set at the point when full maximum rise height is achieved. The young experiments show that only half of the old maximum rise height is achieved. Looking at larger aperture, 0.714mm and 0.900mm the effect of age on the capillary rise is negligible. This is as the larger the aperture, the lower the rise height so therefore the less overall absorption into the cement matrix. Therefore, it is assumed that there is unhydrated cement in younger specimens and therefore more fluid flow into the cement matrix reducing the overall capillary flow. When there is a larger crack aperture the capillary rise is anticipated to be lower, providing a smaller area over which absorption into the cement matrix can occur and therefore less absorption into the cement matrix, hence why the values of old and young are of similar magnitude.

4.5 Effect of specimen saturation

Flow in discrete cracks in saturated concrete is an important area to look at as structures rarely are in a moisture free state in outdoor environments.

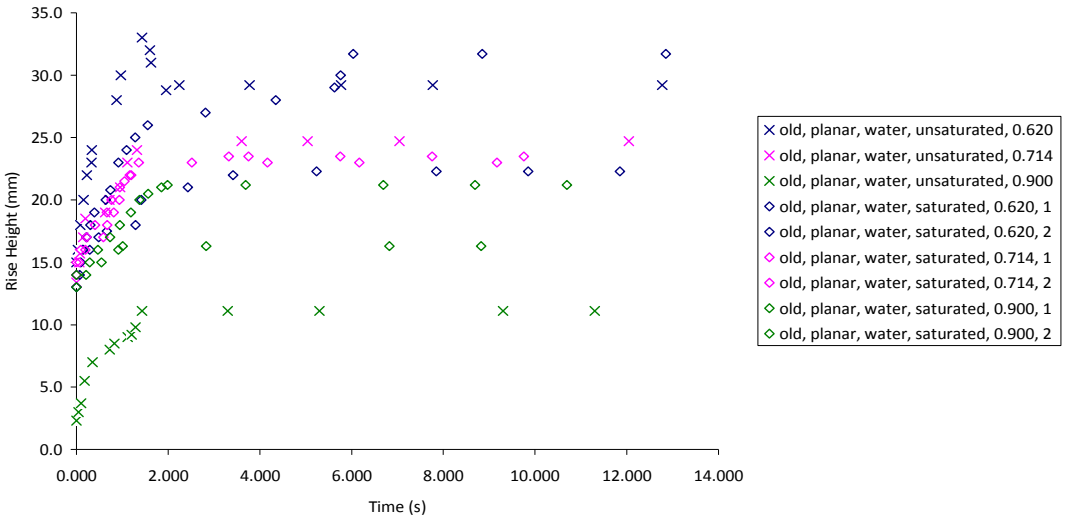

Figure 49: Effect of specimen saturation old planar water saturated and unsaturated

Results in figure 49 show that there is no significant difference between the results for the saturated and unsaturated specimens. It could be assumed that the saturated specimens would overall have a higher rise height than the unsaturated specimens as no fluid would be absorbed into the cement matrix either side of the crack plane.

Differences previously found in data show that with low absorption of fluid into a specimen the capillary rise height is higher than that of high absorption. Images in figure 35 show that the water does absorb into the matrix. This therefore must have significance on the overall rise height potentially decreasing the maximum achievable rise heights.

Looking at capillary rise for saturated and unsaturated, data shows that saturated flow is slower than for unsaturated specimens. This shows that the attractive forces need to develop between the flow agent and the capillary wall to enable the fluid to rise. The development of these forces would be disrupted by the presence of water on the boundary therefore a reduced capillary driving force.

4.6 Main concluding results

Below the equivalent planar crack aperture for natural cracks and the effectiveness of cyanoacrylate to heal has been investigated. This has been completed to determine how reliable the experimental work would be to determine flow through natural cracks in concrete.

4.6.1 Equivalent planar crack for natural cracks

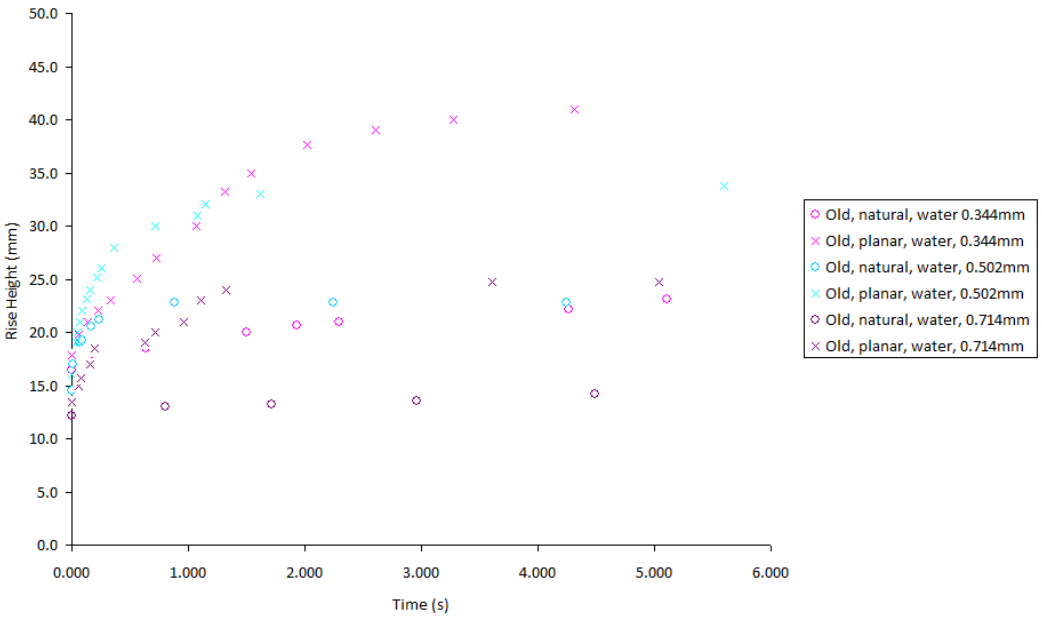

Figure 50: Comparison of natural cracks for planar cracks

Comparisons between natural crack rise height and planar crack rise heights have been made to determine the reliability of results. Therefore, in future fluid flow can be determined for all healing agents with natural cracks based on planar experiments.

Figure 50 clearly shows that the natural crack flow is considerably lower than planar fluid flow. There is a clear correlation between the change in rise height for a natural crack and a planar crack for all crack apertures. Taking forward this information a relationship between a natural crack aperture and a planar crack rise height can be determined.

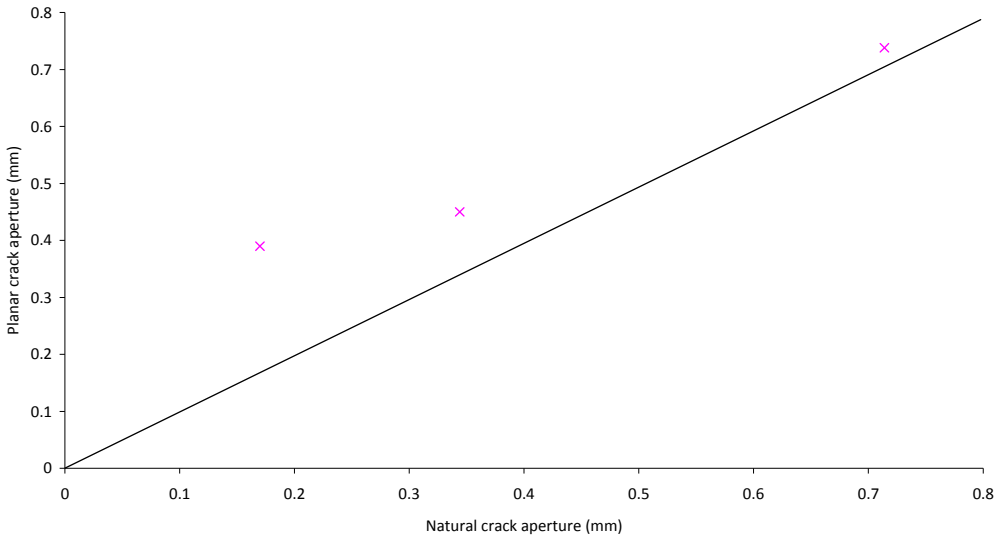

Figure 51: Graph of planar crack aperture compared to natural crack aperture

The rise heights for a series of natural cracks have been examined to determine whether it is possible to predict the capillary rise height for a natural crack of known aperture using an equivalent planar aperture in equation 5.1. The relationship between capillary rise in natural cracks and in an equivalent planar crack is given in figure 51. The relationship is of linear form and demonstrates that as the natural crack aperture increases, the effect of the crack tortuosity and crack surface roughness decreases until there is no observed difference between a natural crack and a planar crack. According to the experiments this appears to happen at a crack aperture greater than 0.3mm. However, without further investigation using wider apertures it is difficult to conclude whether this limit is accurate. This method can be used to determine any property for fluid flow through a natural crack using the properties of fluid flow through a planar crack.

Table 9: Crack aperture calculation

Crack width Natural Crack (mm)	Final rise height for natural crack (mm)	Equivalent planar crack aperture (mm)
0.170	37.5	0.390
0.344	23.3	0.450
0.714	14.2	0.738

4.6.2 Effectiveness of cyanoacrylate flow and potential to heal

Experiments using cyanoacrylate show a general trend that the initial rate of rise is quicker than that of water. Therefore, if a rapid heal is needed a healing agent with the same viscosity as cyanoacrylate should be used instead of one with a lower viscosity.

Other experimental results and readings show that the younger specimens tend to absorb more healing agent into the cement matrix. Therefore for rapid healing in cracks in cementitious materials, a young specimen with a crack aperture less than 0.5mm (as this is the bonding width of cyanoacrylate used) would be recommended.

4.7 Summary of conclusions

Research in this thesis has been completed by looking at different variables that can affect capillarity in cementitious materials. The key conclusions from the experimental work and data are listed below and how they can be applied to self healing mechanisms in cementitious materials is described.

- Crack aperture affects the overall rise height, with higher rise heights observed from smaller crack apertures as predicted by theory. However, the capillary rise height from natural crack apertures does not reach its theoretical value from all crack apertures examined. This may be due to surface roughness of the crack face or the change in surface tension as a result of the addition of fluorescein to the water.
- Results confirm that crack configuration does vary the rate of fluid rise height depending on the crack inclination. Therefore, to determine the fluid flow of a

healing agent through cementitious materials the crack geometry would need to be examined to allow the rate of capillary flow to be determined.

- The flow agent used experimentally does have an effect on the rate of rise due to its viscosity and using equation 5.1 only an approximation on how far the fluid will travel can be made.
- The degree of saturation and the age of the specimen only had an effect on the rate of capillary rise and not on the final level of capillary rise observed. This indicates that along with the degree of saturation and specimen age the healing potential of the self healing cementitious material will be dependant on the curing rate of the healing agent and its ability to flow into the crack before hardening.
- Experiments show that healing with cyanoacrylate occurs in a matter of seconds with a crack width less than 0.502mm. This indicates that natural cracks with a crack aperture less than 0.502mm can be successfully healed in autonomic healing systems. This was seen post experiment when the specimens with this crack width and below had successfully bonded.
- There appears to be a relationship between the final capillary rise height measured for natural cracks and the final capillary rise height predicted for an equivalent planar crack. For a crack aperture less than 0.5mm, the relationship between natural and planar crack apertures is not linear and therefore more experimental work would need to be undertaken to determine the nature of this relationship more accurately. However, it is shown that for crack apertures greater than 0.5mm a linear relationship is observed so therefore if a natural crack aperture is known the fluid rise through that crack can be determined based on a planar crack simulation.

Chapter 5

Theory and Validation of Experimental Results

5. 1 Basic capillary flow equations

Liquid flow against gravity through a capillary or narrow space, such as a thin tube, is known by capillary action or capillarity.

Capillary flow occurs due to the intermolecular forces between liquids and solid surrounding surfaces. As explained in Chapter 2, capillarity is caused by the joint action of the fluid surface tension and the adhesion between the fluid and the solid wall of the capillary.

The adhesion pulls the liquid column up until there is a sufficient mass of liquid for gravitational forces to overcome the intermolecular forces. The contact length (around the edge) between the top of the liquid column and the tube is proportional to the diameter of the tube, while the weight of the liquid column is proportional to the square of the tube's diameter, so a narrow tube will draw a liquid column higher than a wide tube.

The height *z* of a liquid column is given by;

$$z = \frac{2\gamma \cos\theta}{\rho g r} \tag{5.1}$$

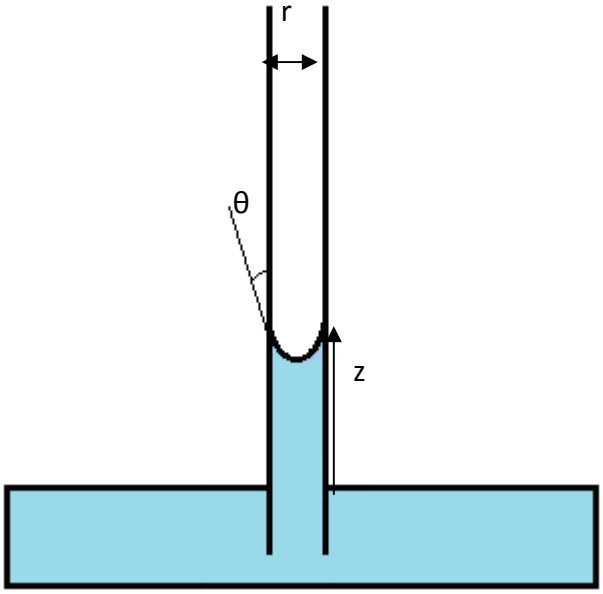

Figure 52: Image of a capillary demonstrating the capillary action formula (Young 2004)

where γ is the liquid-air surface tension in N/m, θ is the angle that the meniscus forms with crack/solid face in degrees, ρ is the density of liquid in kg/m^3, g is the force due to gravity acting on the fluid in the capillary in m/s^2, and r is radius of the capillary in mm and μ is the dynamic viscosity in Ns/m^2.

5.2 Analysis of the Lucas-Washburn equation

The Lucas-Washburn equation (L-W) (Hamraoui and Nylander. 2002) given below in equation 5.2, describes the dynamic flow of liquid in a capillary tube. The forces considered in the equation are the inertia, surface tension (adhesion), gravity, and dynamic viscosity.

$$\rho\pi r^2 \frac{\partial}{\partial t}\left(z(t)\frac{\partial z(t)}{\partial t}\right) = 2\pi r\gamma\cos(\theta) - \pi r^2\rho g z(t) - 8\pi\mu z(t)\frac{\partial z(t)}{\partial t} \qquad (5.2)$$

Where t is the time in seconds.

The L-W equation has been applied to capillary flow through porous materials Gospodinov (2005). The theory is considered in the context of the experimental arrangement shown in figure 52.

The difference in pressure between the liquid and gas, either side of the liquid surface in a capillary, i.e. either side of the meniscus, is termed the capillary pressure, which, for a round capillary tube, is given by

$$P_c = \frac{2\gamma\cos(\theta)}{r} \tag{5.3}$$

The inertia term in the L-W equation is considered negligible in most flow problems through porous media. Setting the inertia term to zero and dividing by the r^2 gives the following equation of capillary flow.

$$\frac{2\gamma\cos(\theta)}{r} - \rho g z(t) - \frac{8\mu z(t)}{r^2}\frac{\partial z(t)}{\partial t} = 0 \tag{5.4}$$

Young (2004) used this equation as a basis for developing an approach for modelling flow through planar cracks. Using equation 5.3 in equation 5.4**,** allowing for non-vertical cracks (see Fig 53) and replacing the surface velocity (dz/dt) with v(t), equation 5.4 becomes

$$P_c - \rho g z(t)\sin(\phi) - \frac{\mu}{k}v(t) = 0 \tag{5.5}$$

In which the permeability type term $k = r^2/8$

5.3 Numerical solution

A numerical solution of the flow equation has been used to create a numerical simulation to obtain theoretical results for the estimated rise height with respect to time to fluid flow through planar or tube capillaries in concrete.

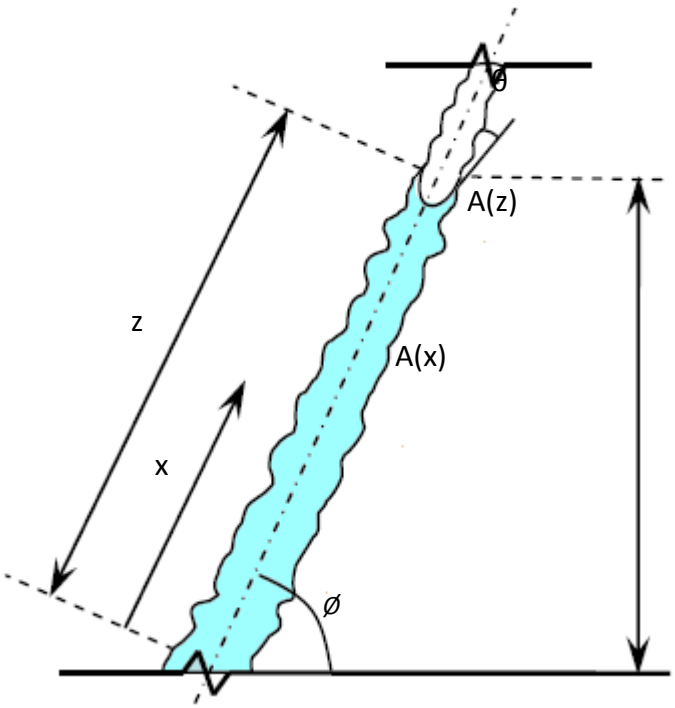

Figure 53: Tube in a reservoir (Joseph et al 2010)

x = coordinate from start of tube in reservoir

v(x) = velocity

A(x) = cross-section

P_c = capillary potential (-p at x=z)

The capillary pressure for a tube was given in equation 5.3, the equivalent expression for a planar opening, formed by a gap between two plates is as follows b = width of opening

$$P_c = \frac{2\gamma \cos\theta}{b} \text{ For plate} \qquad (5.6)$$

To allow for non-uniform capillaries, the last term in equation 5.5 must become an integral since the fluid velocity is no longer uniform along the length of the capillary. Rearranging equation 5.5 gives the following equation in the form presented by Young (2004).

$$\mu \int_0^z \frac{v(x)}{k} dx = \left(p_c - \rho g \sin\phi z\right) \qquad (5.7)$$

From the conservation of mass:

$$\frac{dz}{dt}A(z) = v(x)A(x) \tag{5.8}$$

Using 5.8 in 5.7 gives

$$\frac{dz}{dt} = \frac{1}{\eta}\left(p_c - \rho g \sin\phi z\right) \tag{5.9}$$

$$where \quad \eta = \mu A(z) \int_0^z \frac{1}{k}\frac{1}{A(x)}dx \tag{5.10}$$

For a planar opening, k takes the value $b^2/12$.

To make sure that the time of fluid flow is found, an initial value of z needs to be chosen, and therefore η can be evaluated.

5.3.1. Time stepping algorithm

Equation 5.9 is solved using a direct integration time-stepping procedure, which is outlined below

1. Chose Δt
2. Start with very small $z=z_0$

$t = t + \Delta t$

$where \quad \eta = \mu A(z) \int_0^z \frac{1}{k}\frac{1}{A(x)}dx$

$\Delta z = \frac{\Delta t}{\eta}\left(p_c - \rho g \sin\phi z\right)$

$z = z + \Delta z$

$\text{if } \Delta z < \text{tol}$

A check is undertaken to ensure that the time step is sufficiently small to give converged results.

5.4 Planar and Tapered capillary fluid flow

Fluid flow in a tapered opening thus can be predicted using the above equations and algorithm. This is used to determine the overall rise height z with time for different openings and tapers. This is all explained following in section 5.4.1.

5.4.1. Numerical solution of flow equation for planar and tapered fluid flow

A planar crack is where $b_h=b_o$ and a tapered crack, as shown in figure 54, is one for which there are two different crack openings, b_h and b_0. Using the same algorithm outlined in section 5.3.1, rise heights and time graphs for different crack openings have been calculated.

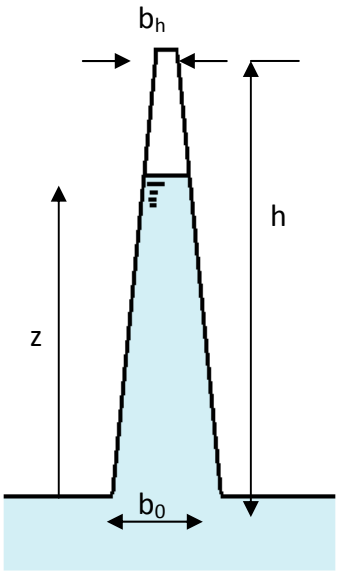

Figure 54: Tapered crack concept

Rise heights versus time graphs from the numerical solution of flow equation are compared with the experimental results for the tapered crack experiments and are shown in section 5.6 of this chapter.

5.5 Validation of the numerical model

The numerical solution involves using an explicit time stepping solution of the temporal equation. Convergence with respect to the time step was checked by reducing the step size until the predicted responses did not change by more than 1% with a halving of the time step.

Specifically, the solutions presented used a time step size of 0.0001s and if reduced to 0.00005s the predicted responses would be indistinguishable from each other on the numerical simulations shown.

In order to establish the generalised response of the system, the capillary flow of water predicted by equation 5.9, in two different glass capillary tubes of 0.3mm and 1.0mm diameter, is compared to that predicted by the standard Lucas Washburn equation.

The standard Lucas Washburn response was obtained by the numerical integration of equation 5.9. However, the numerical response, thus calculated, was checked against the analytical expression given by Fries and Dreyer (2008), with the results from the two calculations being the same to within the precision of the calculation and thus indistinguishable from each other on graphs in figure 55.

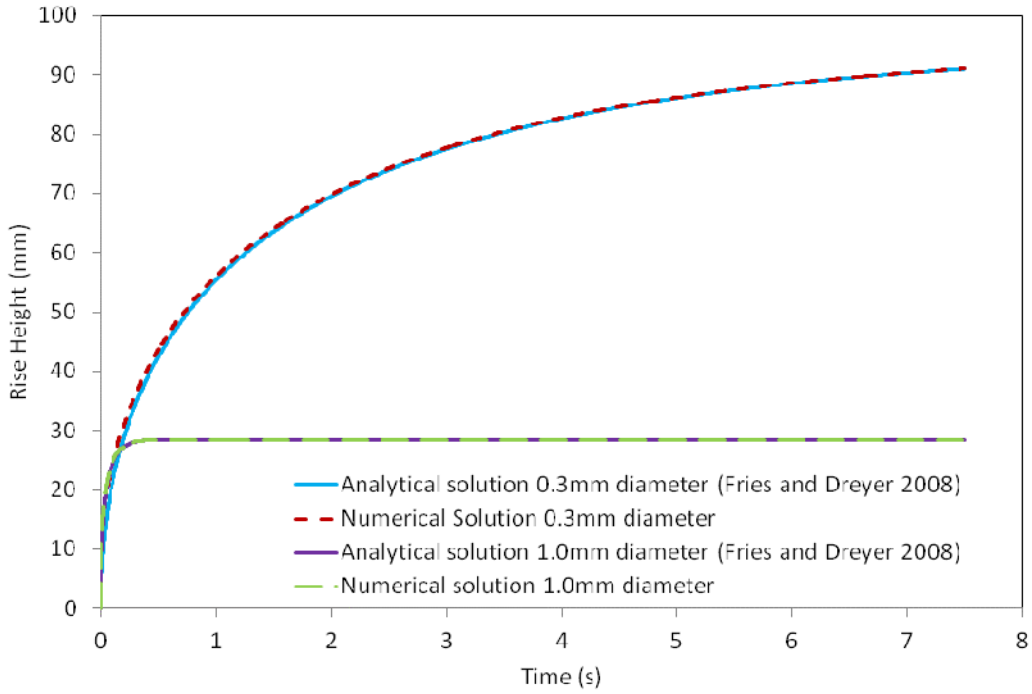

Figure 55: Validation of numerical model with analytical solution

Experimental validation of the numerical model was performed using capillary rise data recorded by Liou et al. (2009) for water in a glass capillary tube of known internal diameter. The parameters used to simulate the experimentally observed capillary rise, as reported by Liou et al. were γ = 0.070 N/m, θ = 30° ρ = 1000kg/m^3 and μ= 0.001 Ns/m^2. Good agreement between the experimental data and the numerical solution is observed for a capillary diameter of 0.1mm, as shown in figure 56. Also presented in Figure 56 is the rate of capillary rise calculated using the analytical solution to the Lucas Washburn equation from Fries and Dreyer (2008).

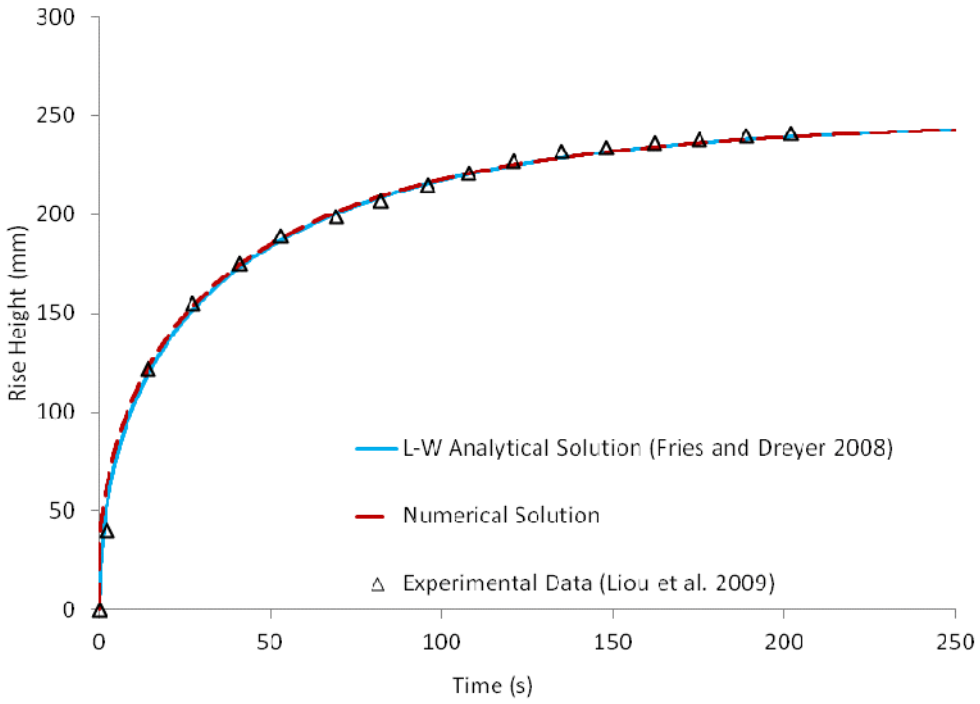

Figure 56: Validation of numerical model with experimental data from Liou et al. (2009)

5.6 Validation of experimental results with theory

This section of the thesis considers the experimental results presented in Section 4 and compares them with numerical flow simulations such that the validity of the model and results can be determined.

5.6.1 Planar fluid flow

In this section results for planar experiments described in chapter 4 are compared with those obtained from the numerical model described above.

5.6.1.1 Planar fluid flow water

Figure 57 displays results the experimental and numerical results for a crack aperture of 0.502mm.

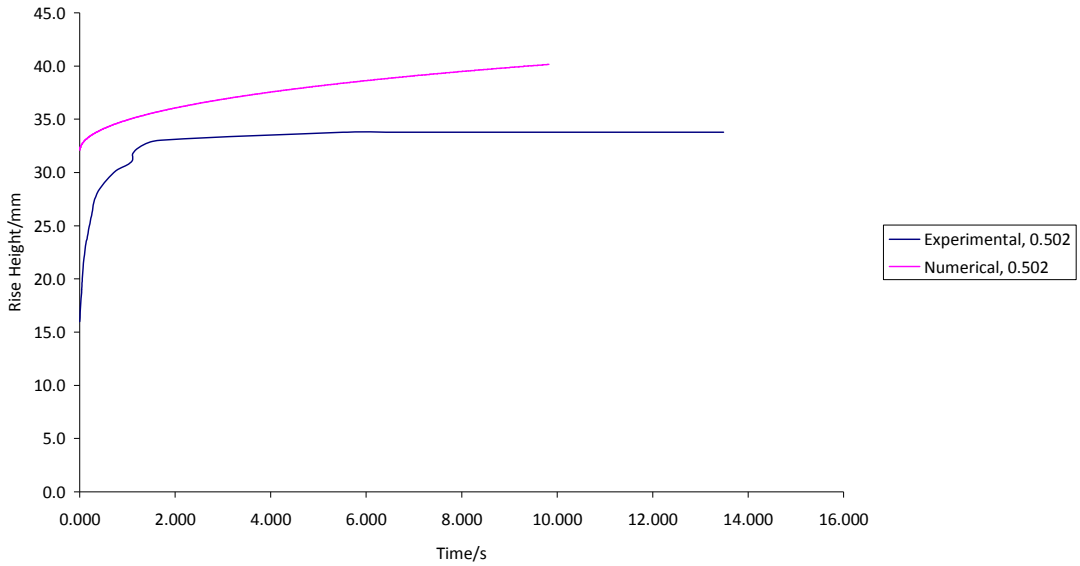

Figure 57: Experimental and numerical results for mature, planar, water with a crack aperture of 0.502mm

The graph shows that the difference between the experimental and numerical response is quite large both in terms of capillary response time and equilibrium rise height. However this could be due to a number of reasons.

As discussed in chapter four, the point taken from the graph starts from 12mm rise height and the time is a time not equal to zero seconds so therefore what is shown by the experimental results is not a full evaluation of capillary flow. However, the data has been corrected by alteration of the origin and the numerical results have been compared with these correct data.

The crack aperture also has shown to vary quite significantly in Chapter 4 which will have also affected the overall final capillary rise height and rate of rise.

5.6.1.2 Planar fluid flow cyanoacrylate

Planar fluid flow of cyanoacrylate has been considered in this section with a numerical solution of the flow equation, presented in Appendix D.

The next topic discussed is how the surface tension and contact angle of cyanoacrylate were determined. These properties were measured as they are a fundamental element of the equation of capillary flow.

The contact angles were measured directly from images of the liquid meniscus within a glass capillary tube, as illustrated in Fig 58.

The image in figure 58 shows the measured contact angle for cyanoacrylate having risen in a tube of radius, 0.315mm, an overall distance z, of 15.96mm. The contact angle between the meniscus of the cyanoacrylate and the tube was measured as 38˚. Three different tubes all of the same radius were used to calculate contact angles and an average value calculated. It was this average value that was used for the numerical simulations.

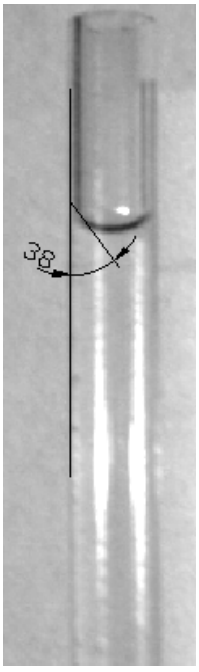

Figure 58: Capillary tube of radius, 0.315mm with a contact angle of 38˚

Equation 5.1 has been used to determine the surface tension. If it is rearranged, the surface tension can be calculated with it being the subject of the equation (equation 5.11);

$$\gamma = \frac{z\rho gr}{2(\cos\theta)} \tag{5.11}$$

The model also requires the viscosity. However, since the curing time for the cyanoacrylate is relatively short it was considered important to determine the change in dynamic viscosity over the duration of a test. Figure 59 shows that the flow changes dramatically for old, planar, cyanoacrylate with a crack aperture of 0.502mm.

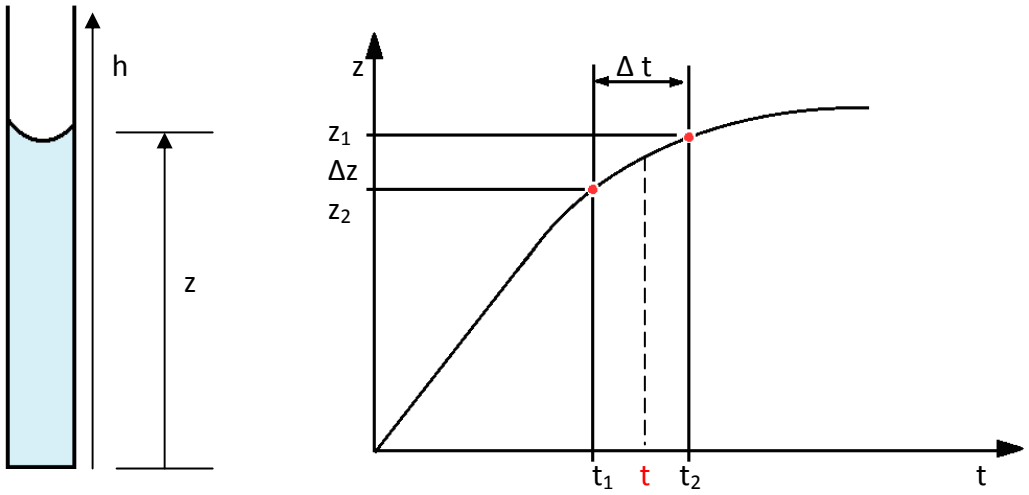

Figure 59: Image of capillary tube and theoretical graph of rise height, z versus time, t

For a thin capillary tube the viscosity can be calculated by cor 2 ing equation 5.9 at time t over a time interval t_1 to t_2 noting that $\Delta t=t_2-t_1$. In this discretized form, equation 5.9 becomes:

$$\frac{z_2 - z_1}{\Delta t} = -\frac{k}{\mu}(p_c - pg(\frac{z_1 + z_2}{2})) \tag{5.12}$$

Rearranging equation 5.12 for the viscosity gives:

$$\mu = -k\frac{\Delta t}{z_2 - z_1}(p_c - pg(\frac{z_1 + z_2}{2})) \tag{5.13}$$

Table 8: Calculation of viscosity

Point	g (m/s^2)	Change in time (s)	k (mm^2x10^{-8})	r (mm)	θ (˚)	Surface tension γ (N/m)	p_c (N)	μ ($Ns/m^2 x10^{-3}$)
1	9.81	0.040	2.1	0.000502	39	0.032	0.099	0.214
2	9.81	0.048	2.1	0.000502	39	0.032	0.099	0.239
3	9.81	0.088	2.1	0.000502	39	0.032	0.099	0.236
4	9.81	3.000	2.1	0.000502	39	0.032	0.099	117.8

Results for the case of a planar crack in mature concrete for an opening of 0.502mm were computed for the following three time intervals 0.016s to 0.056s, 0.088s; to 0.136s and 1.232s to 1.320s. These results are summarised in Table 8.

Figure 60 shows the experimental and the numerical graphical results for capillary flow of cyanoacrylate through a planar crack.

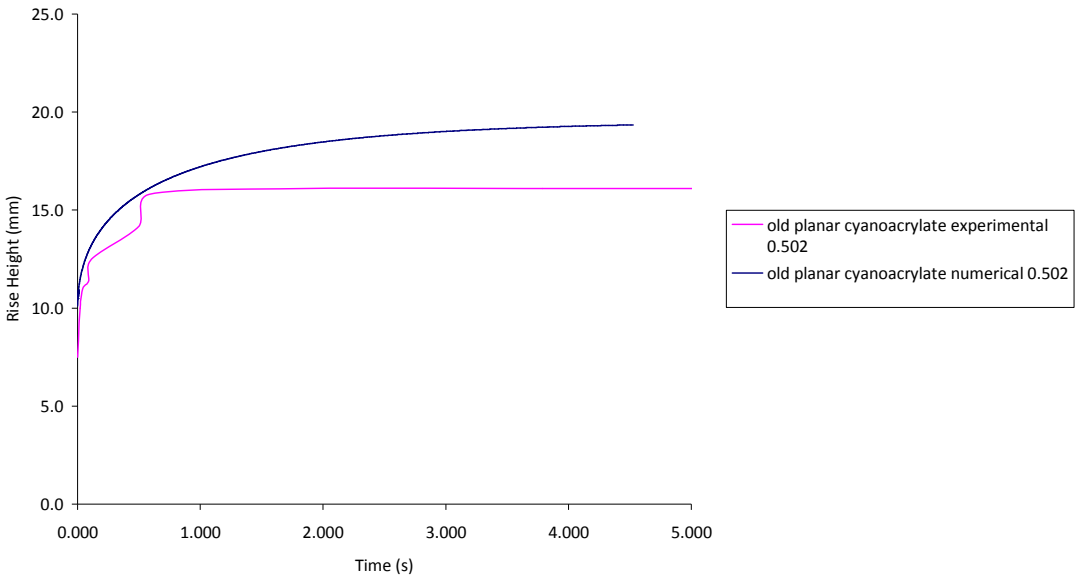

Figure 60: Experimental and numerical results for old, planar, cyanoacrylate with a crack aperture of 0.502mm.

It is evident that yet again there is a difference in final rise height between the numerical and experimental results and readings. An overall difference between the

two is approximately 6mm. This yet again could be due to the changes in the initial point of measurement as spoken about previously.

5.6.2 Tapered fluid flow

Fluid flow in a tube or crack where b_0 is not equal to b_h can be defined as tapered flow. The next two following sections take results from the results chapter 4 and compare them to the numerical values created with the numerical solution given in Appendix D.

5.6.2.1 Tapered fluid flow water

This section discusses the differences found between the numerical and the experimental models for tapered fluid flow in mortar specimens.

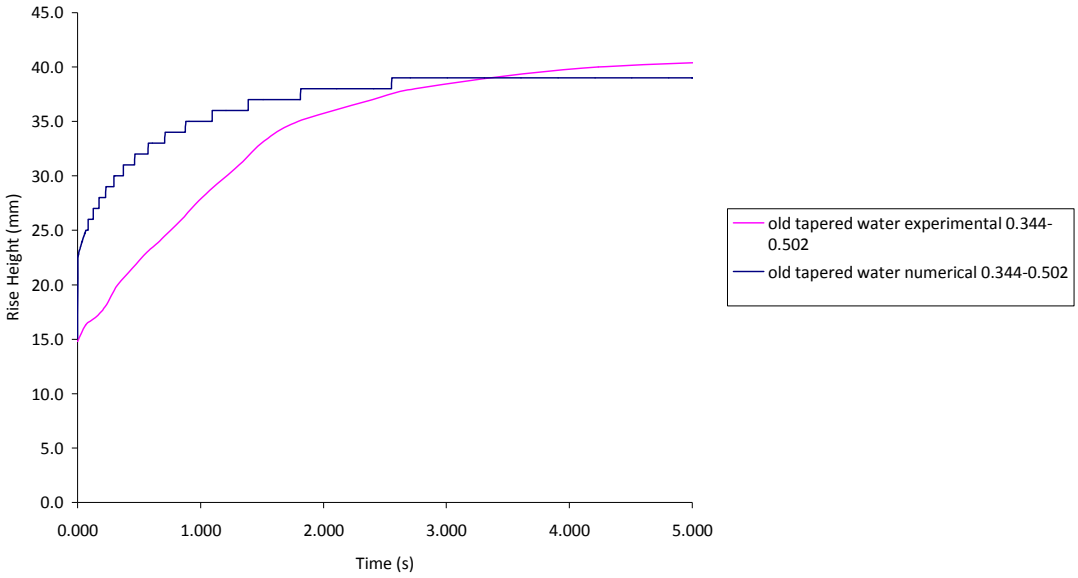

Figure 61: Old, tapered, water 0.344-0.502mm crack aperture for experimental and numerical work

Figure 61 presents the numerical and the experimental results graphically so that the difference between flow rates can be looked at in detail.

The rates of flow, i.e. the gradient for each of the experiments, are shown to be somewhat similar. Therefore, the numerical model validates the flow rate is at a

similar value to that of the experimental. It can be seen that the final rise heights are also in a similar region of value. The differences could be based on how absorption into the cement matrix is not taken into consideration in the model which would affect the overall final rise height by a significant amount. There is still evidence, in figure 61, that additional simulations and amendments are required to accurately model the capillary rise response.

5.6.2.2 Tapered fluid flow cyanoacrylate

Here capillary flow is assessed with cyanoacrylate as the flow agent in experimental and numerical work is looked at in detail.

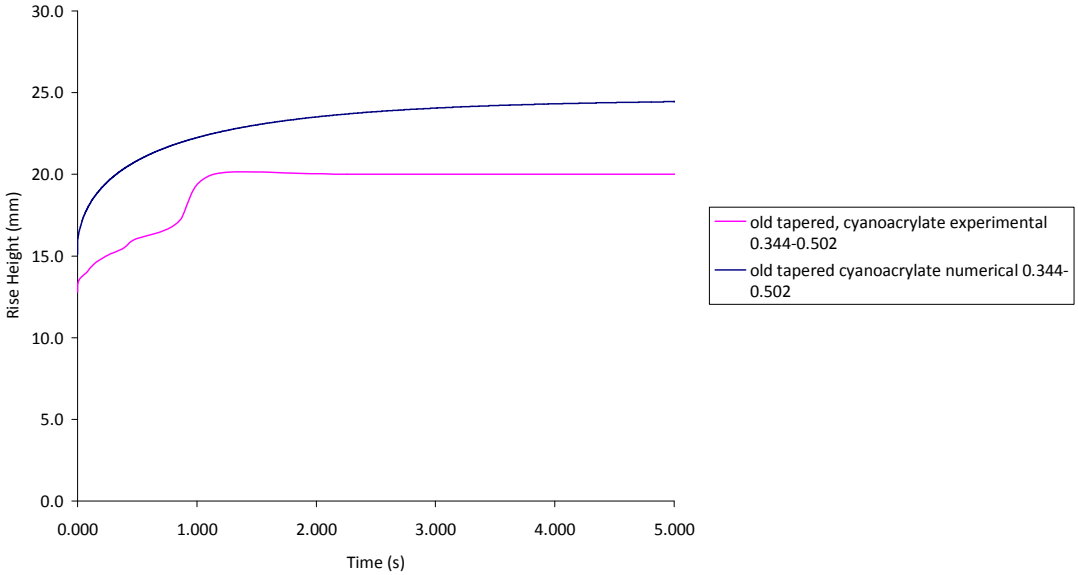

Figure 62: Old, tapered, cyanoacrylate 0.344-0.502mm crack aperture for experimental and numerical work

Similarly to tapered fluid flow of water as to tapered fluid flow of cyanoacrylate, the gradient from 0-1 seconds are similar, indicating that the numerical solution represents the experimental results and readings properly

5.7 Conclusions

The theory in this chapter gives the correct general behaviour. However, further work would be needed to explore the capillary and resistance forces active in this system in order to derive modifications which would allow the experiments to be simulated accurately.

It is evident that the experimental rise heights are lower than the theoretical rise heights. Results also show that the standard Lucas-Washburn theory over estimates the rate and rise height for capillary flow.

Chapter 6

Conclusions and further work

6.1 Introduction

The work reported in this thesis endeavoured to examine some of the factors which affect capillarity through cementitious materials.

The main objectives of this study were detailed in Chapter 1. These objectives covered four areas of investigation and these were detailed in chapter 4 which analyse the experimental results:

1. Effect of crack configuration
2. Effect of flow agent
3. Effect of specimen age
4. Effect of specimen saturation

A detailed review of relevant literature was presented in Chapter 2 and Chapter 5 presented observations made based on the numerical models relating to the experimental work. This comes under the section 5.6 Validation of experimental results.

6.2 Conclusions

The conclusions from each of the investigations have been given at the end of the results chapter. However, a summary of the conclusions is presented here.

6.2.1 Capillary flow experimentation and conclusions

The conclusions in Chapter four state that although the overall experimental procedures were successful for producing some results and readings, however, there are a few issues that could be resolved and are listed below:

- Chapter 4 shows that the data on the graphs starts recording capillary flow mid flow. It is hard to determine when capillary rise through the different crack configurations starts. This is due to the time at which the fluid is poured into the tray and also determining the actual rise height by where capillary action starts. One way to overcome these issues would be to either use a clear scale, where the markings could still be seen and also raising the specimen having the fluid reservoir at the base of the specimen so full capillary flow can be captured. Therefore, the capillary action can be monitored initially from 0 and a full capture of capillary flow can be determined.

6.2.2 Effect of crack configuration

The effect of crack configuration on capillary rise response is one of the variables that has been looked at in detail in this thesis. Simulations of planar, tapered, tortuous and natural cracks are looked at.

- The general trends in the results show that after experimentation where there is a large change in weight there is a lower overall maximum rise height achieved for that particular crack aperture.
- Some results and readings show that using formula 5.1 demonstrating capillary flow that the expected rise height for a crack aperture, the maximum rise height is considerably less. This may be attributed to the actual crack aperture being larger than anticipated.

- Results do show some validity as the natural water experiments show consistency with theory that the greater the crack width of the capillary the lower the overall rise height.
- Unlike the planar or tapered experiments where there is a smaller crack width, it takes longer for fluid flow to reach the maximum rise height; the natural experiments do not display any significant difference in the time taken to achieve maximum rise height.
- Results do not show significant changes in overall maximum rise height for capillary flow for the 3 nodes and 5 nodes tortuous experiments.

6.2.3 Effect of flow agent

Looking at how flow agents affect capillarity with the changes in surface tension and viscosity is an area that has been discussed and explored in chapter 4. The key conclusions from the results are presented below:

- Fluid flow of water shows to have on the whole a larger rate of progression through the simulated capillaries compared to cyanoacrylate. This can be attributed to the low interaction of water with the surfaces together with lower viscosity.
- Cyanoacrylate in the results shows that through capillary flow that there is a significant change in the overall maximum rise height, due to the curing effect that cyanoacrylate has when it comes into contact with air.
- However, when cyanoacrylate is compared to xanthan gum, a fluid with the same density and surface tension properties of cyanoacrylate but without the curing effect, it can be seen that a higher maximum rise height is achieved.

6.2.4 Effect of specimen age

Specimen age is another area of experimentation that has been looked at in detail and yet again the key conclusions presented here:

- Results from experimental work comparing mature and young specimens show that higher capillary flow is achieved for both cyanoacrylate and water in mature specimens.
- For the healing agent to penetrate far into the cracks of cracked concrete specimens, it is therefore concluded that fluid flow of healing agents in mature specimens is better than that in young specimens.
- Comparisons between old and young mortar specimens show that rates of rise are faster in mature mortar specimens than young mortar specimens. This can be attributed to less fluid being absorbed into the cement matrix of a mature specimen.
- Younger specimens show more fluid being absorbed into the cement matrix therefore is good for early age healing.

6.2.5 Effect of specimen saturation

Results and readings in saturated experiments show that there is not a large difference in overall rise heights for saturated or unsaturated specimens. Therefore in the context of how far fluid flows in specimens that need to 'heal' the cracks there would not be a difference in how far the fluid travels based on saturation.

6.3 Numerical models and validity of results

The conclusions for the numerical solutions based on flow through cracks are stated here. Each separate solution and the validity of the results presented in section 5.6 are also touched on.

The numerical solutions of planar and tapered flow are successful in that for any crack aperture, flow agent; graphical results of final rise heights and capillary pore pressures are calculated based on the theory presented through the work of Young (2004).

However, due to the problems occurring of the origins of the graphical results produced from experimental work, comparing these with the numerical simulation graphical has not been very successful. There are many issues that could affect the results produced through the numerical solutions. These are listed below:

- The angle of crack inclination, viscosity of cyanoacrylate and the contact angles for each flow agent used have been calculated experimentally and are not values that the solutions can depend on.
- This is as the experimental values could potentially show some inaccuracy and would therefore affect the numerical simulation of flow.
- These issues are reflected in chapter 5.6 were the validity of the results is discussed more in depth.

6.4 Recommendations for further work

There are many areas that have been touched upon in Chapter 2 where all of the gaps have been noted throughout literature. Chapters 3 – 5 state how the work completed in this thesis has endeavoured to address the shortcomings of this particular research field.

Even though the gaps have been looked at and ways to overcome areas in research filled there are some areas that could be built upon experimentally and numerically.

Ideas for further work are presented below looking individually at experimental and numerical studies:

- In this study only two flow agents have been used. Therefore it would be beneficial to use a larger variety of flow agents with different properties such as surface tension and viscosity.
- Other fluids that have been found to be used more in practise are epoxy resins, PFA in solution and GGBS in solution. Therefore, these could be used to investigate flow properties of other healing agents through cementitious materials.
- Models of sinusoidal capillaries simulated by Gospodinov (2005) simulate different crack apertures of capillaries of varying tortuosity. A potential for further experimentation could be creating different types of capillaries to compare them with the numerical solutions.
- Joseph et al.'s work (2009) spoken about in Chapter 2, show that natural cracks of similar magnitude are looked at for one type of flow agent. Therefore to examine more crack apertures for natural experiments and to find an experimental procedure where the fluid front of cyanoacrylate can be detected in natural specimens.
- Numerical work in this thesis has looked at different flow agents as the viscosity and surface tension parameters could be modified. However, the numerical solutions of flow in this thesis given in appendix C have not included the absorption rates into the cement matrix. Therefore, in future, absorption rates would need to be considered to produce a more accurate model.

References

Azari, M. M., Mangat, P.S. and Tu S.C. 1993. Chloride ingress in microsilica concrete. *Cement and Concrete Composites* 15(4), pp. 215-221.

Bahramian, A. and Danesh, A. 2004. Prediction of solid–fluid interfacial tension and contact angle. *Journal of Colloid and Interface Science,* 279 (1), pp. 206-212.

Erlin, B and Hine, W. 2004. Carbonation of concrete [Online]. Available: http://findarticles.com/p/articles/mi_m0NSX/is_8_49/ai_n6170202/. [Accessed: 12th November 2011]

Cabrera, J. G. 1996. Deterioration of concrete due to reinforcement steel corrosion. *Cement and Concrete Composites* 18(1), pp. 47-59.

Concrete repairs, volume 2, Palladian Publications Limited, 11 Grosvenor Cresent, London, SW1X 7EE, printed by Williams press, Berkshire limited, Maidenhead, Berkshire, England. 1986

Corporatewatch. The construction sector: a brief overview See http://www.corporatewatch.org/?lid=262 for further details. [Accessed 04/06/2009.]

Fries, N. and Dreyer, M. 2008. The transition from inertial to viscous flow in capillary rise. *Journal of Colloid and Interface Science* 327(1), pp. 125–128.

Funada, T. and Joseph, D. D. 2002. Viscous potential flow analysis of capillary instability. *International Journal of Multiphase Flow* 28(9), pp. 1459-1478.

Gardner, D. R., Jefferson, A. D. and Lark, R. J. 2008. An experimental, numerical and analytical investigation of gas flow characteristics in concrete. *Cement and Concrete Research*, 38(3) pp. 360-367.

Gardner, D., Hoffman, A. and Jefferson, A.D., 2011, Capillary flow of healing agents in discrete cracks in cementitious materials. *3rd International Conference on Self-Healing Materials. Bath, UK*

Gospodinov, P. N. 2005. Numerical simulation of 3D sulfate ion diffusion and liquid push out of the material capillaries in cement composites. *Cement and Concrete Research* 35(3), pp. 520-526.

Gowripalan, N., Sirivivatnanon, V., Lim. C.C., 2000. Chloride diffusivity of concrete cracked in flexure. *Cement and Concrete Research* 30(5), pp. 725-730.

Granju, J.-L. and Balouch, S. U. 2005. Corrosion of steel fibre reinforced concrete from the cracks. *Cement and Concrete Research* 35(3), pp. 572-577.

Halstead, P.E., Durability of concrete, Construction Publications Ltd, elm house, elm street, London WC1X 0BP. Civil Engineering, Building and Reinforced Concrete contractor. A supplement to the consulting engineer, April/May 1971.

Hamaroui, A. & Nylander, T. 2002. Analytical Approach for the Lucas-Washburn Equation. *Journal of Colloid and Interface Science,* 250(2), pp. 415-421.

Hannant, D. J. and Keer, J. G. 1983. Autogenous healing of thin cement based sheets. *Cement and Concrete Research* 13(3), pp. 357-365.

Hanzic, L., Kosec, L. and Anzel , I. 2010. Capillary absorption in concrete and the Lucas-Washburn equation. *Cement and Concrete Composites*, 32(1), pp., 84-91.

Hoffman, A. 2009; An investigation into capillary flow in cementitious materials. Third Year Undergraduate BEng Project, Cardiff University School of Engineering, Cardiff University.

Jefferson, A., Joseph, C., Lark, R., Issaacs, B., Dunn, S. & Weager, B. 2010. A new system for crack closure of cementitious materials using shrinkable polymers. *Cement and Concrete Research,* 40(5), pp. 795-801.

Jonkers, H. 2010. Bio-Concrete:A Novel Bio-Based Material European Council of Applied Sciences and Engineering, U.S. National Academy of Engineering, EU-US Frontiers of Engineering Symposium, Cambridge, U.K.

Joseph, C., Gardner, D., Jefferson, A, Lark, R and Isaacs, B. 2010. Self Healing Cementitious Materials. *Proceedings of the ICE - Construction Materials*. 164(1), pp. 29-41.

Lepech, M. D. and Li, V. C. 2009. Water permeability of engineered cementitious composites. *Cement and Concrete Composites* 31(10), pp. 744-753.

Li V.C., Lim Y.M. and Chan Y.-W. 1998. Feasibility study of a passive smart self-healing cementitious composite. *Composites Part B: Engineering* 29(6), pp. 819-827.

Liou, W. W., Peng Y. and Parker, E. 2009. Analytical modeling of capillary flow in tubes of nonuniform cross section. *Journal of Colloid and Interface Science* 333(1), pp. 389-399.

Marshall A.L. (1990) Behaviour of Plain Concrete. In *Marine Concrete*. Blackie, Glasgow & London, 1990, pp. 122-211.

Martys, N. S. and Ferraris, C. F. 1997. Capillary transport in mortars and concrete. *Cement and Concrete Research,* 27 (5), pp. 747-760.

McAlpine, K. 2010. *For self-healing concrete, just add bacteria and food* [Online]. Available at: http://www.newscientist.com/article/dn19386-for-selfhealing-concrete-just-add-bacteria-and-food.html [Accessed: 05th April 2011]

Neville, A. M. Properties of Concrete. 1999. 2nd Edition. Pearson Education Ltd, Essex.

Qian, S., Zhou, M.R. de Rooij., Schlangen, E., Van Breugel G. and K. van Brugel. 2009. Self-healing behavior of strain hardening cementitious composites incorporating local waste materials. *Cement and Concrete Composites* 31(9), pp. 613-621.

Roels, S., Vandersteen, K. and Carmeliet, J. 2003. Measuring and simulating moisture uptake in a fractured porous medium. *Advances in Water Resources*, 26(3) pp. 237-246.

Song, H-W., Lee, C-H. and Ann, K. Y. 2008. Factors influencing chloride transport in concrete structures exposed to marine environments. *Cement and Concrete Composites* 30(2), pp. 113-121.

Song, H.-W. and Kwon, S.-J. 2007. Permeability characteristics of carbonated concrete considering capillary pore structure. *Cement and Concrete Research* 37(6), pp. 909-915.

Song, H.-W. Kwon, S-J. Byun, K. Park. C-K. 2006. Predicting carbonation in early-aged cracked concrete. *Cement and Concrete Research* 36(5), pp. 979-989.

Steffens, A. 2002. Modeling carbonation for corrosion risk prediction of concrete structures. *Cement and Concrete Research* 32(6), pp. 935-941.

Stevens, N., Dinkler D. and Ahrens, H. 2009. The uniform capillary model for packed beds and particle wettability. *Journal of Colloid and Interface Science* 337(1), pp. 162-169.

Van Tittelboom, K. De Belie, N, De Muynck, W. and Verstraete W. 2010. Use of Bacteria to Repair Cracks in Concrete. *Cement and Concrete Research* 40(1), pp. 157-166.

Vidal, T. Castel, A. François , R. 2007. Corrosion process and structural performance of a 17 year old reinforced concrete beam stored in chloride environment. *Cement and Concrete Research* 37(11), pp. 1551-1561.

Young, W.-B. 2004. Analysis of capillary flows in non-uniform cross-sectional capillaries. *Colloids and Surfaces A: Physicochemical and Engineering Aspects,* 234(1-3) pp. 123-128.

Zhmud, B. V., Tiberg. F. and Hallstensson K. 2000. Dynamics of Capillary Rise. *Journal of Colloid and Interface Science* 228(2), pp. 263-269.

APPENDIX A

- **Experimental information**

Age of specimen	Crack type	Fluid used	Crack aperture (mm)	Quantity of tests for each crack aperture
Old	Planar	Water	0.094 0.110 0.237 0.254 0.261 0.344 0.502 0.620 0.714 0.900 1.170	4 3 4 3 2 3 3 3 3 1 1
Old	Tapered	Water	0.094 0.110 0.237 0.344 0.502 0.714 0.900	3 3 3 3 2 3 3
Old	Tortuous 3 nodes	Water	0.094 0.170 0.254 0.344 0.502 0.714 0.900	3 3 3 2 3 3 1
Old	Tortuous 5 nodes	Water	0.094 0.170 0.280 0.344 0.502 0.714 0.900	3 3 3 3 3 3 1
Old	Natural Crack	Water	0.170 0.280 0.344 0.502 0.620 0.714	4 1 1 1 3 1

Age of specimen	Crack type	Fluid used	Crack aperture (mm)	Quantity of tests for each crack aperture
Old	Planar	Cyanoacrylate	0.110 0.261 0.344 0.502 0.714 1.214	2 3 2 2 3 2
Old	Tapered	Cyanoacrylate	0.094-0.110 0.110-0.254 0.254-0.344 0.344-0.502 0.502-0.714 0.254-0.714	3 1 2 3 3 2
Old	Tortuous 3 nodes	Cyanoacrylate	0.170 0.344 0.502 0.714	1 3 3 3
Old	Tortuous 5 nodes	Cyanoacrylate	0.094 0.170 0.344 0.502 0.714	2 3 2 3 2
Young	Planar	Water	0.094 0.110 0.344 0.502 0.714 0.900	1 1 3 3 3 3
Young	Tapered	Water	0.094-0.170 0.170-0.280 0.280-0.502 0.502-0.714 0.714-0.900 0.094-0.502	1 1 1 1 1 1
Young	Planar	Cyanoacrylate	0.261 0.344 0.502 0.714	1 1 1 1
Young	Tapered	Cyanoacrylate	0.094-0.170 0.170-0.280 0.280-0.502 0.502-0.714 0.714-0.900 0.094-0.502	1 1 1 1 1 1
Old	Planar	Xanthan Gum	0.170	1

Age of specimen	Crack type	Fluid used	Crack aperture (mm)	Quantity of tests for each crack aperture
			0.280 0.344 0.502	1 1 1
Old, Saturated	Planar	Water	0.620 0.714 0.900	1 1 1

APPENDIX B

Data sheets

1. **Cyanoacrylate technical data**

CYANOTEC TECHNICAL DATA FOR PC 20

TYPICAL APPLICATIONS

PC 20 is specially formulated for the bonding of plastics, rubbers, wood, metals and other common substrates. Recommended for use on assemblies with very close fitting parts and smooth, even surfaces.
Can be used as a post-assembly adhesive to wick into parts.

PRODUCT DESCRIPTION

Procure PC 20 is a very low viscosity (5 cPs) modified Ethyl Cyanoacrylate adhesive.
PC 20 is suitable for bonding a very wide range of materials, including some porous ones, where very fast cure speed is required.

PROPERTIES OF UNCURED MATERIAL

		Value
Chemical type		Ethyl
Appearance		Clear
Specific Gravity		1.06
Viscosity cPs[1]		
– range		2-5
– typical value		4
Tensile Strength[2]	(N/mm^2)	21
Fixture Time	(secs)	1-20
Full Cure	(hours)	24
Flash Point	(°C)	> 85
Shelf Life @ 5°C	(months)	12
Max Gap Fill	(mm)	0.05
Operating Temperature Range	(°C)	-50 to +80

[1] ISO 3104/3105
[2] ISO 6922

TYPICAL CURING PERFORMANCE

Typical Speed:

Steel/steel	<15 seconds
ABS/ABS	<5 seconds
Rubber/Rubber	<5 seconds
Wood (balsa)	<3 seconds

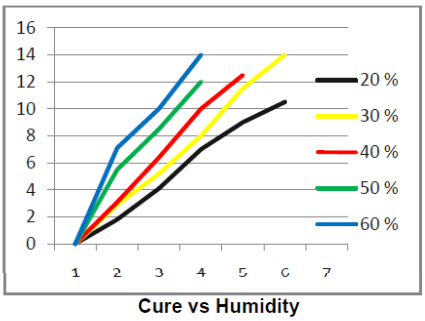

Cure vs Humidity

Cure speed vs. environmental conditions

Cyanoacrylates require surface moisture on the substrates in order to initiate the curing mechanism. The speed of cure is reduced in low-humidity conditions. Low temperatures will also reduce cure speed. All figures relating to cure speed are tested at 21°C .

Cure speed vs. substrate

The speed of cure of Cyanoacrylates varies according to the substrates to be bonded. Acidic surfaces such as paper and leather will have longer cure times than most plastics and rubbers. Some plastics with very low surface energies, such as polyethylene, polypropylene and Teflon® require the use of Procure 77 Primer
(see PC 77 TDS for further info).

Cure speed vs. activator

Activators 780 and 750 may be used in conjunction with cyanoacrylates where cure speed needs to be accelerated.

Cure speeds of less than 2 seconds can be obtained with most cyanoacrylates.

The use of an activator can reduce the final bond strength by up to 30% Testing on the parts to measure the effect is recommended.

Cure speed vs. bond gap

PROCURE/REACT Cyanoacrylates give best results on close fitting parts. The product should be applied in a very thin line in order to ensure rapid polymerisation and a strong bond. Excessive bond gaps will result in slower cure speeds. PROCURE / REACT Cyanoacrylate Activators may be used to greatly increase cure speeds
(see PC780 and PC750 TDS for further info).

TYPICAL ENVIRONMENTAL RESISTANCE HOT STRENGTH

PROCURE/REACT cyanoacrylates are suitable for use at temperatures up to 80°C. At 80°C the bond will be approximately 70% of the strength at 21°C. The bond strength at 100°C is approximately 50% of full strength at 21°C.

CYANOTEC LTD
Bay 2 building 62 Third Avenue Pensnet Trading Estate Dudley DY67XT
TEL 0845 618 3120 FAX 0845 618 3121 EMAIL SALES @CYANOTEC.COM

PC20
V1.2
OCT 08

CYANOTEC TECHNICAL DATA FOR PC 20

Chemical / Solvent Resistance
Cyanoacrylates exhibit excellent chemical resistance to most oils and solvents including motor oil, leaded petrol, ethanol, propanol and freon.
Cyanoacrylates are **not** resistant to high levels of moisture or humidity over time.

STORAGE

Store in a cool area out of direct sunlight. Refrigeration to 5° C gives optimum storage stability.

REMOVAL OF CURED CYANOACRYLATE

Cured cyanoacrylate may be removed from most substrates, and parts disassembled, with a Debonder.
It is not possible to fully remove cyanoacrylate from fabrics

PRESENTATION Cyanoacrylates are supplied in 20g,50g,500g and bulk packs

DIRECTIONS FOR USE

Bond speed is very fast so ensure that parts are properly aligned before bonding.

Activators may be required if there are gaps or porous surfaces. Some plastics may require application of Primer.

Ensure parts are clean, dry and free from oil and grease.

Product is normally hand applied from the bottle. Apply sparingly to one surface and press parts firmly together until handling strength is achieved. As a general rule, as little cyanoacrylate as possible should be used – over application will result in slow cure speed and lower bond strength.

Please contact your representative for further advice on dispensing solutions.

GENERAL INFORMATION

For safe handling of this product consult the Material Safety Data Sheet.

NOTES AND DISCLAIMER
The information contained herein is produced in good faith and is believed to be reliable but is for guidance only. CYANOTEC Ltd. and its agents cannot assume liability or responsibility for results obtained in the use of its product by persons whose methods are outside or beyond our control. It is the user's responsibility to determine the suitability of any of the products and methods of use or preparation prior to use mentioned in our literature and furthermore the user's responsibility to observe and adapt such precautions as may be advisable for the protection of personnel and property in the handling and use of any of our products.

CYANOTEC LTD
Bay 2 building 62 Third Avenue Pensnet Trading Estate Dudley DY67XT
TEL 0845 618 3120 FAX 0845 618 3121 EMAIL SALES @CYANOTEC.COM

PC20
V1.2
OCT 08

Section 11: Potential respiratory effects information was deleted.
Section 11: Potential effects from ingestion information was deleted.
Section 11: Potential effects from skin contact information was deleted.
Section 12: No data available information was deleted.
Section 12: Environmental risk information was deleted.
Section 6: Personal precautions information was deleted.
Section 6: Environmental procedures information was deleted.
Section 6: Methods for cleaning up information was deleted.
Section 2: Other hazards heading was deleted.
Section 2: Notes on labelling heading was deleted.
Reference to R phrase explanation in Section 16 was deleted.
Section 16: Restrictions on use was deleted.

DISCLAIMER: The information on this Safety Data Sheet is based on 3M's experience and is correct to the best of 3M's knowledge at the date of publication. 3M does not accept liability for any loss, damage or injury resulting from its use (except as required by law). The information may not be valid for any use not referred to in this Data Sheet or use of the product in combination with other materials. For these reasons, it is important that customers carry out their own test to satisfy themselves as to the suitability of the product for their own intended applications.

3M United Kingdom MSDSs are available at www.3M.com/uk

APPENDIX C
EXPERIMENTAL DATA AND RESULTS

Graphical results and readings:

1. **Old Planar Water**
2. **Old Tapered Water**
3. **Old Tortuous 3 and 5 Nodes Water**
4. **Old Natural Water**
5. **Old Planar Cyanoacrylate**
6. **Old Tapered Cyanoacrylate**
7. **Old Tortuous 3 and 5 Nodes Cyanoacrylate**
8. **Young Planar Water**
9. **Young Tapered Water**
10. **Young Planar Cyanoacrylate**
11. **Young Tapered Cyanoacrylate**
12. **Old Planar Xanthan Gum**
13. **Mortar contact angles**

1. Old Planar Water

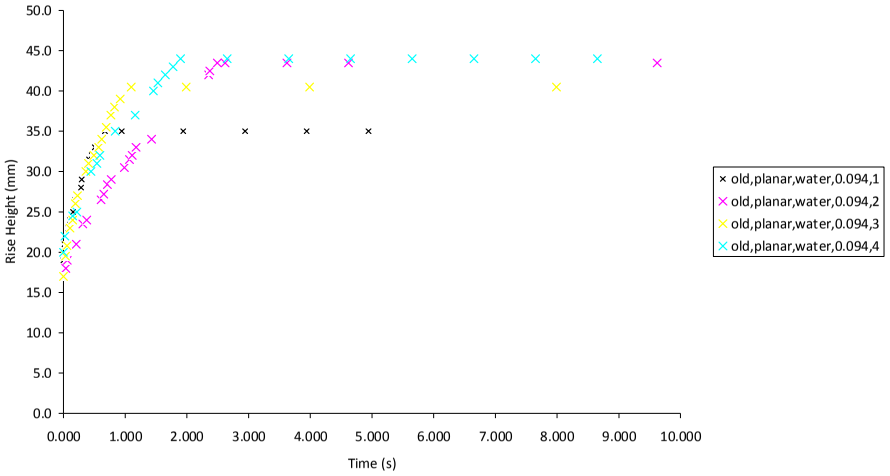

(a)

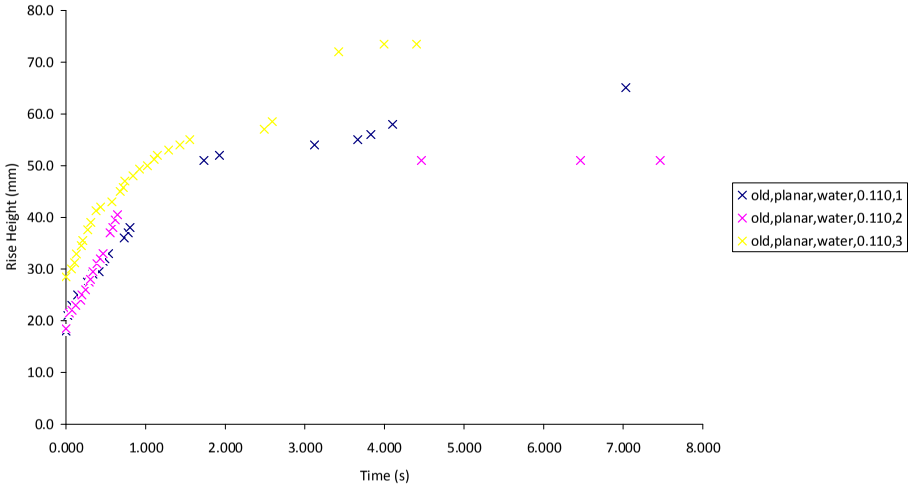

(b)

C2

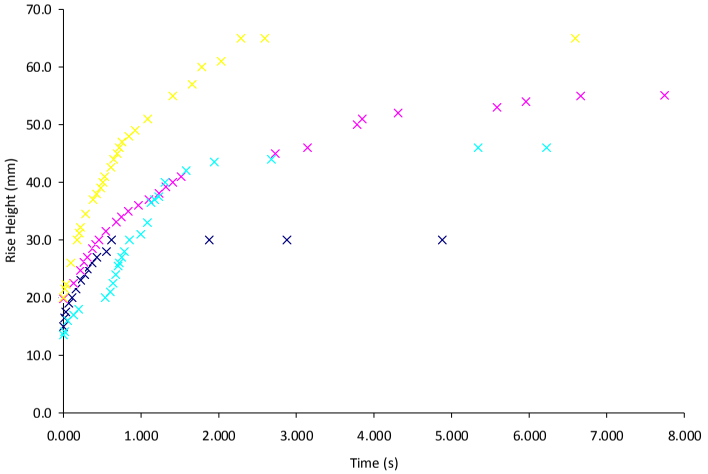
Rise Height (mm)
70.0
60.0
50.0
40.0
30.0
20.0
10.0
0.0
0.000
1.000
2.000
3.000
4.000
5.000
6.000
7.000
8.000
Time (s)
old,planar,water,0.237,1
old,planar,water,0.237,2
old,planar,water,0.237,3
old,planar,water,0.237,4

(c)

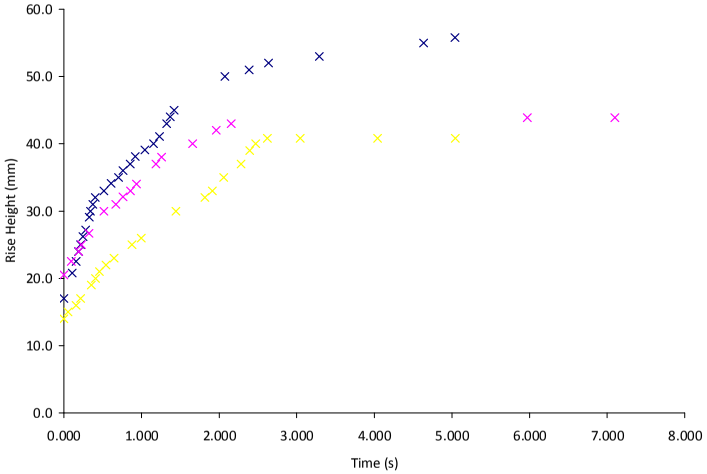
Rise Height (mm)
60.0
50.0
40.0
30.0
20.0
10.0
0.0
0.000
1.000
2.000
3.000
4.000
5.000
6.000
7.000
8.000
Time (s)
old,planar,water,0.254,1
old,planar,water,0.254,2
old,planar,water,0.254,3

(d)

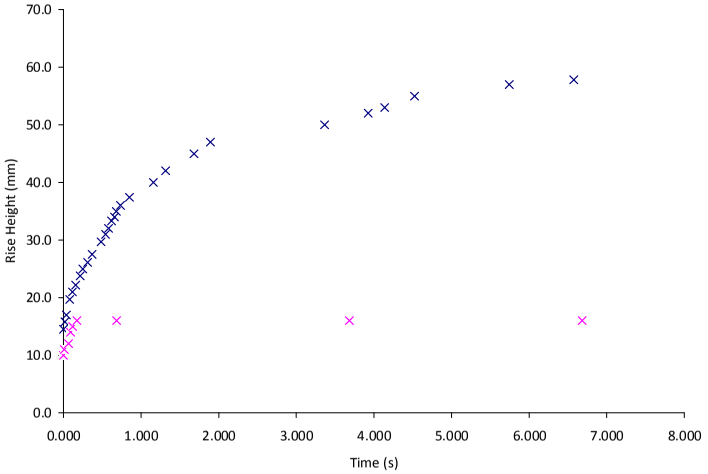
Rise Height (mm)
70.0
60.0
50.0
40.0
30.0
20.0
10.0
0.0
0.000
1.000
2.000
3.000
4.000
5.000
6.000
7.000
8.000
Time (s)
old,planar,water,0.261,1
old,planar,water,0.261,2

(e)

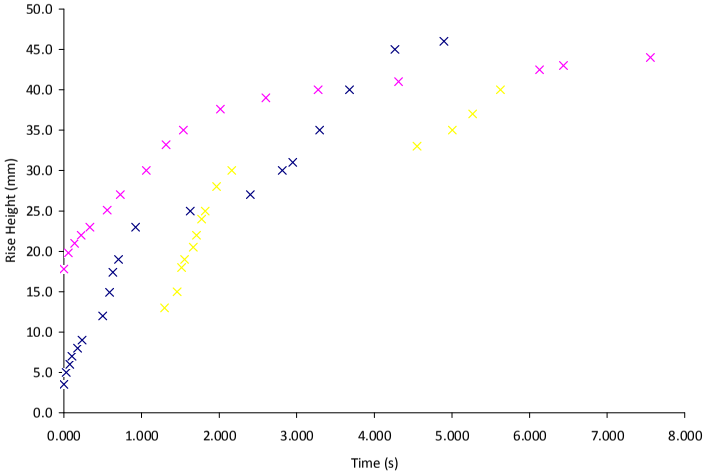
Rise Height (mm)
50.0
45.0
40.0
35.0
30.0
25.0
20.0
15.0
10.0
5.0
0.0
0.000
1.000
2.000
3.000
4.000
5.000
6.000
7.000
8.000
Time (s)
old,planar,water,0.344,1
old,planar,water,0.344,2
old,planar,water,0.344,3

(f)

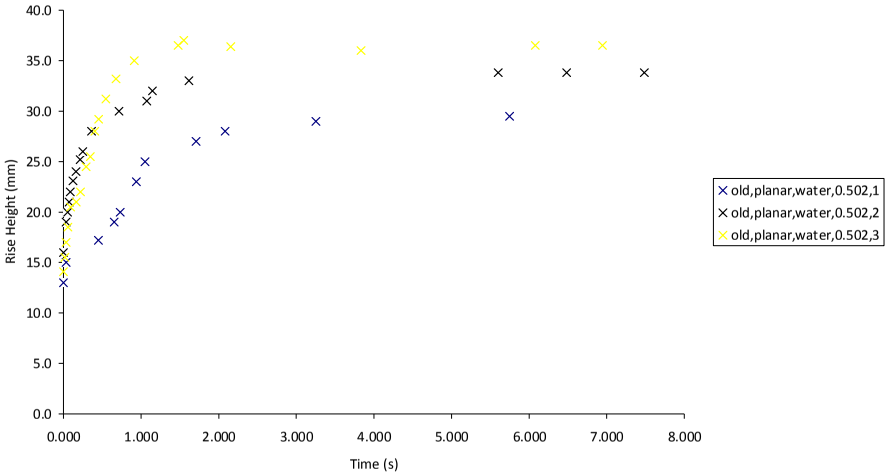
Rise Height (mm)
Time (s)
old,planar,water,0.502,1
old,planar,water,0.502,2
old,planar,water,0.502,3

(g)

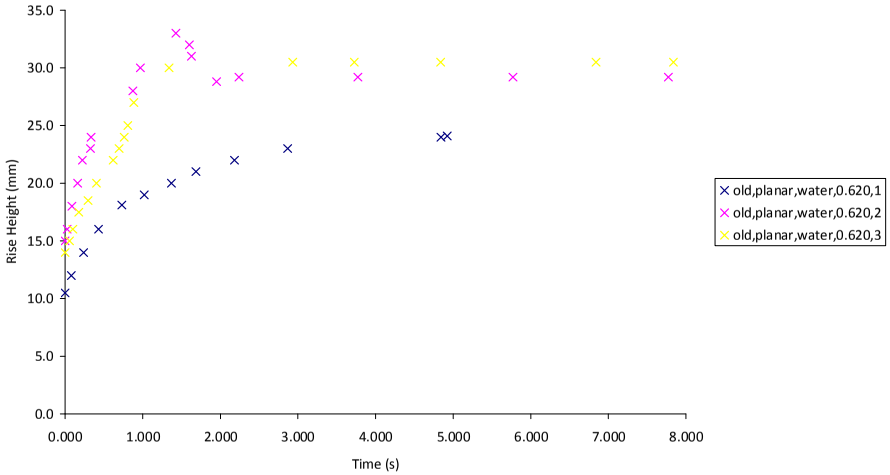
Rise Height (mm)
Time (s)
old,planar,water,0.620,1
old,planar,water,0.620,2
old,planar,water,0.620,3

(h)

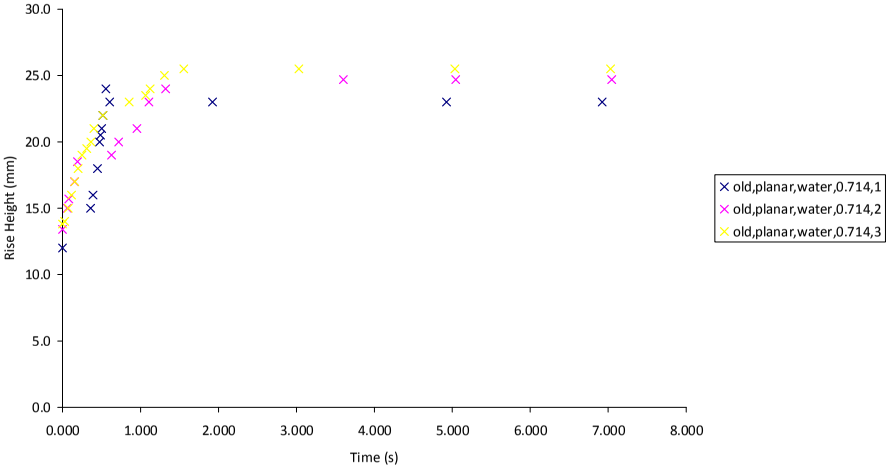
Rise Height (mm)
Time (s)
old,planar,water,0.714,1
old,planar,water,0.714,2
old,planar,water,0.714,3

(i)

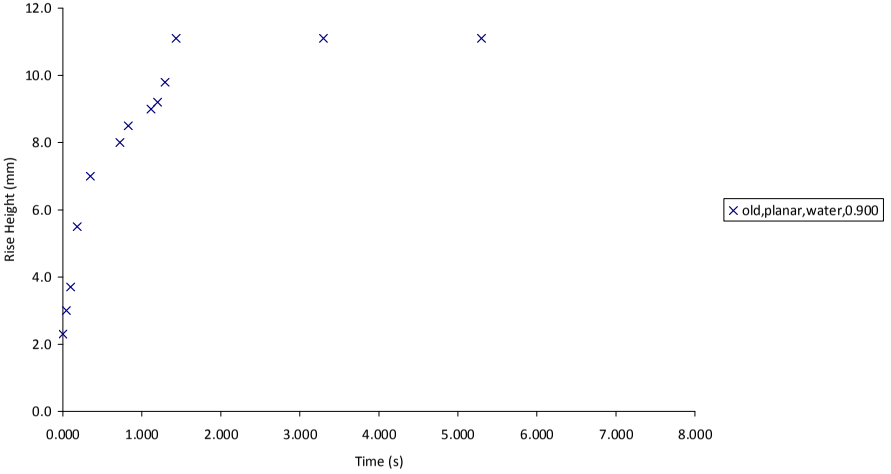
Rise Height (mm)
Time (s)
old,planar,water,0.900

(j)

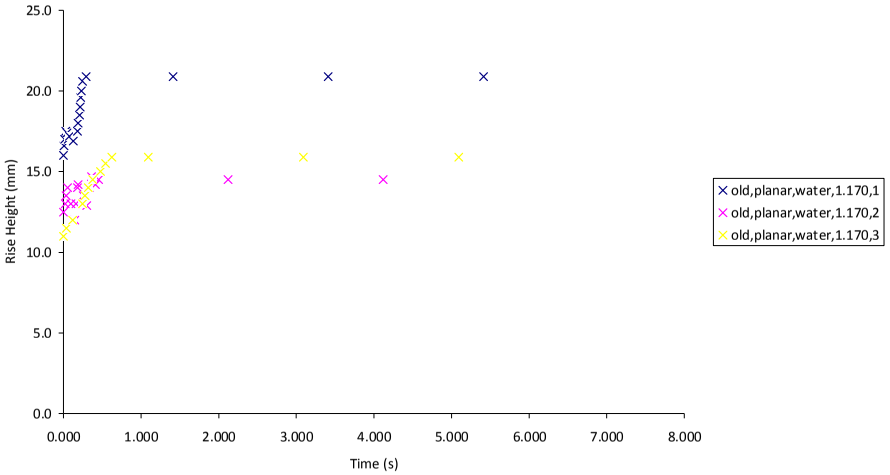

(k)

Figure_C1: Old, planar, water graphs for wire thicknesses a-k respectively, a(0.094mm), b(0.110mm), c(0.237mm), d(0.254mm), e(0.261mm), f(0.344mm), g(0.502mm), h(0.620mm), i(0.714mm), j(0.900mm), k(1.170mm)

2. Old Tapered Water

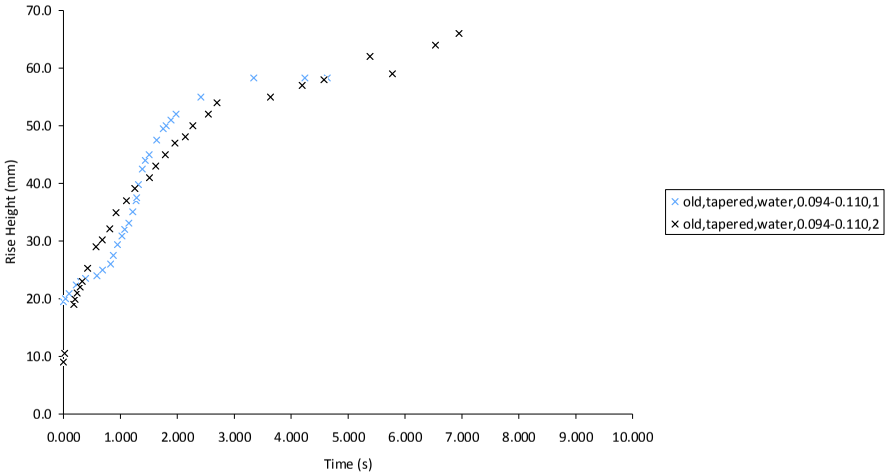

(a)

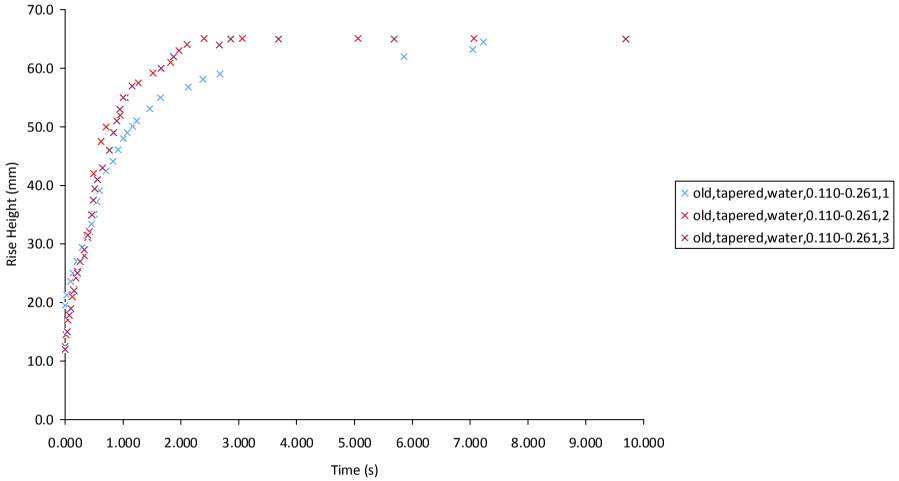

(b)

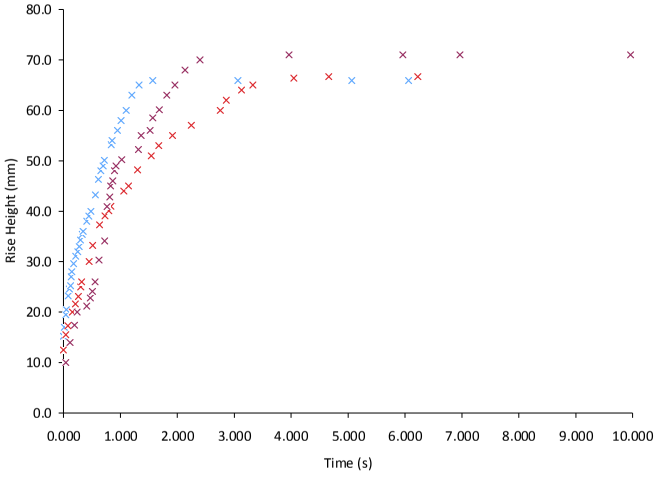
Rise Height (mm)
Time (s)
old,tapered,water,0.237-0.344,1
old,tapered,water,0.237-0.344,2
old,tapered,water,0.237-0.344,3

(c)

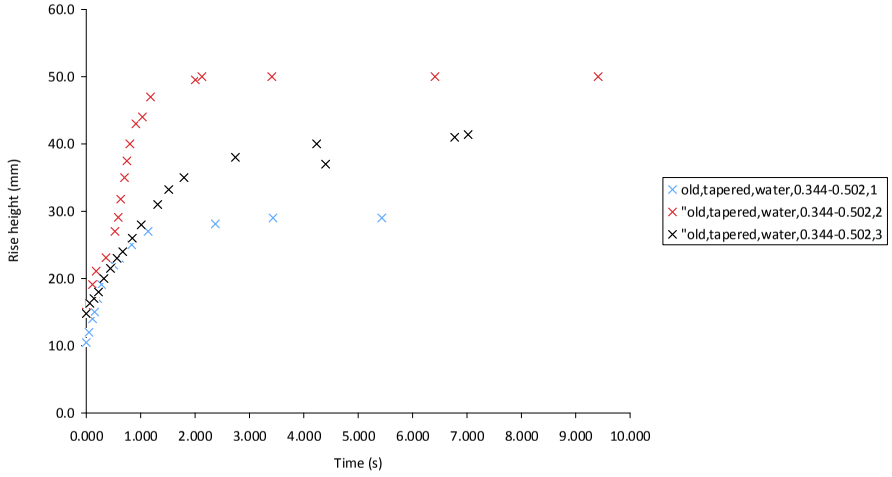
Rise height (mm)
Time (s)
old,tapered,water,0.344-0.502,1
"old,tapered,water,0.344-0.502,2
"old,tapered,water,0.344-0.502,3

(d)

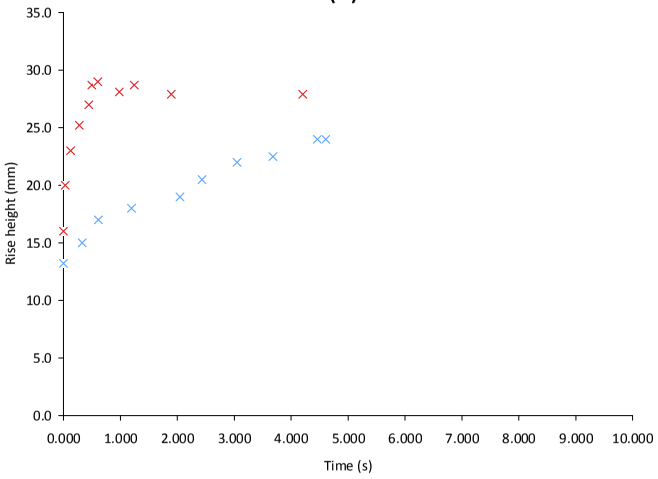
Rise height (mm)
Time (s)
old,tapered,water,0.502-0.714,1
old,tapered,water,0.502-0.714,2

(e)

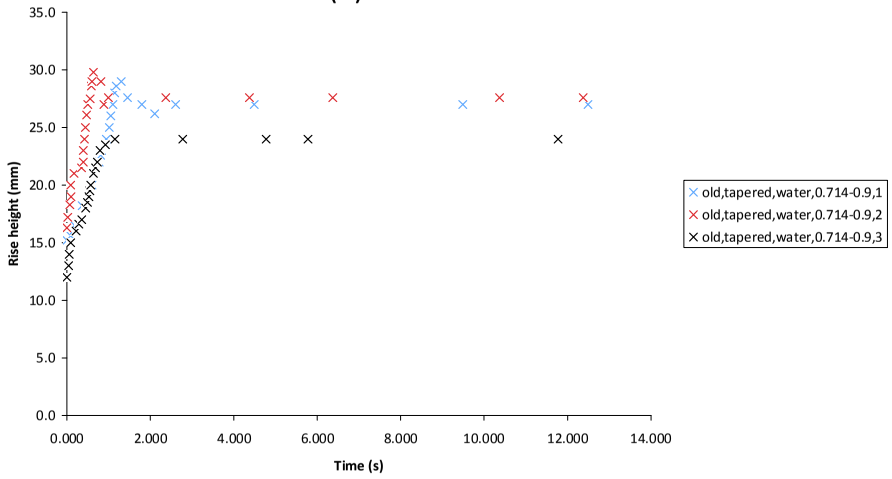
Rise height (mm)
Time (s)
old,tapered,water,0.714-0.9,1
old,tapered,water,0.714-0.9,2
old,tapered,water,0.714-0.9,3

(f)

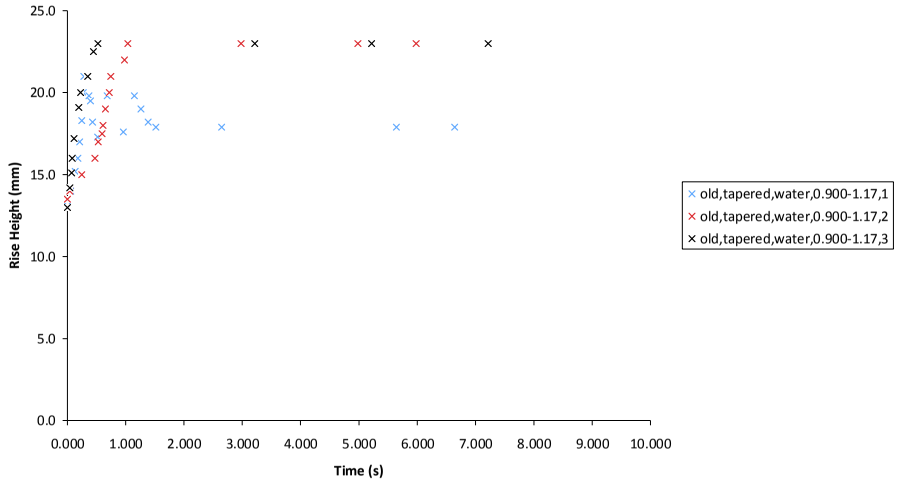

(g)

Figure_C2: Old, tapered, water graphs for crack apertures a-g respectively, a(0.094-0.110mm), b(0.110-0.261mm), c(0.237-0.344mm), d(0.344-0.502mm), e(0.502-0.714mm), f(0.714-0.900mm), g(0.900-1.170mm)

3. Old Tortuous 3 and 5 Nodes Water

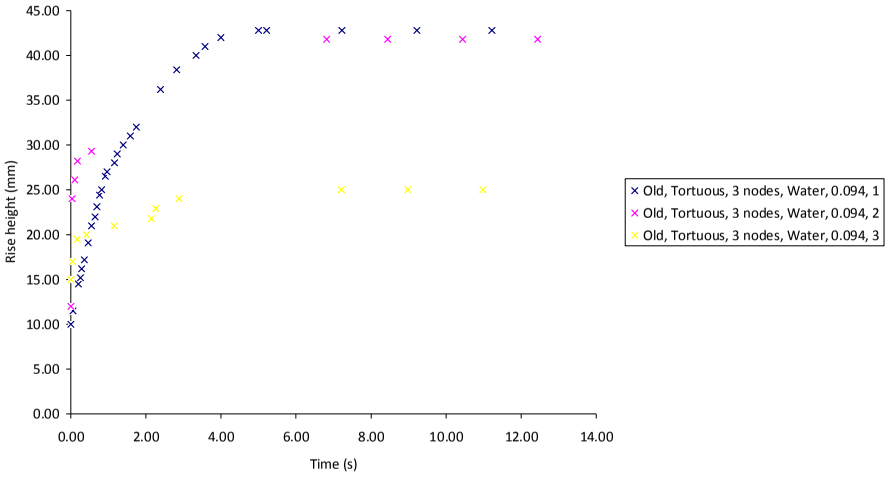

(a)

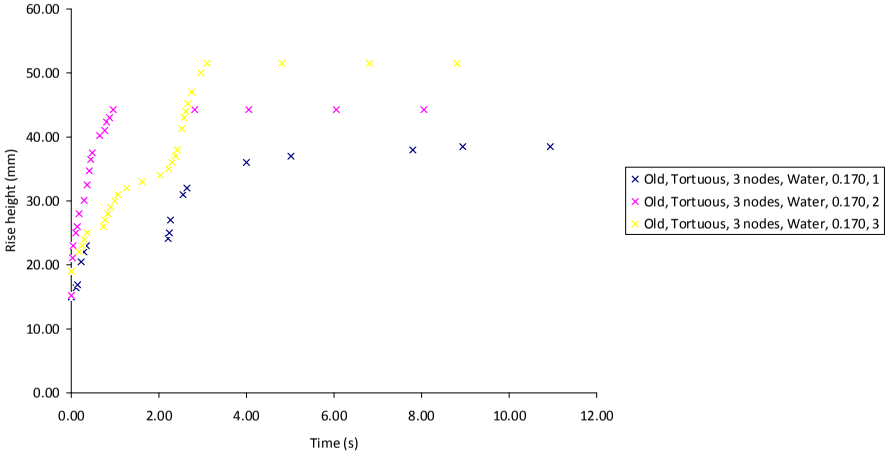

(b)

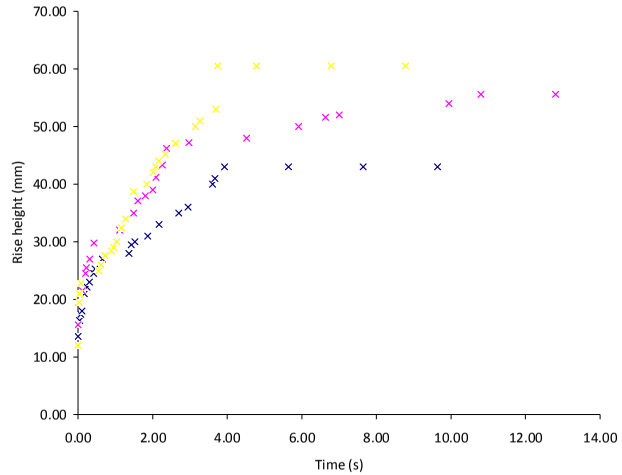
70.00
60.00
50.00
40.00
30.00
20.00
10.00
0.00
Rise height (mm)
0.00
2.00
4.00
6.00
8.00
10.00
12.00
14.00
Time (s)
Old, Tortuous, 3 nodes, Water, 0.254, 1
Old, Tortuous, 3 nodes, Water, 0.254, 2
Old, Tortuous, 3 nodes, Water, 0.254, 3

(c)

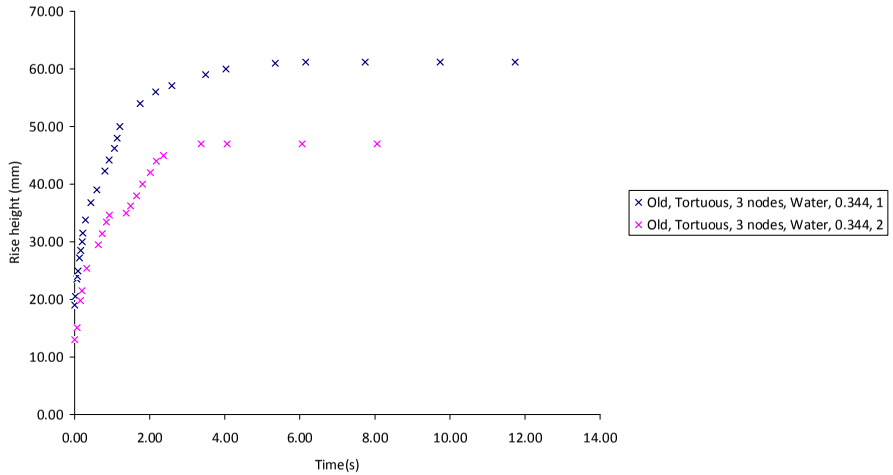
70.00
60.00
50.00
40.00
30.00
20.00
10.00
0.00
Rise height (mm)
0.00
2.00
4.00
6.00
8.00
10.00
12.00
14.00
Time(s)
Old, Tortuous, 3 nodes, Water, 0.344, 1
Old, Tortuous, 3 nodes, Water, 0.344, 2

(d)

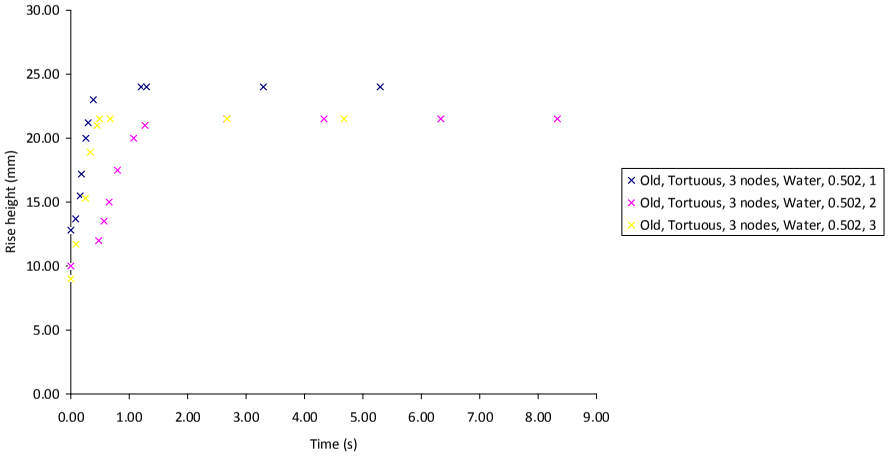
30.00
25.00
20.00
15.00
10.00
5.00
0.00
Rise height (mm)
0.00
1.00
2.00
3.00
4.00
5.00
6.00
7.00
8.00
9.00
Time (s)
Old, Tortuous, 3 nodes, Water, 0.502, 1
Old, Tortuous, 3 nodes, Water, 0.502, 2
Old, Tortuous, 3 nodes, Water, 0.502, 3

(e)

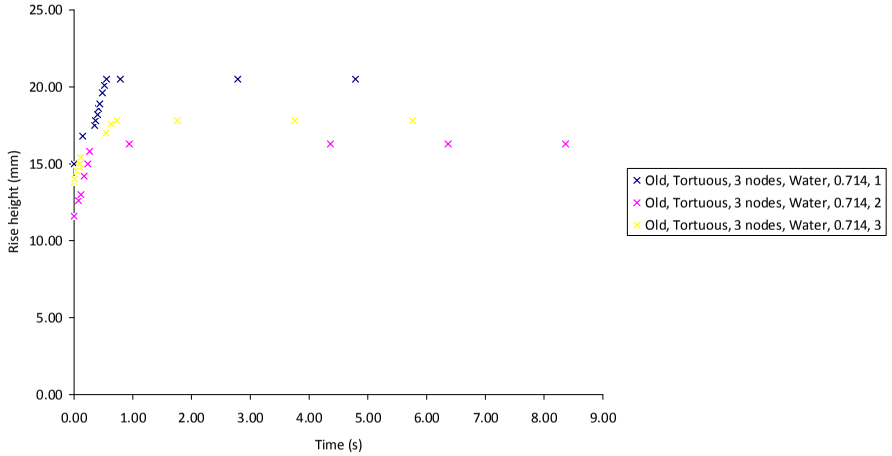
25.00
20.00
15.00
10.00
5.00
0.00
Rise height (mm)
0.00
1.00
2.00
3.00
4.00
5.00
6.00
7.00
8.00
9.00
Time (s)
Old, Tortuous, 3 nodes, Water, 0.714, 1
Old, Tortuous, 3 nodes, Water, 0.714, 2
Old, Tortuous, 3 nodes, Water, 0.714, 3

(f)

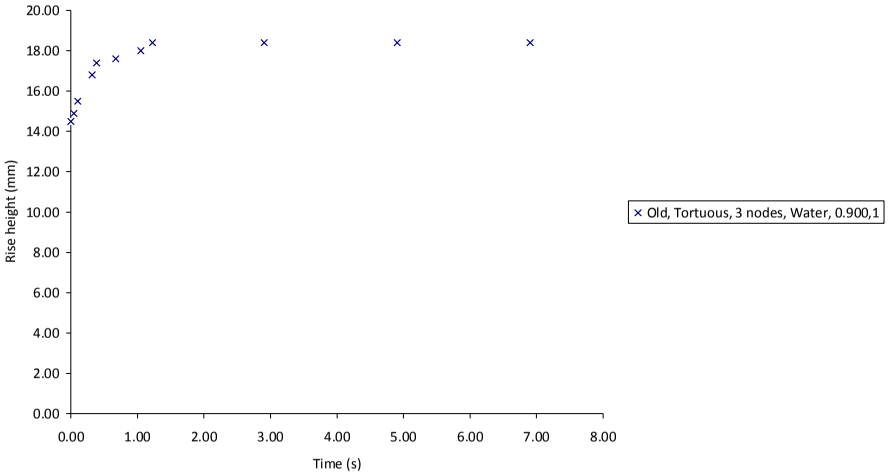
Rise height (mm)
Time (s)
Old, Tortuous, 3 nodes, Water, 0.900,1

(g)

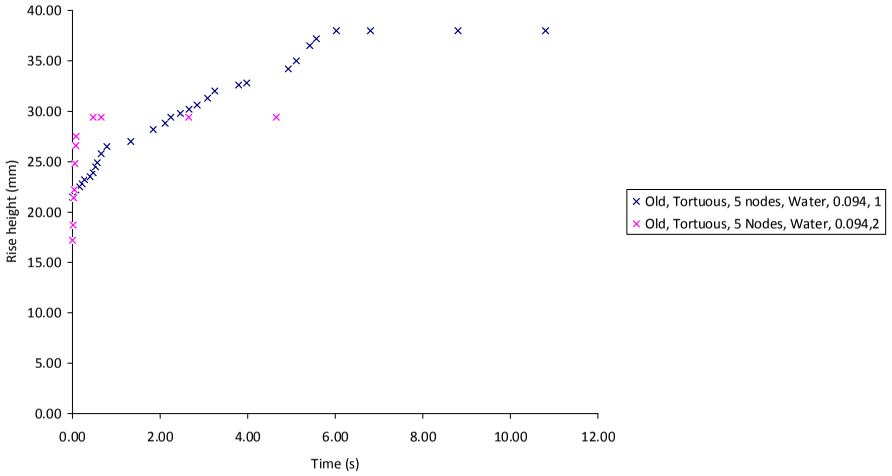
Rise height (mm)
Time (s)
Old, Tortuous, 5 nodes, Water, 0.094, 1
Old, Tortuous, 5 Nodes, Water, 0.094,2

(h)

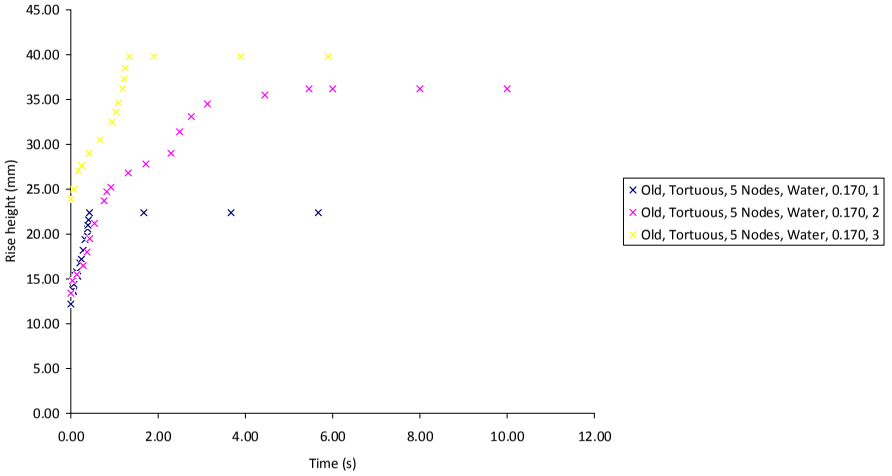
Rise height (mm)
Time (s)
Old, Tortuous, 5 Nodes, Water, 0.170, 1
Old, Tortuous, 5 Nodes, Water, 0.170, 2
Old, Tortuous, 5 Nodes, Water, 0.170, 3

(i)

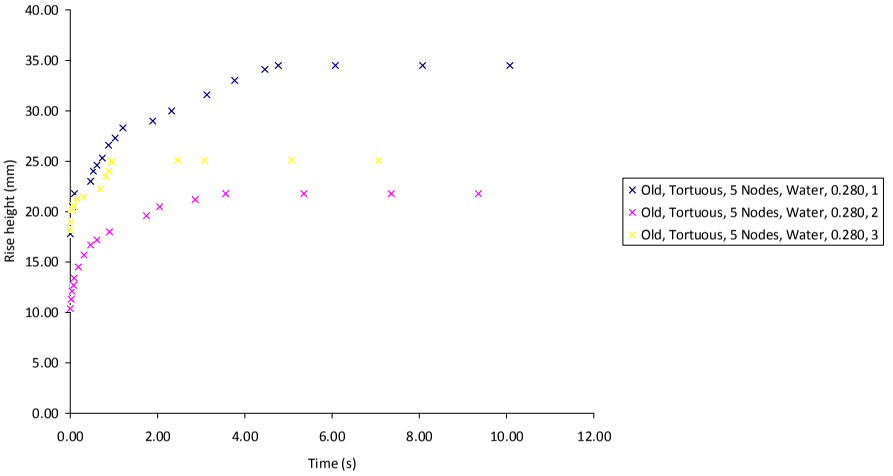
Rise height (mm)
Time (s)
Old, Tortuous, 5 Nodes, Water, 0.280, 1
Old, Tortuous, 5 Nodes, Water, 0.280, 2
Old, Tortuous, 5 Nodes, Water, 0.280, 3

(j)

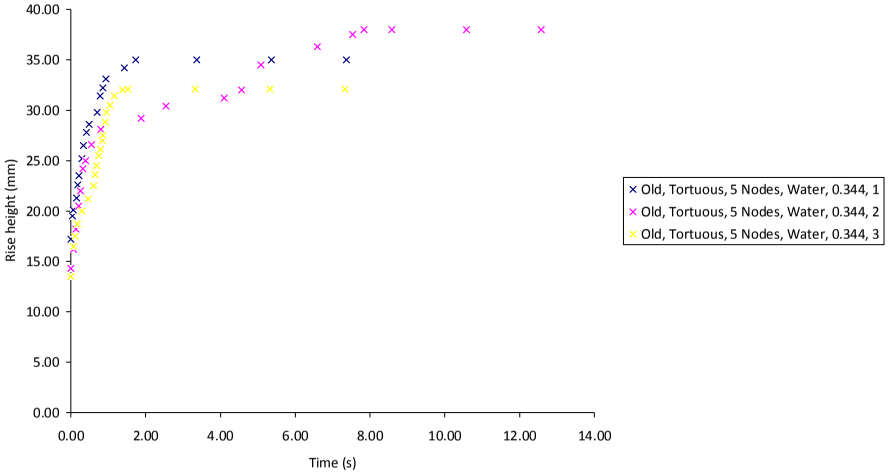
Rise height (mm)
Time (s)
Old, Tortuous, 5 Nodes, Water, 0.344, 1
Old, Tortuous, 5 Nodes, Water, 0.344, 2
Old, Tortuous, 5 Nodes, Water, 0.344, 3

(k)

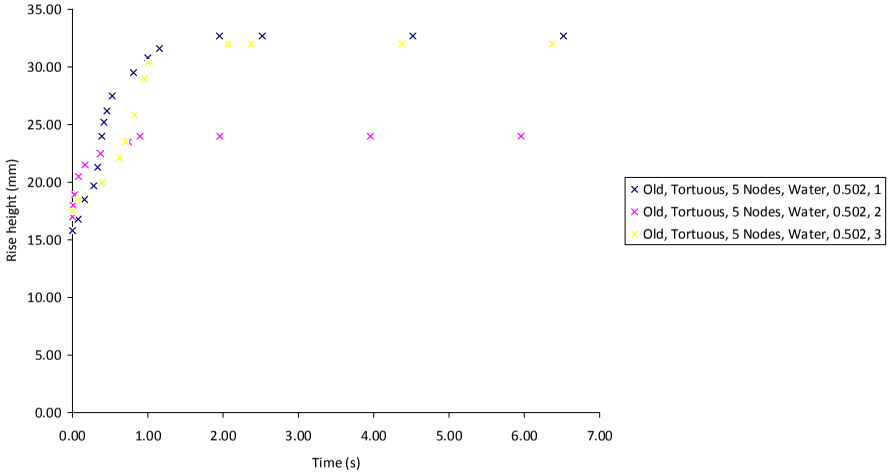
Rise height (mm)
Time (s)
Old, Tortuous, 5 Nodes, Water, 0.502, 1
Old, Tortuous, 5 Nodes, Water, 0.502, 2
Old, Tortuous, 5 Nodes, Water, 0.502, 3

(l)

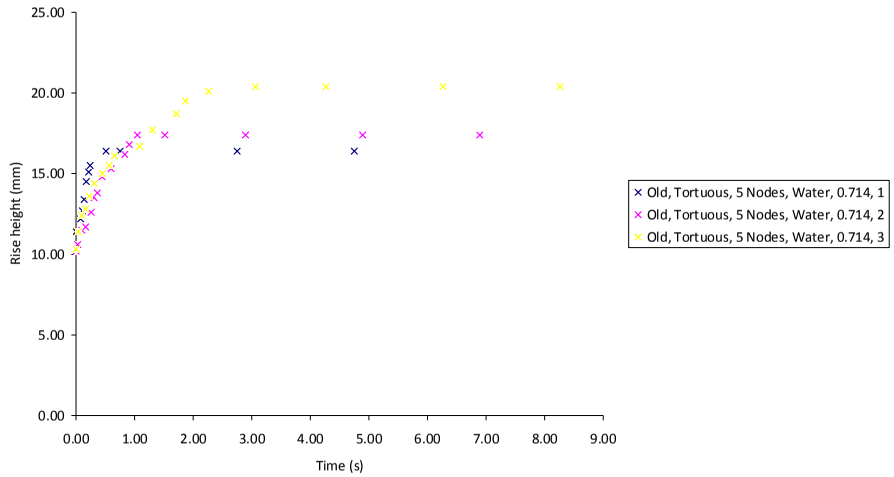

(m)

Figure_C3: Old, tortuous, water graphs for crack apertures a-m respectively, a(3 nodes-0.094mm), b(3 nodes-0.170mm), c(3 nodes-0.254mm), d(3 nodes- 0.344mm), e(3 nodes- 0.502mm), f(3 nodes- 0.714mm), g(3 nodes- 0.900mm), h(5 nodes- 0.094mm), i(5 nodes- 0.170mm), j(5 nodes- 0.280mm), k(5 nodes- 0.344mm), l(5 nodes- 0.502mm), m(5 nodes- 0.714mm)

4. Old Natural Water

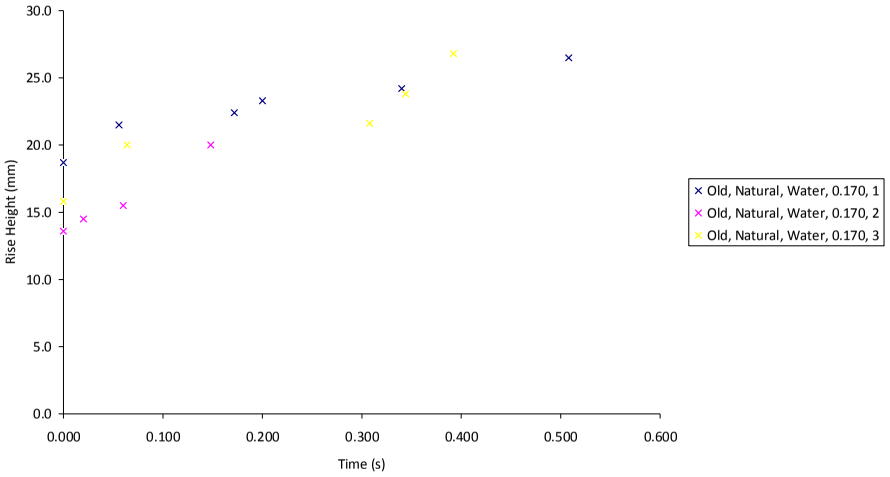

(a)

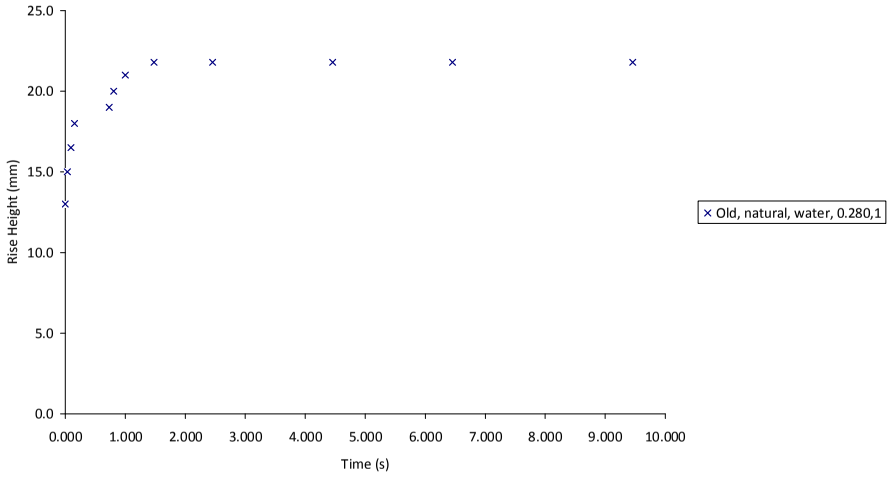

(b)

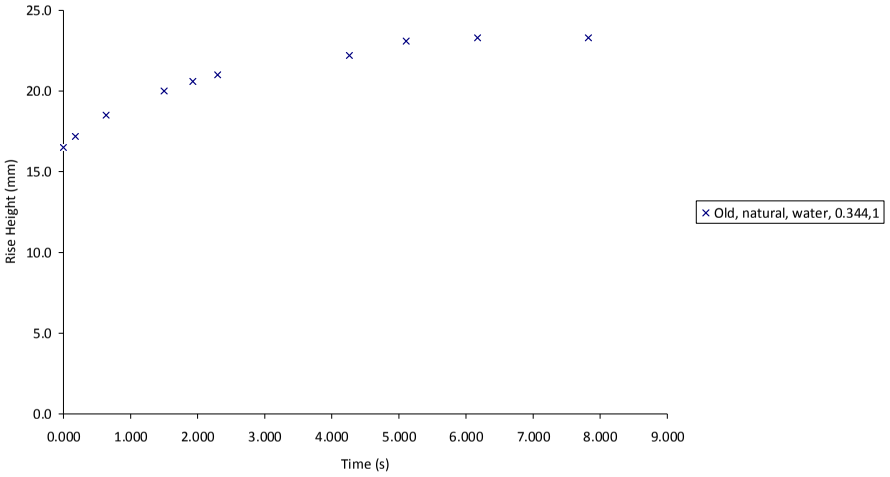
25.0
20.0
15.0
10.0
5.0
0.0
Rise Height (mm)
0.000
1.000
2.000
3.000
4.000
5.000
6.000
7.000
8.000
9.000
Time (s)
Old, natural, water, 0.344,1

(c)

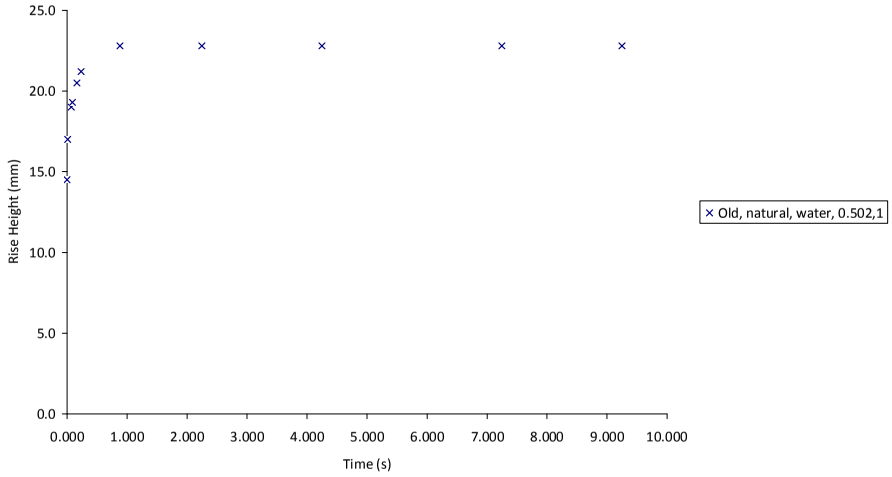
25.0
20.0
15.0
10.0
5.0
0.0
Rise Height (mm)
0.000
1.000
2.000
3.000
4.000
5.000
6.000
7.000
8.000
9.000
10.000
Time (s)
Old, natural, water, 0.502,1

(d)

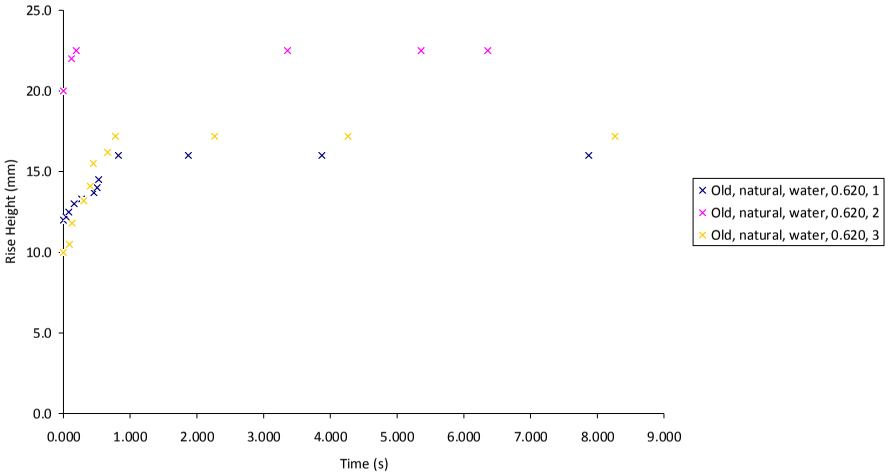

(e)

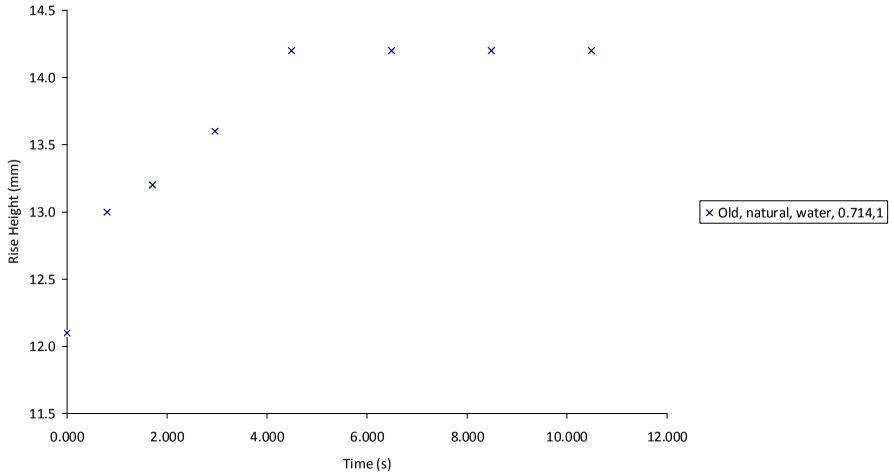

(f)

Figure_C4: Old, natural, water graphs for crack apertures a-f respectively, a(0.170mm), b(0.280mm), c(0.344mm), d(0.502mm), e(0.620mm), f(0.714mm)

5. Old Planar Cyanoacrylate

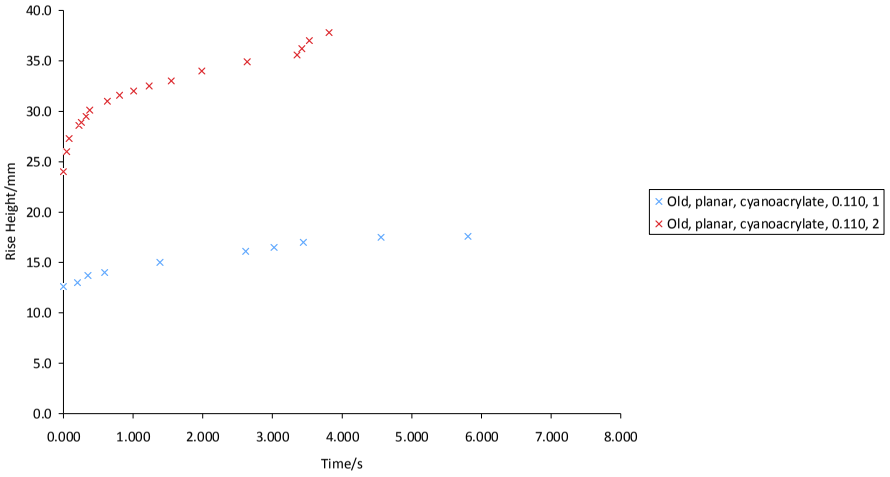

(a)

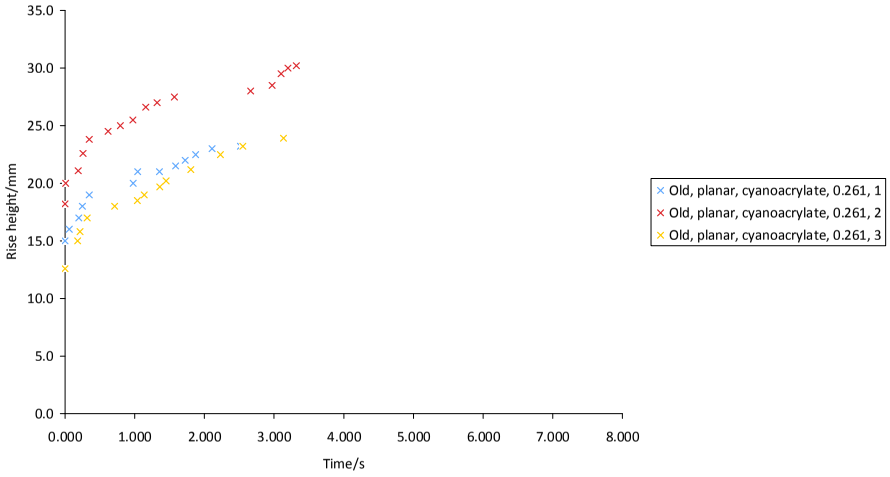

(b)

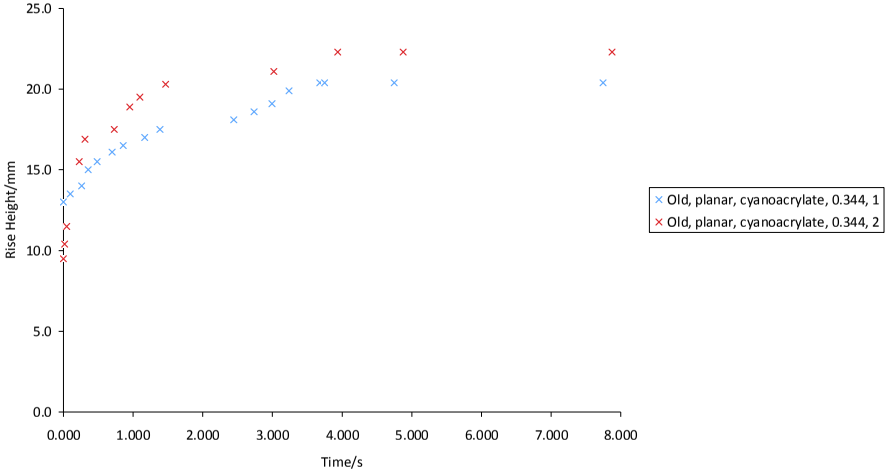

(c)

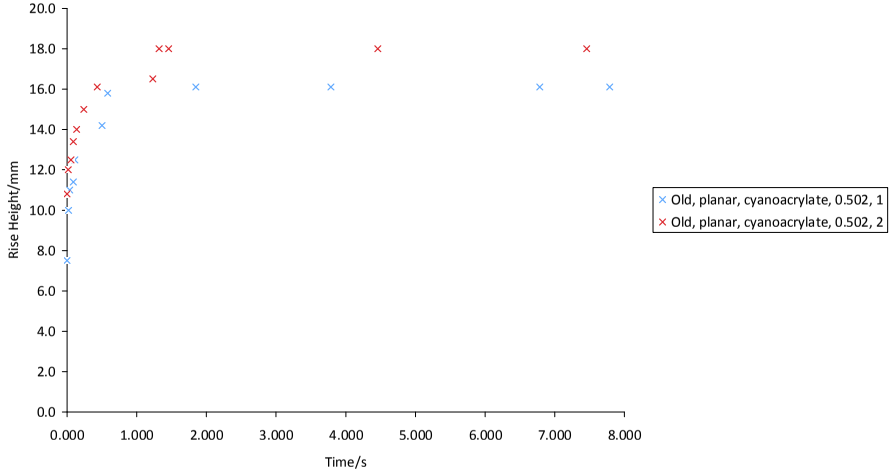

(d)

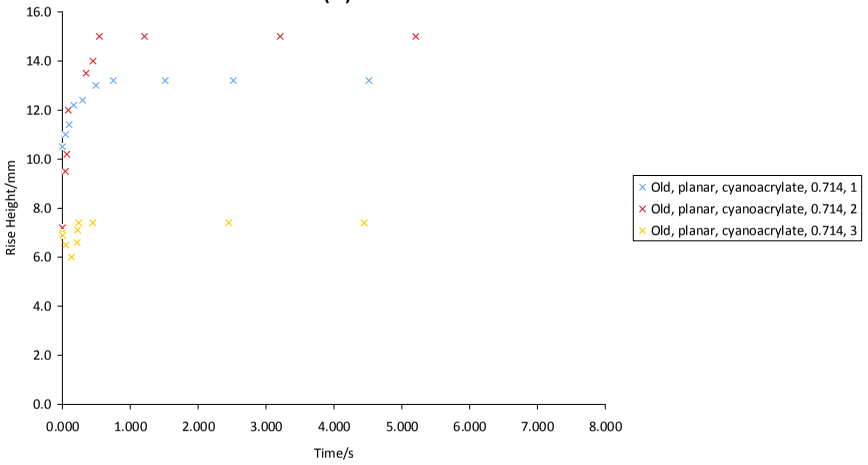

(e)

Figure_C5: Old, planar, cyanoacrylate graphs for wire thicknesses a-e respectively, a(0.110mm), b(0.261mm), c(0.344mm), d(0.502mm), e(0.714mm)

6. Old Tapered Cyanoacrylate

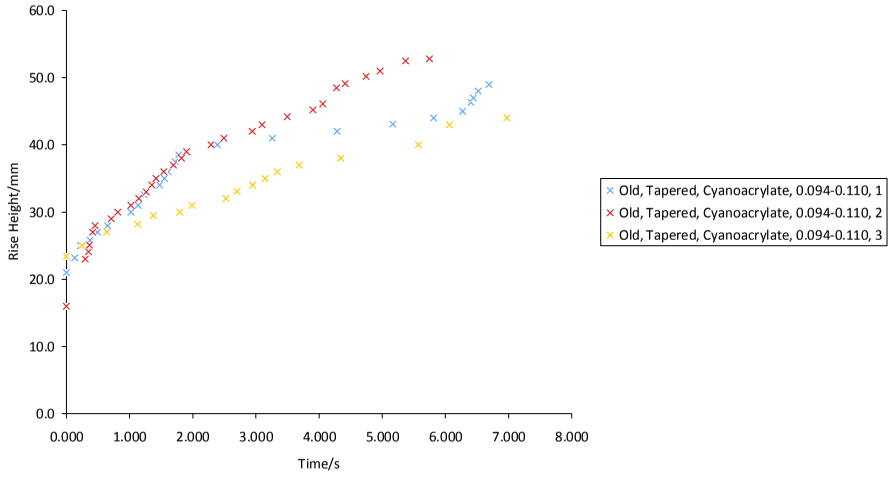

(a)

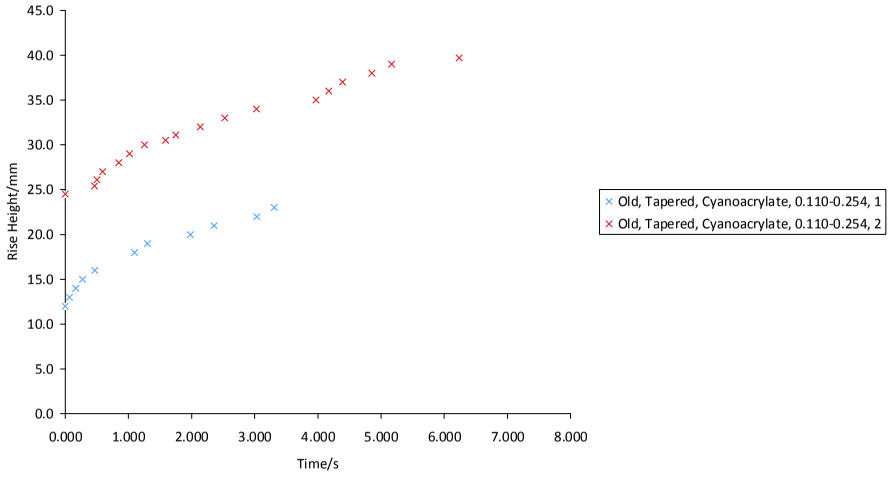

(b)

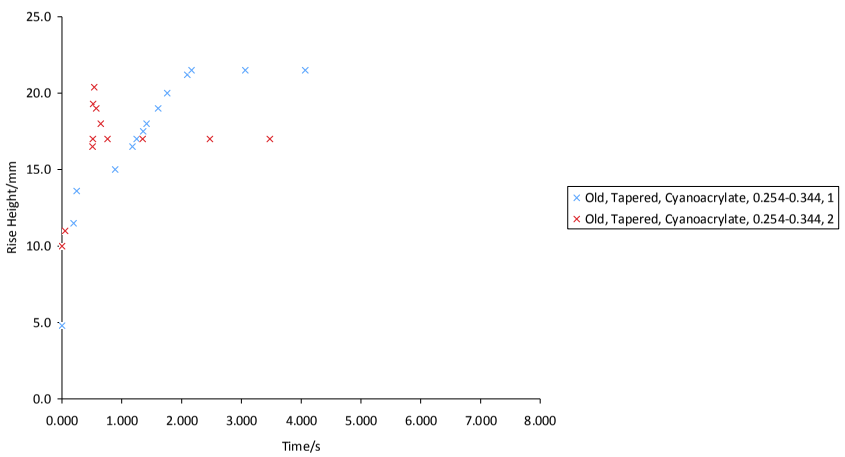

(c)

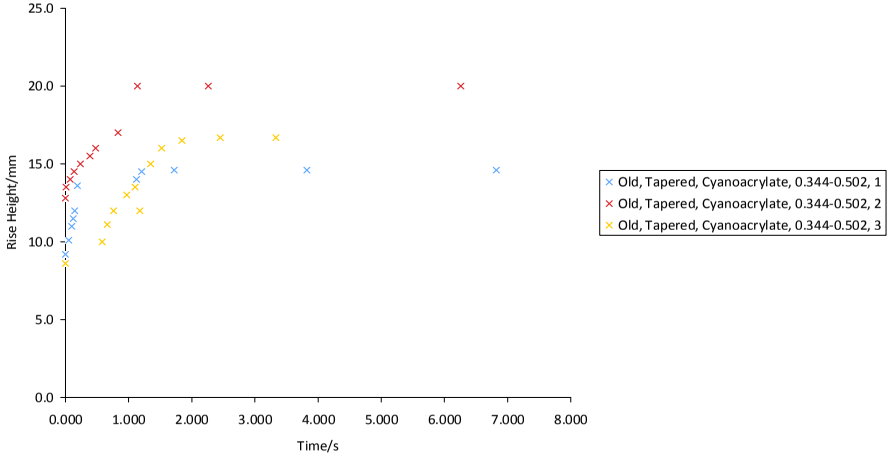

(d)

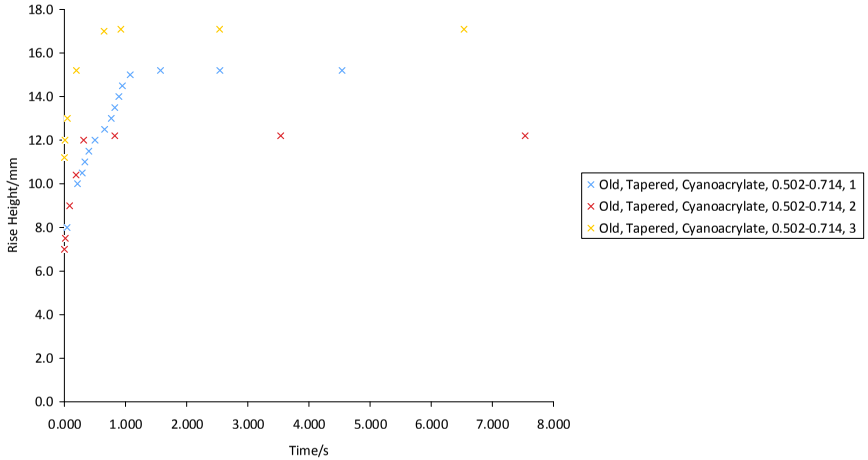

(e)

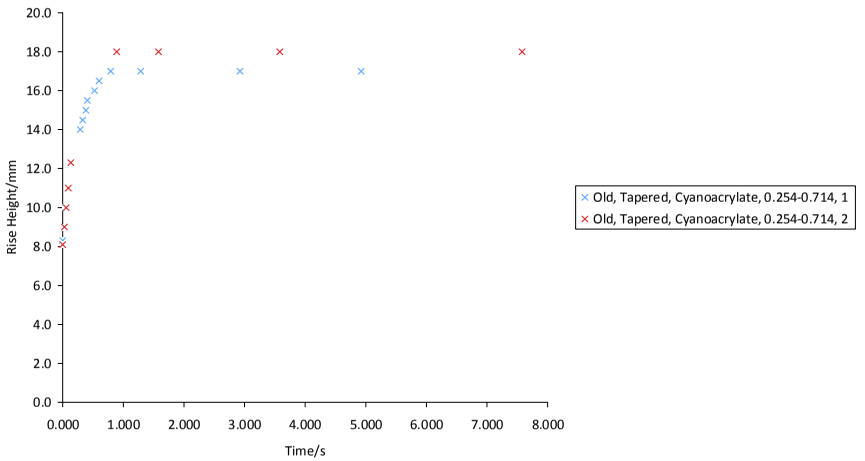

(f)

Figure_C6: Old, tapered, cyanoacrylate graphs for wire thicknesses a-f respectively, a(0.094-0.110mm), b(0.110-0.254mm), c(0.254-0.344mm), d(0.344-0.502mm), e(0.502-0.714mm), f(0.254-0.714mm)

7. Old Tortuous 3 and 5 Nodes Cyanoacrylate

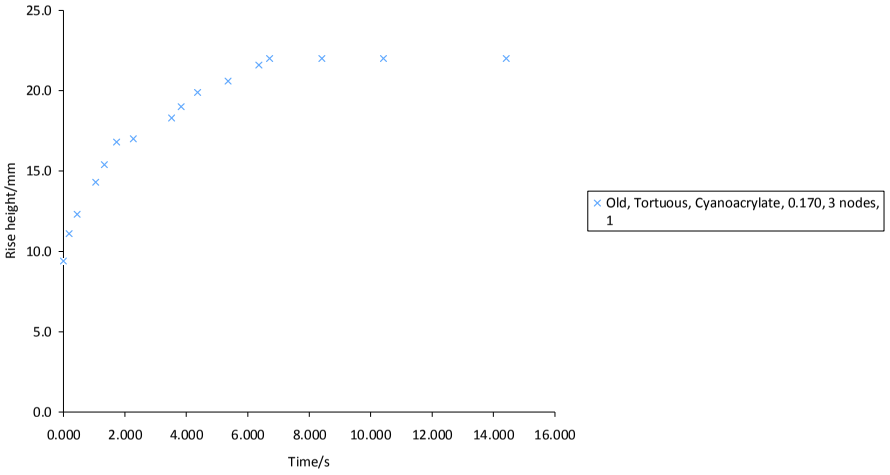

(a)

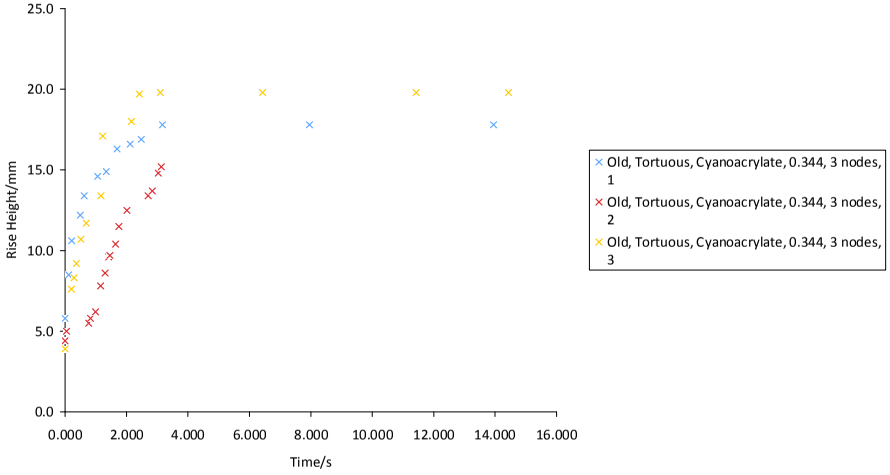

(b)

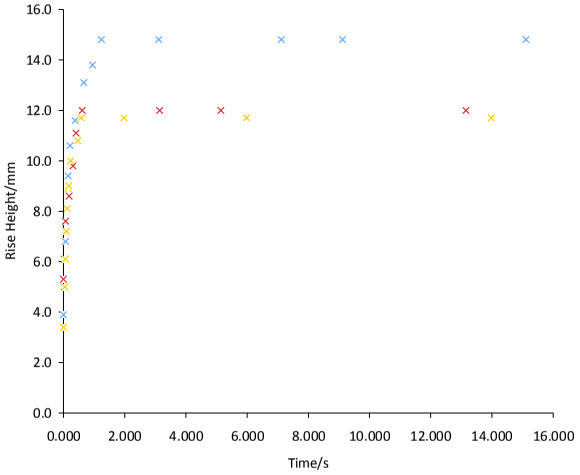
Rise Height/mm
Time/s
0.0
2.0
4.0
6.0
8.0
10.0
12.0
14.0
16.0
0.000
2.000
4.000
6.000
8.000
10.000
12.000
14.000
16.000

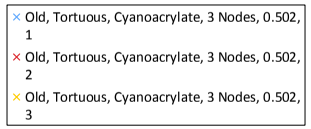
Old, Tortuous, Cyanoacrylate, 3 Nodes, 0.502, 1
Old, Tortuous, Cyanoacrylate, 3 Nodes, 0.502, 2
Old, Tortuous, Cyanoacrylate, 3 Nodes, 0.502, 3

(c)

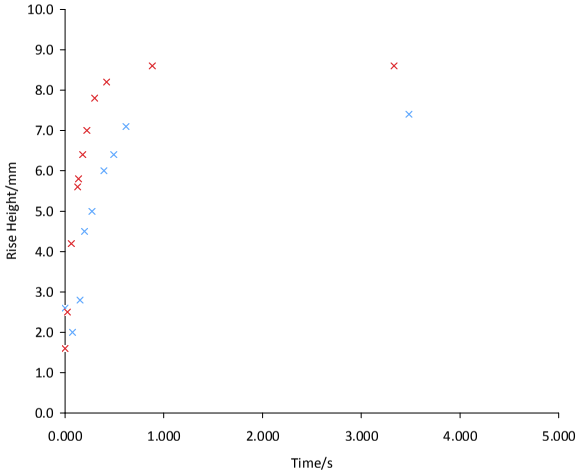
Rise Height/mm
Time/s
0.0
1.0
2.0
3.0
4.0
5.0
6.0
7.0
8.0
9.0
10.0
0.000
1.000
2.000
3.000
4.000
5.000

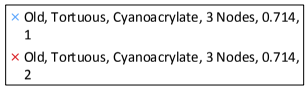
Old, Tortuous, Cyanoacrylate, 3 Nodes, 0.714, 1
Old, Tortuous, Cyanoacrylate, 3 Nodes, 0.714, 2

(d)

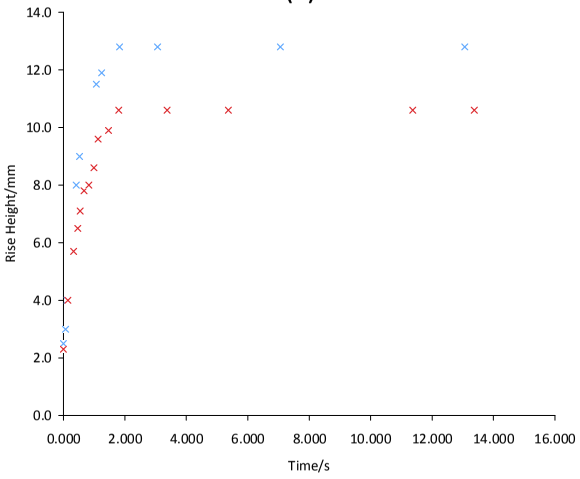
Rise Height/mm
Time/s
0.0
2.0
4.0
6.0
8.0
10.0
12.0
14.0
0.000
2.000
4.000
6.000
8.000
10.000
12.000
14.000
16.000

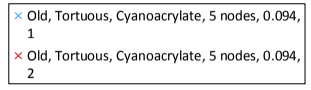
Old, Tortuous, Cyanoacrylate, 5 nodes, 0.094, 1
Old, Tortuous, Cyanoacrylate, 5 nodes, 0.094, 2

(e)

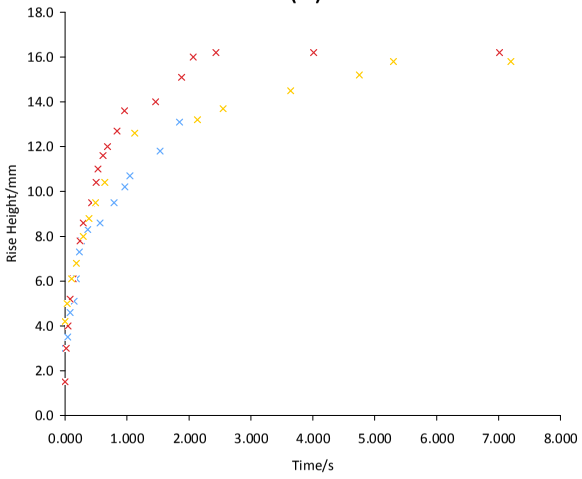
Rise Height/mm
Time/s
0.0
2.0
4.0
6.0
8.0
10.0
12.0
14.0
16.0
18.0
0.000
1.000
2.000
3.000
4.000
5.000
6.000
7.000
8.000

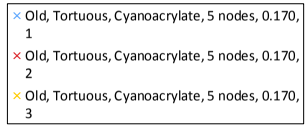
Old, Tortuous, Cyanoacrylate, 5 nodes, 0.170, 1
Old, Tortuous, Cyanoacrylate, 5 nodes, 0.170, 2
Old, Tortuous, Cyanoacrylate, 5 nodes, 0.170, 3

(f)

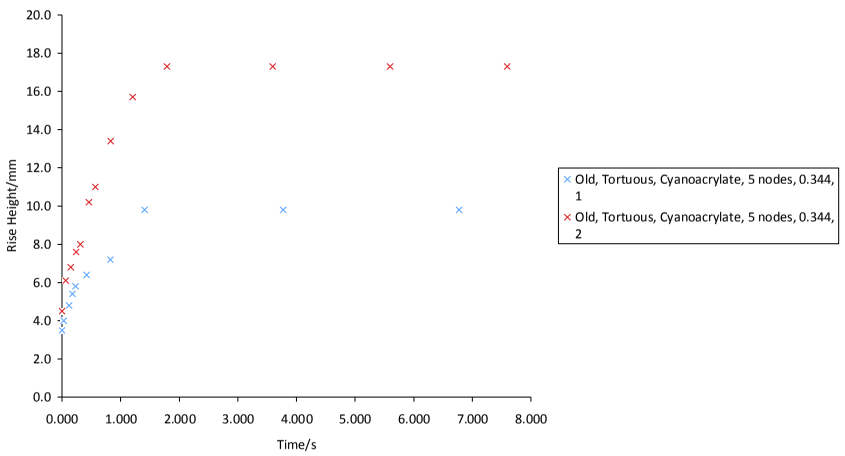

(g)

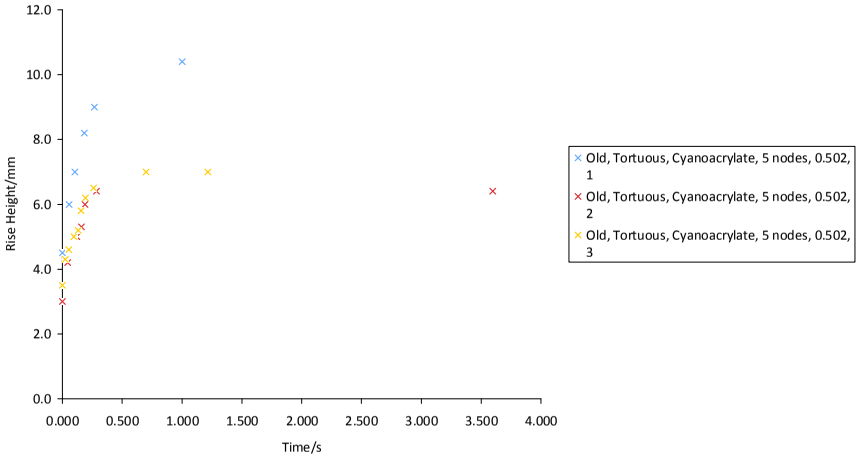

(h)

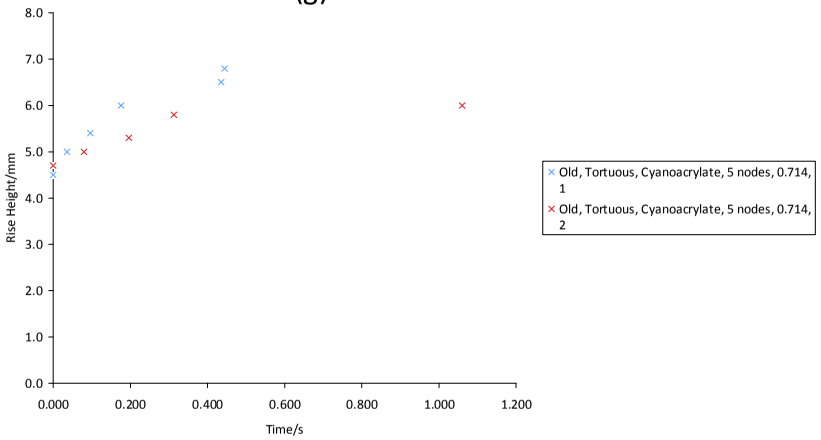

(i)

Figure_C7: Old Tortuous 3 and 5 Nodes Cyanoacrylate water graphs for wire thicknesses a-i respectively, a(3 nodes, 0.170mm), b(3 nodes, 0.344mm), c(3 nodes, 0.502mm), d(3 nodes, 0.714mm), e(5 nodes, 0.094mm), f(5 nodes, 0.170mm), g(5 nodes, 0.344mm), h(5 nodes, 0.502mm), i(5 nodes, 0.714mm)

8. Young Planar Water

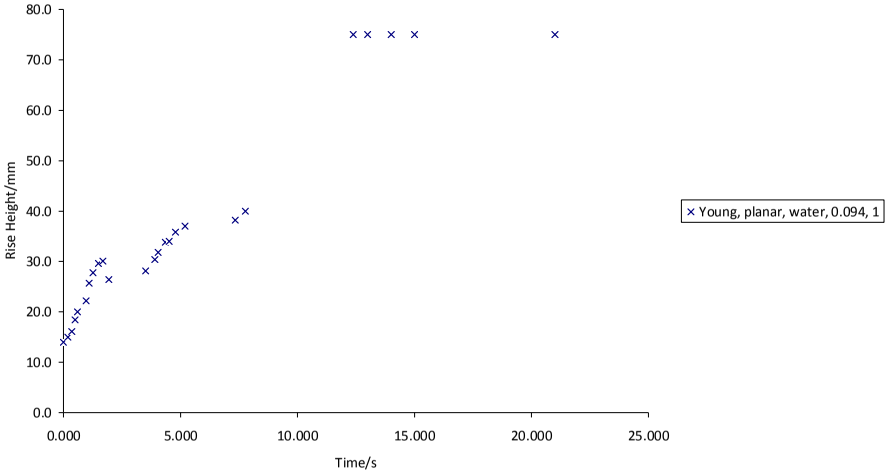

(a)

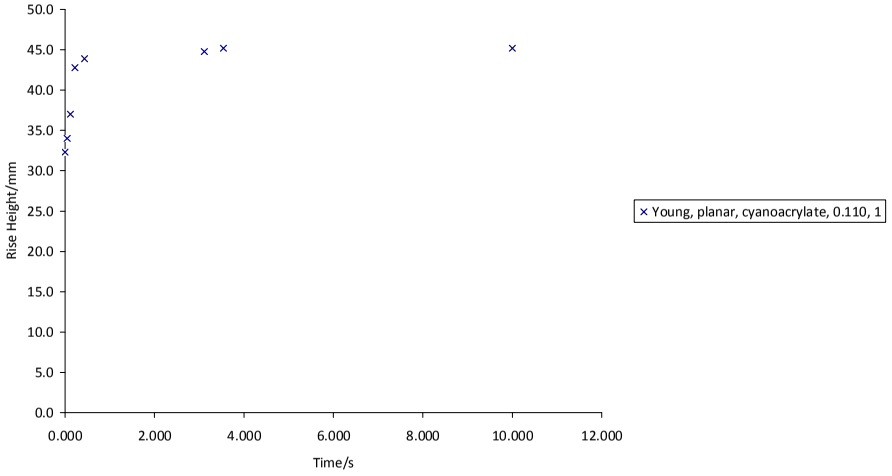

(b)

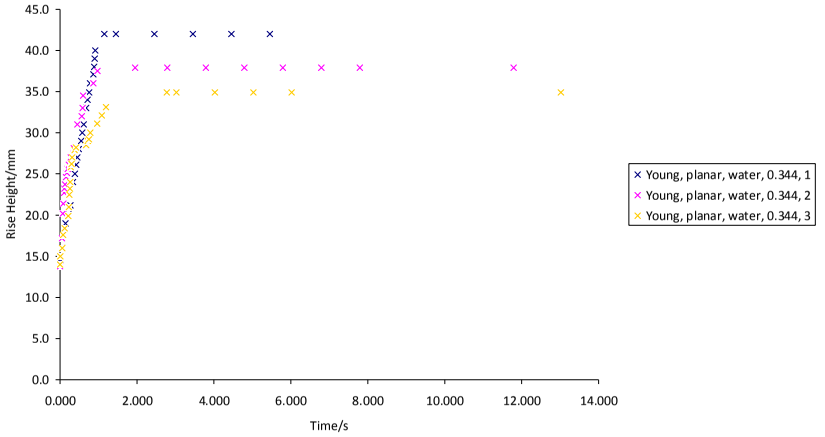

(c)

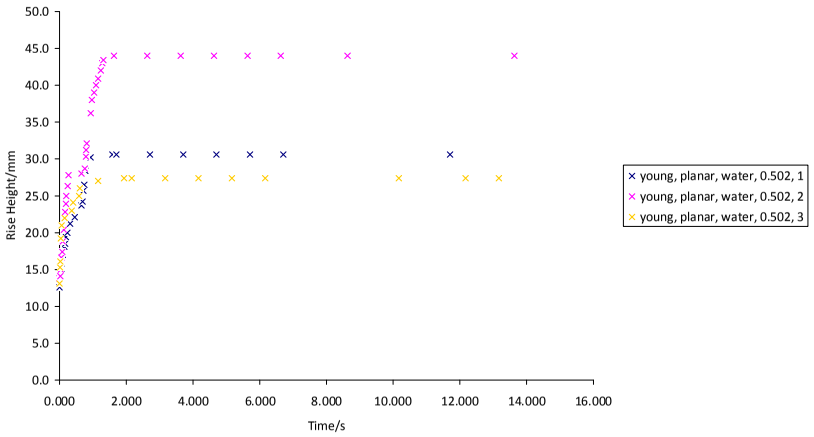

(d)

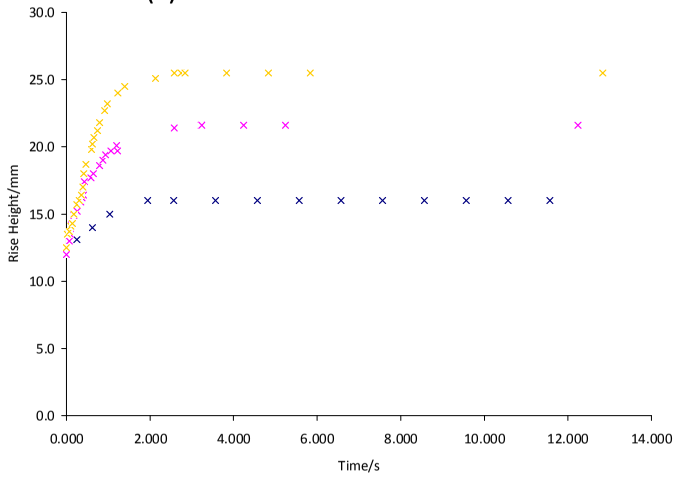

(e)

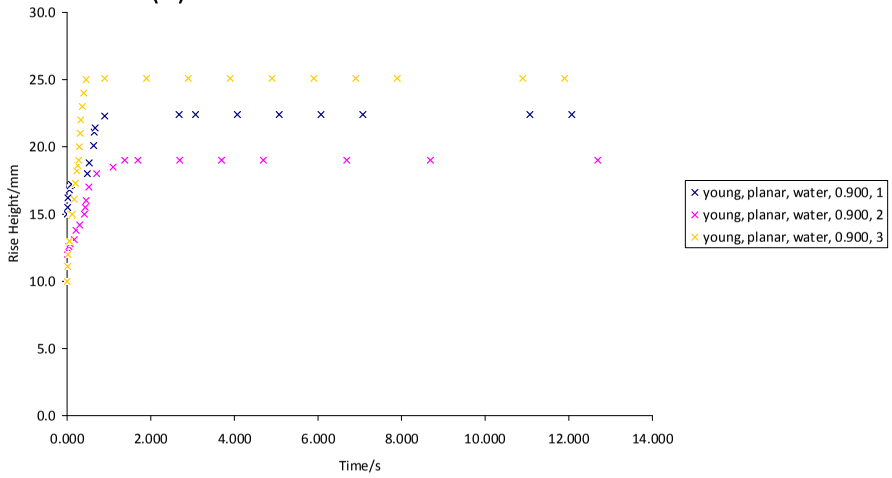

(f)

Figure_C8: Young planar water graphs for wire thicknesses a-f respectively, a(0.094mm), b(0.110mm), c(0.344mm), d(0.502mm), e(0.714mm), f(0.900mm)

9. Young Tapered Water

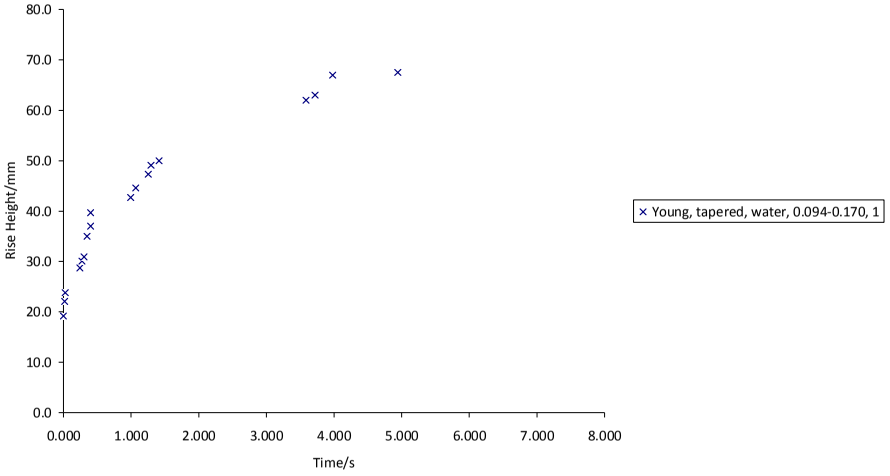

(a)

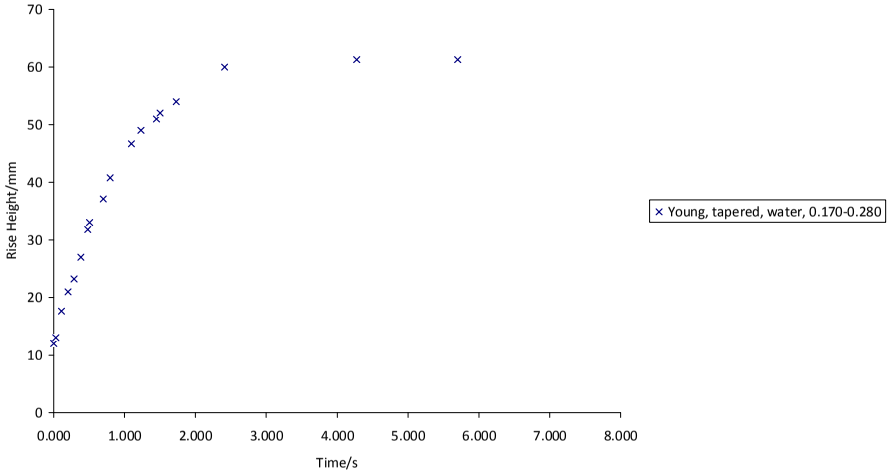

(b)

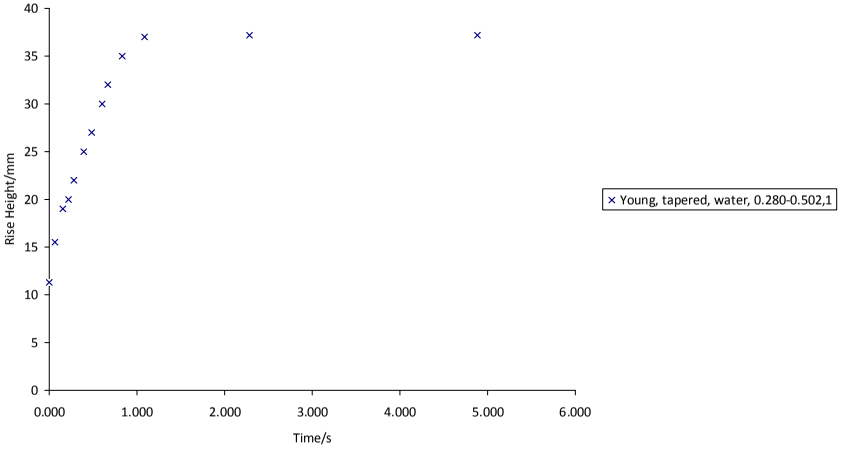

(c)

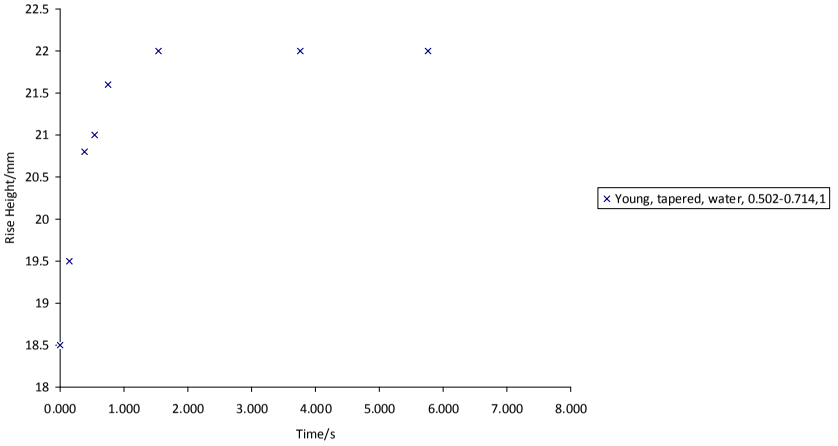

(d)

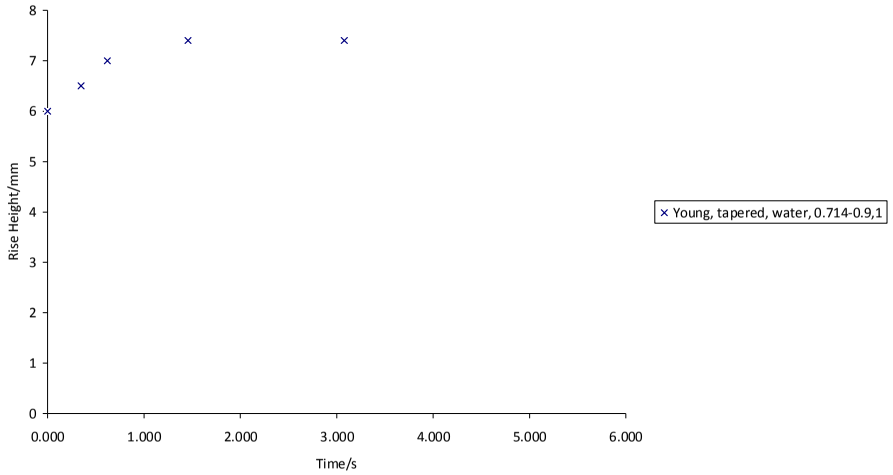

(e)

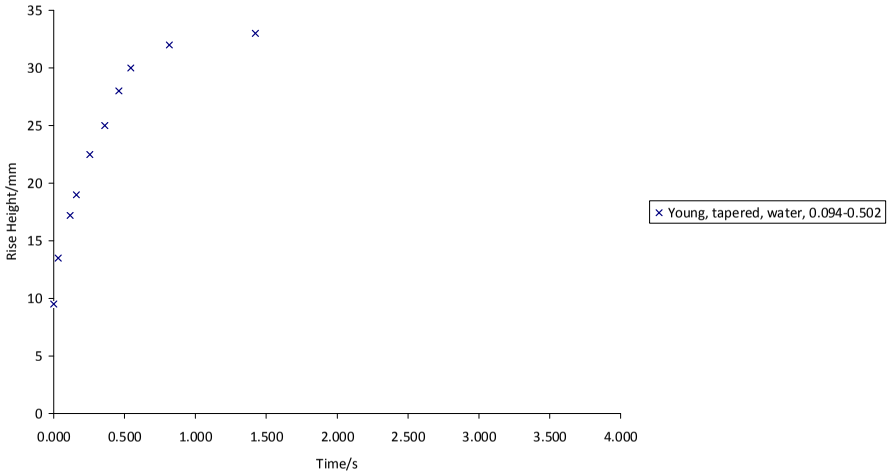

(f)

Figure_C9: Young, tapered, water graphs for wire thicknesses a-k respectively, a(0.094-0.170mm), b(0.170-0.280mm), c(0.344-0.502mm), d(0.502-0.714mm), e(0.714-0.900mm), f(0.094-0.502mm)

10. Young Planar Cyanoacrylate

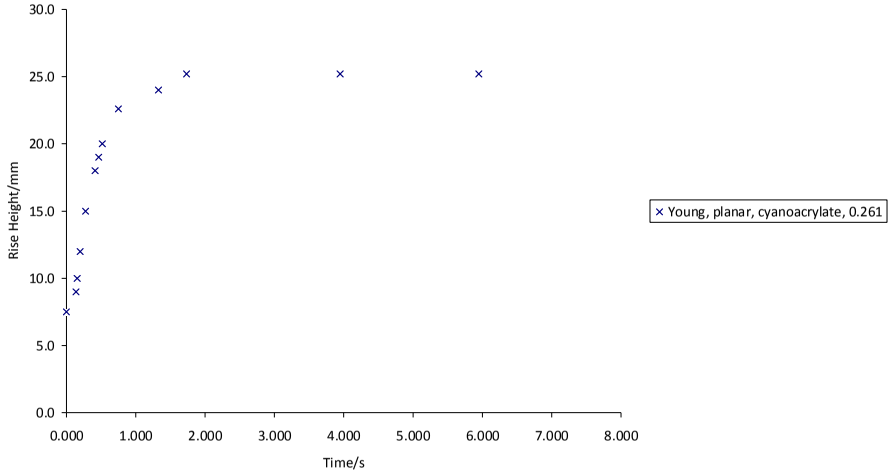

(a)

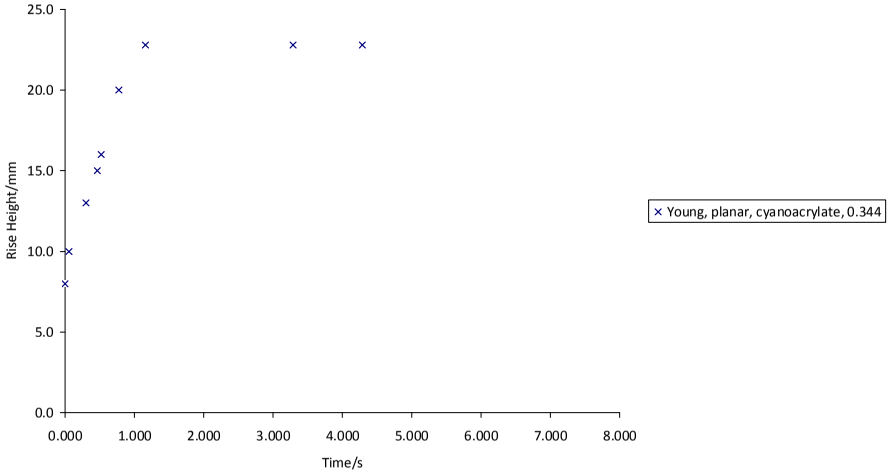

(b)

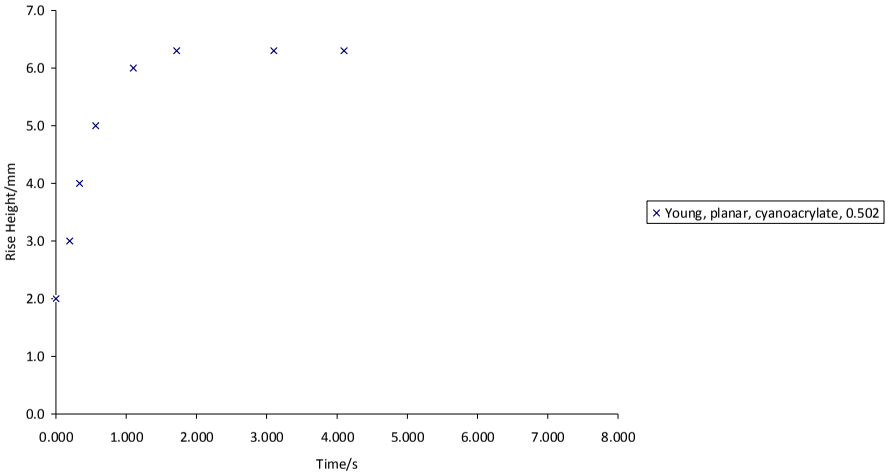

(c)

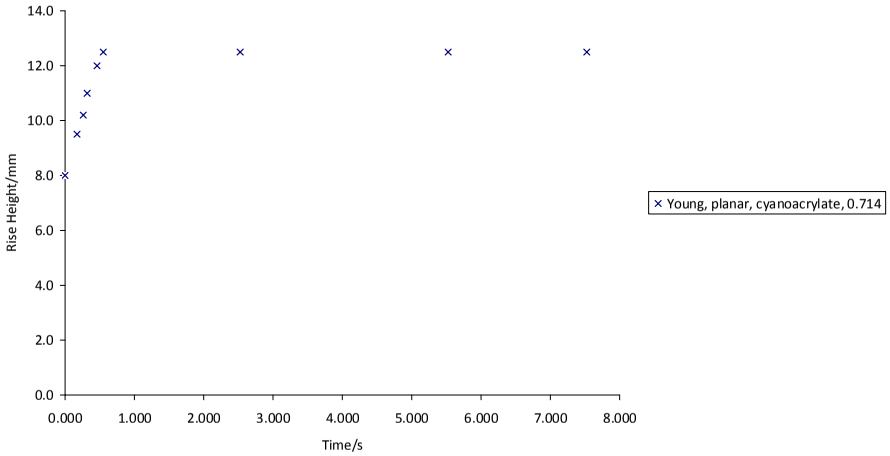

(d)

Figure_C10: Young planar cyanoacrylate graphs for wire thicknesses a-d respectively, a(0.261mm), b(0.344mm), c(0.502mm), d(0.714mm)

11. Young Tapered Cyanoacrylate

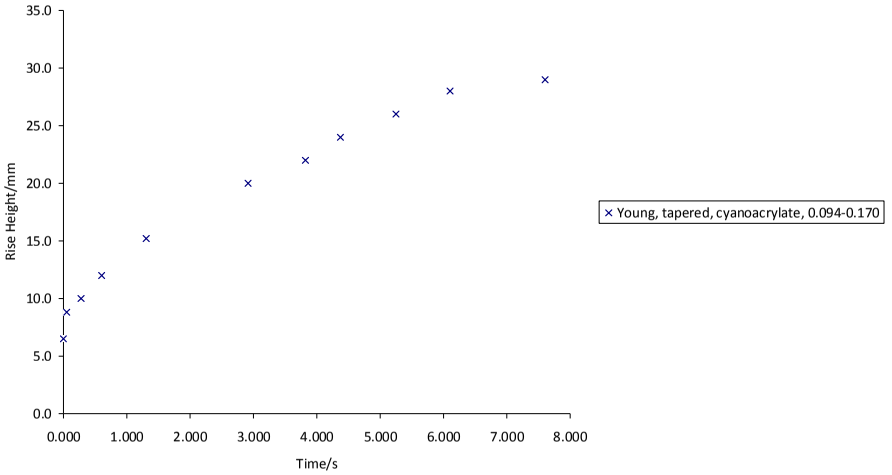

(a)

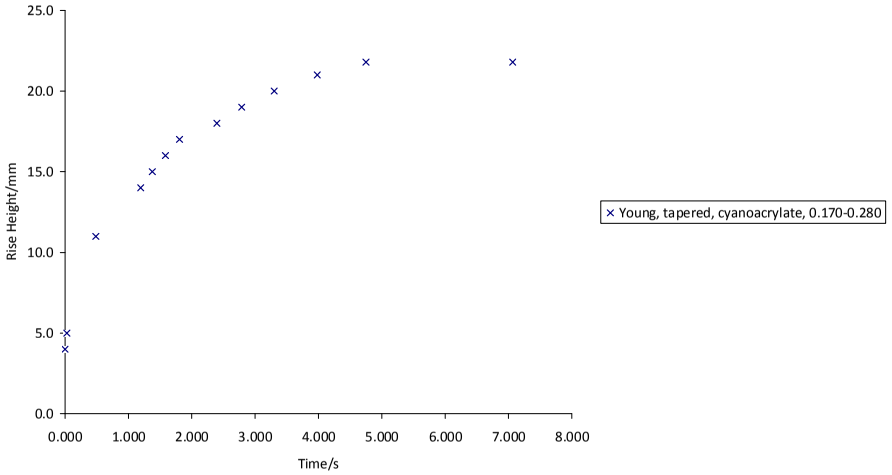

(b)

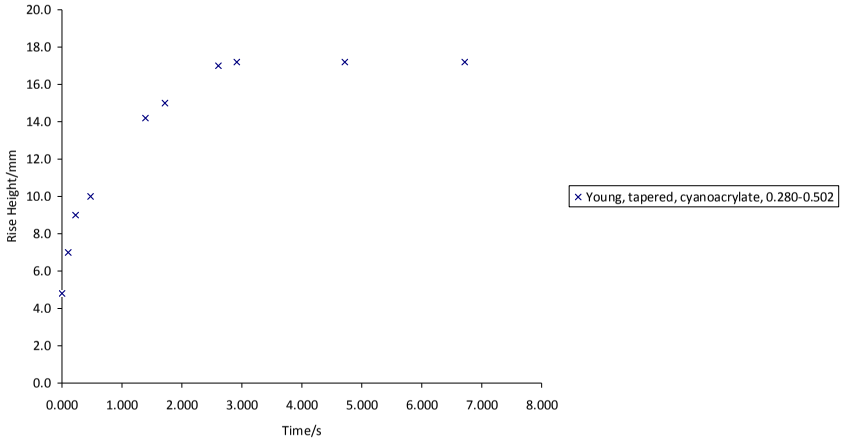

(c)

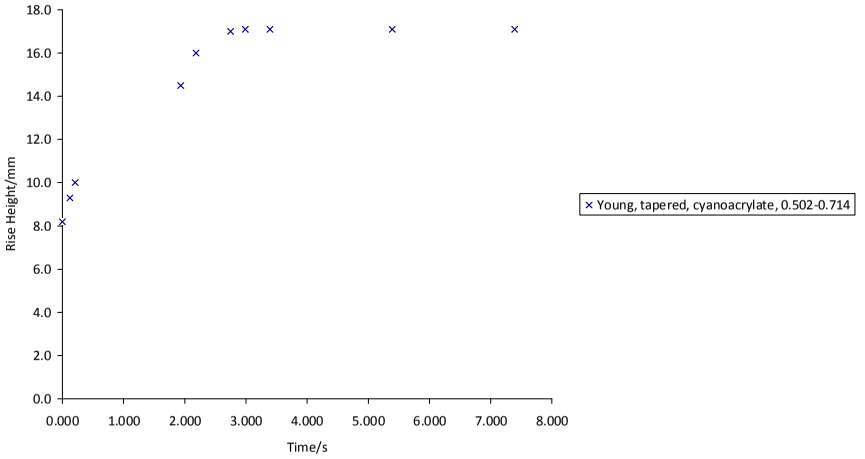

(d)

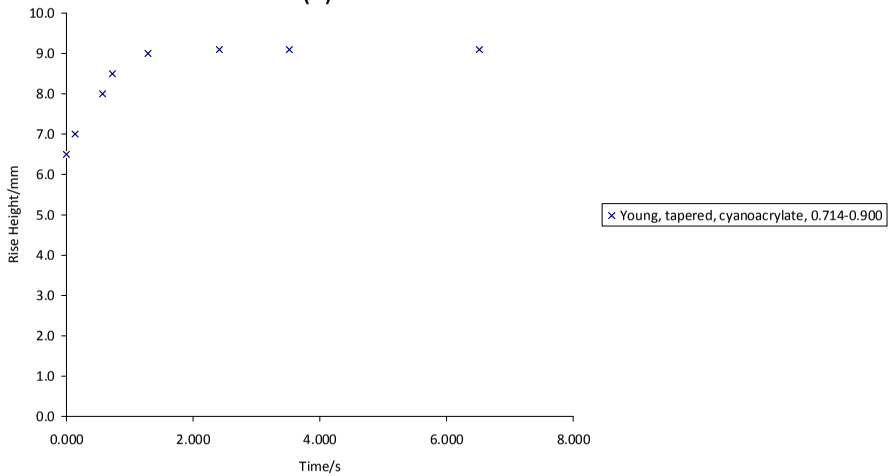

(e)

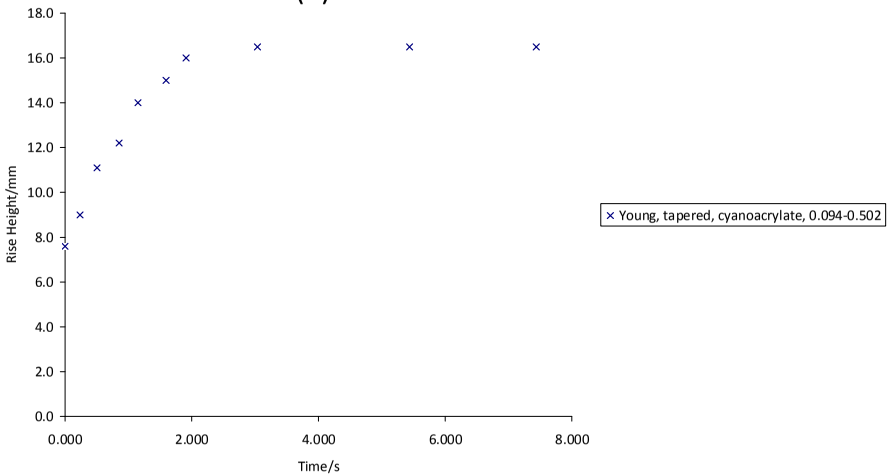

(f)

Figure_C11: Young, tapered, cyanoacrylate graphs for wire thicknesses a-f respectively, a(0.094-0.110mm), b(0.110-0.254mm), c(0.254-0.344mm), d(0.344-0.502mm), e(0.502-0.714mm), f(0.254-0.714mm)

12. Old Planar Xanthan Gum

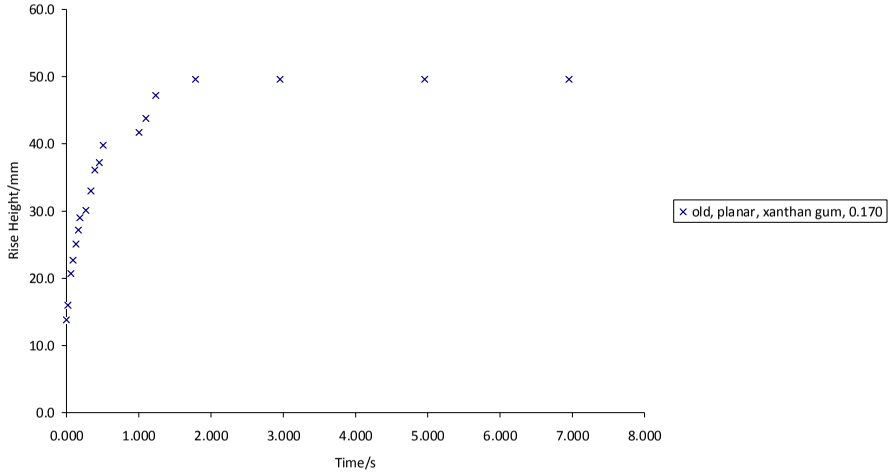

(a)

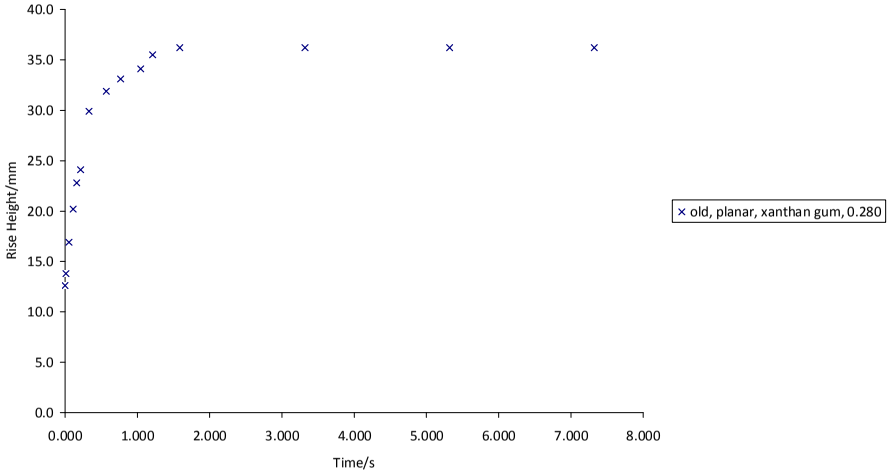

(b)

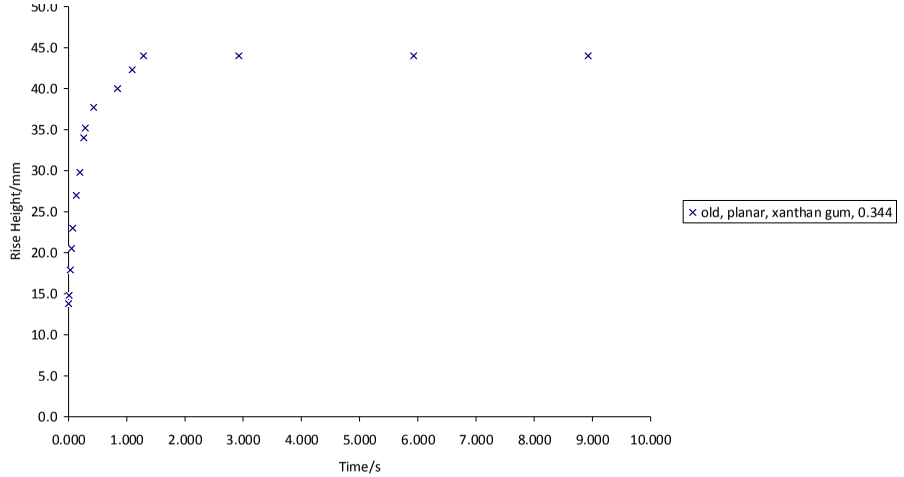

(c)

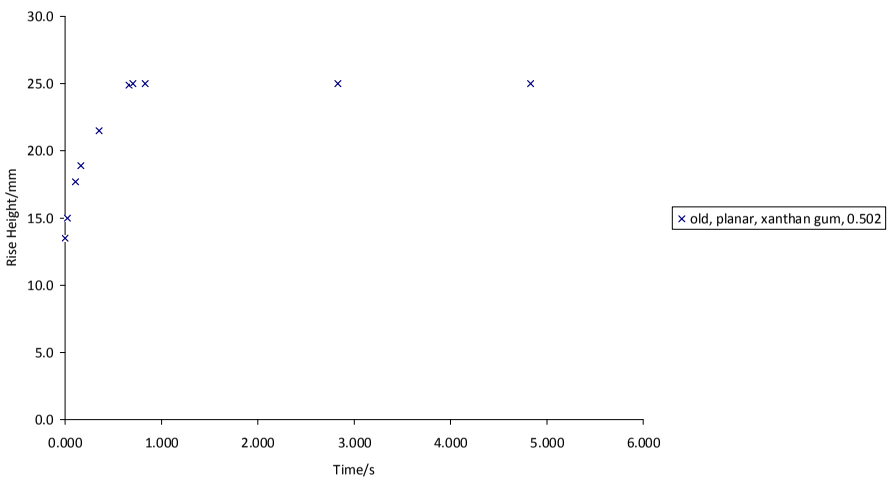

(d)

Figure_C12: Old, planar, xanthan gum graphs for wire thicknesses a-k respectively, a(0.170mm), b(0.280mm), c(0.344mm), d(0.502mm)

13. Mortar contact angles

Age of specimen	Wet/dry	Fluid	Wire thickness	Angle	°	Average angle/ deg
old	dry	water	0.094	1	bad image	**36**
				2	39	
				3	33	
				4	39	
				5	33	
old	dry	water	0.170	1	37	**31**
				2	24	
old	dry	water	0.150	1	55	**45**
				2	51	
				3	43	
				4	30	
old	dry	water	0.502	1	42	**33**
				2	44	
				3	28	
				4	19	
old	dry	water	0.170	1	14	**23**
				2	31	
old	dry	water	0.237	1	23	**20**
				2	16	
old	dry	water	0.280	1	46	**42**
				2	55	
				3	26	
old	dry	water	0.502	1	39	**46**
				2	49	
				3	49	
old	dry	water	0.620	1	47	**33**
				2	24	
				3	32	
				4	30	
old	dry	water	0.714	1	42	**34**
				2	35	
				3	25	
old	dry	water	0.900	1	bad image	**38**
				2	42	
				3	34	
young	dry	water	0.170	1	16	**21**
				2	25	
young	dry	water	0.280	1	32	**28**
				2	19	
				3	29	
				4	30	
young	dry	water	0.502	1	21	**21**
				2	bad image	
				3	20	
young	dry	water	0.714	1	13	**19**
				2	16	
				3	28	
young	dry	water	0.620	1	29	**34**
				2	25	
				3	49	
old	wet	water	0.170	1	31	**31**
				2	31	
old	wet	water	0.280	1	36	**32**
				2	28	
				3	20	
				4	45	
old	wet	water	0.502	1	21	**19**
				2	16	
old	wet	water	0.714	1	34	**31**
				2	27	
old	wet	cyanoacrylate	0.17	1	27	**19**
				2	11	
				3	19	
old	wet	cyanoacrylate	0.28	1	bad image	**28**
				2	28	
old	wet	cyanoacrylate	0.502	1	40	**39**
				2	50	
				3	28	
old	wet	cyanoacrylate	0.714	1	33	**30**
				2	26	

APPENDIX D

Numerical Models and CDs

1. **Planar experimental videos**
2. **Tapered experimental videos**
3. **Tortuous and natural experimental videos**
4. **Planar and tapered flow model**